

University of Windsor

## Scholarship at UWindor

---

Electronic Theses and Dissertations

Theses, Dissertations, and Major Papers

---

7-17-1969

### An experimental study of the decay of anisotropic turbulence.

Syed Firasat Ali  
*University of Windsor*

Follow this and additional works at: <https://scholar.uwindsor.ca/etd>

---

#### Recommended Citation

Ali, Syed Firasat, "An experimental study of the decay of anisotropic turbulence." (1969). *Electronic Theses and Dissertations*. 6550.

<https://scholar.uwindsor.ca/etd/6550>

This online database contains the full-text of PhD dissertations and Masters' theses of University of Windsor students from 1954 forward. These documents are made available for personal study and research purposes only, in accordance with the Canadian Copyright Act and the Creative Commons license—CC BY-NC-ND (Attribution, Non-Commercial, No Derivative Works). Under this license, works must always be attributed to the copyright holder (original author), cannot be used for any commercial purposes, and may not be altered. Any other use would require the permission of the copyright holder. Students may inquire about withdrawing their dissertation and/or thesis from this database. For additional inquiries, please contact the repository administrator via email ([scholarship@uwindsor.ca](mailto:scholarship@uwindsor.ca)) or by telephone at 519-253-3000ext. 3208.

## INFORMATION TO USERS

This manuscript has been reproduced from the microfilm master. UMI films the text directly from the original or copy submitted. Thus, some thesis and dissertation copies are in typewriter face, while others may be from any type of computer printer.

**The quality of this reproduction is dependent upon the quality of the copy submitted.** Broken or indistinct print, colored or poor quality illustrations and photographs, print bleedthrough, substandard margins, and improper alignment can adversely affect reproduction.

In the unlikely event that the author did not send UMI a complete manuscript and there are missing pages, these will be noted. Also, if unauthorized copyright material had to be removed, a note will indicate the deletion.

Oversize materials (e.g., maps, drawings, charts) are reproduced by sectioning the original, beginning at the upper left-hand corner and continuing from left to right in equal sections with small overlaps.

ProQuest Information and Learning  
300 North Zeeb Road, Ann Arbor, MI 48106-1346 USA  
800-521-0600

UMI<sup>®</sup>



AN EXPERIMENTAL STUDY OF  
THE DECAY OF  
ANISOTROPIC TURBULENCE

A Thesis

Submitted to the Faculty of Graduate Studies Through  
the Department of Mechanical Engineering in Partial  
Fulfillment of the Requirements for the Degree  
of Master of Applied Science at the  
University of Windsor

by

Syed Firasat Ali

B.E.(Mechanical), The University of Karachi,  
Karachi, Pakistan, 1965

Windsor, Ontario, Canada

1969

UMI Number:EC52732

UMI<sup>®</sup>

---

UMI Microform EC52732  
Copyright 2007 by ProQuest Information and Learning Company.  
All rights reserved. This microform edition is protected against  
unauthorized copying under Title 17, United States Code.

---

ProQuest Information and Learning Company  
789 East Eisenhower Parkway  
P.O. Box 1346  
Ann Arbor, MI 48106-1346

APPROVED BY:

Henry J. Tucker

W. J. [unclear]

[unclear]

254493

## ABSTRACT

Strongly anisotropic and approximately axisymmetric homogeneous turbulence was obtained in a parallel flow section by passing nearly isotropic grid turbulence through a  $5 \frac{3}{4} : 1$  axisymmetric contraction. Measurement of the three components of turbulence in the parallel flow section indicated strong tendency of anisotropic turbulence towards isotropy in the initial period of decay and the decay rate of the total turbulent energy was found to follow nearly the same power law as isotropic turbulent flow. Measurement of one dimensional energy spectra for the three components was also carried out at two different stations in the parallel flow section. Decay rate and energy spectra in the nearly isotropic turbulence obtained with the grid inserted at the starting of the parallel flow section were also measured mainly for comparison purposes.

In both of the above studies a perforated steel sheet grid was used for generating the turbulence but on comparison with other investigations the characteristics of turbulence were found to be nearly the same as obtained by the commonly used biplane grids.

The wind tunnel used had considerably high free stream turbulence which was undesirable in the study of anisotropic turbulence because of low grid turbulence intensity obtainable after the contraction.



## ACKNOWLEDGEMENTS

I wish to express my gratitude to Professor Henry J. Tucker for his supervision and valuable advices throughout this work. Gratitude is also due to my parents for their moral and financial support.

The technical assistance given by Mr. L. Cory and Mr. B. Gordon is gratefully acknowledged. I further wish to thank Mr. Roy Allen for taking pains to type this work.

The work was financially supported by the National Research Council of Canada under Grant No. 691.

## CONTENTS

	Page
ABSTRACT	iii
ACKNOWLEDGEMENTS	v
TABLE OF CONTENTS	vi
LIST OF FIGURES	viii
NOMENCLATURE	xi
1. INTRODUCTION	1
1.1 Definitions	1
1.2 Present Study	2
1.2.1 Type of Field	2
1.2.2 Realization of the Field	2
1.2.3 Experimental Program	4
2. LITERATURE SURVEY	6
2.1 Isotropic Turbulence	6
2.2 Anisotropic Turbulence	12
3. THEORY	15
4. APPARATUS AND INSTRUMENTATION	19
4.1 Wind Tunnel	19
4.2 Grid	19
4.3 Instrumentation	21
4.4 Probing Technique	22

	Page
5. EXPERIMENTS	24
5.1 Types of Field	24
5.2 Properties and their Measurement	25
5.3 Homogeneity Check	25
5.4 Effects of Acoustical and Free Stream Turbulence and other Inaccuracies	26
6. RESULTS AND DISCUSSIONS	28
6.1 Computation	28
6.2 Homogeneity of Turbulence	29
6.3 Isotropic Turbulence	30
6.3.1 Decay Rate	30
6.3.2 Isotropy	32
6.3.3 Energy Spectra	33
6.4 Anisotropic Turbulence	34
6.4.1 Decay Rate	34
6.4.2 Isotropy	34
6.4.3 Energy Spectra	35
Tables 6.1 - 6.4	37
7. CONCLUSIONS	40
BIBLIOGRAPHY	42
APPENDICES	47
FIGURES	95
VITA AUCTORIS	141

## FIGURES

Figure	Page
1	Coordinate system w.r.t. the wind tunnel section and the pipe. <span style="float: right;">95</span>
2a	Turbulence generating grid used in present study. <span style="float: right;">96</span>
2b	Typical grids for generating nearly isotropic turbulence. <span style="float: right;">97</span>
3	Isotropic turbulence decay, $(\bar{U}/u')^2$ and $(\bar{U}/v')^2$ vs. $(x/M)$ at $\bar{U} = 27.0$ ft/sec. <span style="float: right;">98</span>
4	Isotropic turbulence decay, $(\bar{U}/u')^2$ and $(\bar{U}/v')^2$ vs. $(x/M)$ at $\bar{U} = 35.7$ ft/sec. <span style="float: right;">99</span>
5	Isotropic turbulence decay, $3(\bar{U}/q)^2$ vs. $(x/M)$ <span style="float: right;">100</span>
6	Anisotropic turbulence decay, $(\bar{U}/u')^2$ , $(\bar{U}/v')^2$ and $(\bar{U}/w')^2$ vs. $(x/M)$ at 39.2 ft/sec. <span style="float: right;">101</span>
7	Anisotropic turbulence decay, $(\bar{U}/u')^2$ , $(\bar{U}/v')^2$ and $(\bar{U}/w')^2$ vs. $(x/M)$ at 53.3 ft/sec. <span style="float: right;">102</span>
8	Anisotropic turbulence decay, $3(\bar{U}/q)^2$ vs. $(x/M)$ <span style="float: right;">103</span>
9	Change in $u'/v'$ nearly isotropic turbulence during decay. <span style="float: right;">104</span>
10	Change in $u'/v'$ and $u'/w'$ in anisotropic turbulence during decay. <span style="float: right;">105</span>
11	Energy spectra of $u'$ in nearly isotropic turbulence at $\bar{U} = 27.1$ ft/sec. <span style="float: right;">106</span>
12	Energy spectra of $u'$ in nearly isotropic turbulence at $\bar{U} = 36.0$ ft/sec. <span style="float: right;">107</span>
13	Energy spectra of $v'$ and $w'$ in nearly isotropic turbulence at $\bar{U} = 27.1$ ft/sec. <span style="float: right;">108</span>
14	Energy spectra of $v'$ and $w'$ in nearly isotropic turbulence at $\bar{U} = 36.0$ ft/sec. <span style="float: right;">109</span>
15	Energy spectra of $u'$ in anisotropic turbulence at $\bar{U} = 39.2$ ft/sec. <span style="float: right;">110</span>

Figure	Page
16 Energy spectra of $u'$ in anisotropic turbulence at $\bar{U} = 53.3$ ft/sec.	111
17 Energy spectra of $v'$ and $w'$ in anisotropic turbulence at $\bar{U} = 39.2$ ft/sec.	112
18 Energy spectra of $v'$ and $w'$ in anisotropic turbulence at $\bar{U} = 53.3$ ft/sec.	113
19 Homogeneity of turbulence in a plane normal to the direction of flow in nearly isotropic turbulence at $x/M = 52.4$	114
20 Homogeneity of turbulence in a plane normal to the direction of flow in nearly isotropic turbulence at $x/M = 261.8$	115
21 Homogeneity of turbulence in a plane normal to the direction of flow in anisotropic turbulence.	116
22 General view of the wind tunnel.	117
23 Mean velocity of flow along the centre line of the test section.	118
24 Longitudinal component of free stream turbulence (plus instrument noise) at different velocities and frequency ranges.	119
25 Transverse component of free stream turbulence (plus instrument noise) at different velocities and frequency ranges.	120
26 Longitudinal component of free stream turbulence in different frequency ranges.	121
27 Transverse component of free stream turbulence in different frequency ranges.	122
28 Energy spectra of $u'$ in free stream turbulence at $\bar{U} = 26.7$ ft/sec.	123
29 Energy spectra of $u'$ in free stream turbulence at $\bar{U} = 35.3$ ft/sec.	124
30 Energy spectra $u'$ in free stream turbulence at $\bar{U} = 47.6$ ft/sec.	125
31 Energy spectra of $v'$ and $w'$ in free stream turbulence at $\bar{U} = 26.7$ ft/sec.	126

Figure	Page
32 Energy spectra of $v'$ and $w'$ in free stream turbulence at $\bar{U} = 35.3$ ft/sec.	127
33 Energy spectra of $v'$ and $w'$ in free stream turbulence at $\bar{U} = 47.6$ ft/sec.	128
34 Homogeneity of turbulence in a plane normal to the direction of flow in free stream turbulence.	129
35 Arrangements of measuring instruments for different turbulence quantities.	130
36 Schematic view of probing arrangement in the test section.	131
37a (i) Linear relationship between $E^2$ and $U^a$ for a hot wire.	132
(ii) Positions of normal and slanting wires w.r.t. the flow direction for measuring the three turbulence intensities.	132
37b Magnified views of normal, slanting and X hot wire probes.	133
38 Calibration of the normal and slanting hot wire probes (excluding the readings at zero velocity).	135
39 Calibration of the normal and slanting hot wire probes (including the readings at zero velocity).	136
40 Calibration of a slanting hot wire probe using linearizer in the circuit.	137
41 Mean velocity profile in turbulent flow in a pipe and values of $k$ of slanting hot wire determined from the known Reynolds shear stress distribution.	138
42 Comparison of radial Reynolds shear stress distribution by hot wire anemometer assuming different vales of $k$ , with that obtained from pressure drop along the pipe.	139
43 Calibration of WL slanting tube micromanometer against Flow Corporation micromanometer.	140

## NOMENCLATURE

Symbol	Description	Units
a	exponent of velocity in hot wire response equation	(dimensionless)
c	contraction ratio of flow section	(dimensionless)
E	instantaneous output voltage of hot wire	(volt)
$\bar{E}$	d.c. voltage across hot wire corresponding to $\bar{U}$	(volt)
$\bar{E}_l$	d.c. voltage across hot wire when linearizer is used in circuit	(volt)
$\bar{E}_0$	d.c. voltage across hot wire when it is not exposed to flow	(volt)
$E_1, E_2, E_3$	one dimensional spectrum functions of turbulence kinetic energy corresponding to $u'$ , $v'$ and $w'$ respectively	$(L^3/t^2)$
e	output fluctuating voltage of hot wire	(volt)
$e'$	r.m.s. value of fluctuating voltage	(volt)
f	coefficient of spatial longitudinal velocity correlation	(dimensionless)
$f'$	r.m.s. value of any turbulent velocity component in general, $u'$ , $v'$ or $\sqrt{q^2/3}$	$(L/t)$
g	gravitational acceleration	$(L/t^2)$

$g_0$	propotionality constant in Newton's law	(M/F L/t <sup>2</sup> )
I	electric heating current through hot wire	(ampere)
$k_t$	coefficient of spatial triple velocity correlation	(dimensionless)
k	constant appearing in empirical effective velocity expression for slanting hot wire	(dimensionless)
$k_1$	one dimensional wave number in the direction of mean flow	(1/L)
$L_x$	spatial integral scale correspond- ing to the direction of mean flow	( L )
M	mesh length	(L)
Nu	Nusselt number	(dimensionless)
n	frequency	(1/t)
n	exponent in decay law	(dimensionless)
P	static pressure	(F/L <sup>2</sup> )
Pr	Prandtl number	(dimensionless)
p	turbulent fluctuation of static pressure	(F/L <sup>2</sup> )
q	$\overline{u_i u_i}$ = twice mean energy of turbulence	(L/t <sup>2</sup> )
$R_w$	electric resistance of hot wire at operating conditions	(ohm)
$R_g$	electric resistance of hot wire at gas temperature	(ohm)



Re	Reynolds number	(dimensionless)
Re <sub>M</sub>	Reynolds number based on mesh length = $\bar{U}M/\nu$	(dimensionless)
Re <sub>λ</sub>	turbulence Reynolds number = $u'\lambda/\nu$	(dimensionless)
r	coordinate in radial direction, r = 0 corresponds to pipe centre	(L)
r <sub>0</sub>	pipe radius	(L)
r <sub>1</sub>	distance between two points	(L)
S	sensitivity of hot wire	(volt t/L)
S <sub>S</sub>	sensitivity of slanting hot wire	(volt t/L)
S <sub>n</sub>	sensitivity of normal hot wire	(volt t/L)
t	time	(t)
t <sub>0</sub>	time lapse between actual starting point and virtual origin	(t)
U	instantaneous total velocity	(L/t)
$\bar{U}$	time average of the velocity of flow	(L/t)
U <sub>n</sub>	component of velocity of flow normal to the hot wire	(L/t)
U <sub>t</sub>	component of velocity of flow tangential to the hot wire	(L/t)
U <sub>eff</sub>	effective instantaneous velocity for slanting hot wire	(L/t)
U*	shear stress velocity; $U^* = -\nu \left( \frac{du}{dr} \right)_{r=a}$	(L/t)

$u, v, w$	instantaneous values of velocity fluctuations in $x, y$ and $z$ directions, respectively in cartesian coordinates and in $x, r$ and $\theta$ directions, respectively in cylindrical coordinates	(L/t)
$u'v'w'$	root mean square values of $u, v$ and $w$ respectively.	(L/t)
w.r.t.	refers to 'with respect to'	
$x, r, \theta$	cylindrical coordinates	(L, L, dimensionless)
$x, y, z$	rectangular cartesian coordinates	(L)
$x_0$	distance along $x$ -axis between physical and virtual origin	(L)
$\tau_0$	wall shear stress in pipe flow	(F/L <sup>2</sup> )
$\theta$	azimuthal coordinate	(dimensionless)
$\lambda$	spatial micro scale of turbulence	(L)
$\nu$	fluid kinematic viscosity	(L <sup>2</sup> /t)
$\rho$	fluid mass density	(M/L <sup>3</sup> )
$\sigma$	grid solidity	(dimensionless)
$Q$	angle which the slanting wire makes with the mean velocity of flow	(dimensionless)

parallel flow section

refers to the flow section in which  
mean flow stream lines are in one  
direction.

## Subscripts

- e indicates condition at the exit of contraction
  - p indicates precontraction condition
  - $\ell$  indicates use of linearizer in hot wire circuit
  - M denotes mesh length
  - n normal direction
  - t tangential direction
  - $\lambda$  denotes micro scale of turbulence
- x , y , y , z , z indicate different positions of hot wire

## 1. INTRODUCTION

### 1.1 Definitions

Turbulent flow is a certain type of irregular flow, in which the velocities vary in a random way with the distance and time at all points in the field. Recently Lin and Reid (22) stated, "It is often desirable to limit the term turbulence only to such random fluctuating motions of a fluid having statistical properties which are definite and experimentally reproducible."

Among conceivable turbulent flows the simplest is the isotropic homogeneous turbulence. The term isotropic means that all statistical functions are invariant to rotation of axes and to reflection with respect to the coordinate planes. The term homogeneous turbulence is used for the random motion where statistical properties of the field are independent of translation of the coordinate system. In brief, in isotropic turbulent flow field  $\overline{u^2} = \overline{v^2} = \overline{w^2}$  at any point irrespective of the orientation of the coordinate system; and  $\overline{uv} = \overline{vw} = \overline{wu} = 0$ .

It has been found that if a uniform stream is passed through a regular array of holes in a rigid sheet or a grid of bars held at right angles to the stream, the turbulence thus generated is nearly isotropic and statistically homo-

geneous in any plane parallel to the grid.

An isotropic homogeneous turbulence field would be statistically non stationary in time. The reason is the absence of Reynolds stresses necessary for the continuous generation of turbulent energy to compensate for the dissipation of this energy. The rate of turbulent energy decay has been one of the principal objects of theoretical and experimental works on homogeneous isotropic turbulence since the pioneering paper by Taylor (4). Though considerable research has been carried out in this field, it has to be admitted that no sound and experimentally confirmed hypothesis exists which can be used to determine the exact law of decay of isotropic turbulence.

## 1.2 Present Study

1.2.1 Type of Field: The kinds of turbulent flow which are encountered in nature or in the engineering applications are usually anisotropic and non homogeneous. The extreme complexity of such a field can be well imagined by appreciating the difficulties encountered even in the study of isotropic turbulence which is considered to be the most simple. Moreover the study of such a field would preclude comparison of the results obtained, with the existing experimental and theoretical information. Since there is extensive research information for the case of the ideal situation of isotropic turbulence it was decided to consider a type second in simplicity, that is anisotropic axisymmetric homogeneous field under a steady mean flow. This type of turbulence has sym-

metry about a given direction. The main flow is assumed to be in this direction and uniform. If  $U$  is the mean velocity then  $\overline{w^2} = \overline{v^2} \neq \overline{u^2}$  corresponds to this type of flow.

The perforated sheet grid used for generating turbulence was not the common biplane grid used by other workers for the study of grid turbulence. Therefore it was felt necessary to study the nearly isotropic turbulence obtained by perforated sheet grid in order to compare the present results with those obtained by other investigators using regular biplane grids.

1.2.2 Realization of the Field: For obtaining nearly isotropic turbulence a regular periodic grid was inserted at the beginning of the constant area working section of the wind tunnel. For obtaining anisotropic axisymmetric turbulence a variety of ways could be employed. In order to achieve simplicity in measurement and reproducibility, only two methods are considered.

The first method is to take nearly isotropic flow downstream of a periodic grid and pass it through an extremely fine mesh gauze of moderately high resistance. The passage of turbulence through the gauze has the effect of attenuating the longitudinal component of the turbulence more than the transverse components and the turbulence emerges anisotropic and axisymmetric. Experimental results reported by Townsend (26) indicate that an appreciable degree of anisotropy may be achieved only when the attenuation of turbulence intensities by the screen is very high. This means that the anisotropic turbulence obtained with this arrangement would consist of very low turbulence in-

tensities.

The second method of obtaining anisotropic turbulence is to pass isotropic turbulence through a distorted passage and then allow it to recover in a parallel flow section. The turbulence is acted on by the mean velocity gradient and is made strongly anisotropic. If the distorted passage is an axisymmetric contraction, the emerging turbulence is also axisymmetric. Calculations made by Ribner and Tucker and independently by Batchelor (32) show that

$$\frac{\overline{u^2}_e}{\overline{u^2}_p} \approx (3c^2/4) (\log 4c^3 - 1) \quad \text{for } c \gg 1 \quad (1.1)$$

$$\frac{\overline{v^2}_e}{\overline{v^2}_p} \approx 3c/4 \quad \text{for } c \gg 1 \quad (1.2)$$

where subscripts p and e correspond to entrance and exit, respectively, of the contraction.

High degree of anisotropy and appreciable intensity and homogeneity of turbulence were the main requirements in the present study. Keeping this in mind the use of the second method was preferable to the first and hence the second method was used.

1.2.3 Experimental Program: The present experiments were undertaken to study the decay of anisotropic turbulence in steady mean flow, to find the rate of decay of turbulent energy and also any possible tendency of turbulence towards isotropy. For this purpose an existing large wind tunnel, which is described later in section 4.1 was used. A per-

forated grid was located in front of the wind tunnel contraction which produced anisotropic turbulence in the test section by the second method discussed in the preceding section. The three fluctuating components of the anisotropic turbulence were measured at points along the centre line of the constant area test section. In addition the energy spectra for  $u'$ ,  $v'$  and  $w'$  were measured at two different stations downstream of the grid. For comparison, the same measurements were also carried out in the case of nearly isotropic grid turbulence when the grid was located after the contraction at the beginning of the constant area test section.

Anisotropic turbulence was studied at two different mean velocities of 39 ft/sec and 53 ft/sec and isotropic turbulence was studied at the mean velocities of 27 ft/sec and 36 ft/sec.



## 2. LITERATURE SURVEY

### 2.1. Isotropic Turbulence

The concept of isotropic turbulence was first given by G.I. Taylor in 1935 (4). Prior to this time, as pointed out by Batchelor (4), theories of turbulence were based on analogies with the kinetic theory of gases which assumes discontinuous collisions between discrete entities. Taylor described measurements which showed that the turbulence generated by passing a uniform stream through a regular array of rods was approximately homogeneous and isotropic. Later measurements were reported by Dryden, Schubauer, Mock and Skramstad (10). Isotropy of the grid turbulence was also confirmed by the experimental study by McPhail (23).

A systematic theoretical approach to the dynamical problems was used by von Karman (4) who introduced, for the purposes of simplification, the assumption of self preservation of the shape of the velocity product functions during decay. In 1938 von Karman and Howarth (19, p.160) arrived at the following differential equation as a result of a theoretical analysis involving double and triple velocity correlations.

$$\frac{\partial}{\partial t}(u'^2 f) - u'^3 \frac{1}{r_1^4} \frac{\partial}{\partial r_1}(r_1^4 k_t) = 2 \nu u'^2 \frac{1}{r_1^4} \frac{\partial}{\partial r_1} \left( r_1^4 \frac{\partial f}{\partial r_1} \right)$$

This equation played an important role in later studies of

the dynamic behaviour of isotropic turbulence.

In 1941 Kolmogoroff (10) suggested the decay law,  $\frac{1}{q^2} = D (t-t_0)^{10/7}$ , where D is a constant. One of his main assumptions was the constancy of the Leitzianskii integral. The same law was derived by Comte-Bellot and Corrsin (10) using spectra method in 1966.

In 1943 Dryden (13) carried out a survey of the available experimental data on isotropic grid turbulence. He analysed the results obtained by Hall, by von Karman and by himself and his associates. He concluded that  $\left(\frac{\bar{U}}{u'}\right)^2$  varies during decay as some power of t lying between 1 and 2.

Batchelor (2), making use of Karman-Howarth equation, derived the so called linear decay law. He assumed partially self preserving solutions for the correlation functions near  $r = 0$  at decay times which are not large. The results can be presented as

$$\begin{aligned} u'^2 &\sim t^{-1} \\ \lambda^2 &= 10 \nu t \\ Re_\lambda &= u' \lambda / \nu = \text{const.} \end{aligned}$$

Experiments with the grid turbulence were carried out by Batchelor and Townsend (6,7). The results verified the above linear decay law for the values of  $Re_M$  at least down to 600, for distances upto about 150 mesh lengths from the grid. They suggested a division of the life history of the turbulence into an initial, a transition and a final period. This is considered with respect to time but for turbulence produced by a grid it applies to consecutive regions downstream of the grid (as  $\frac{\partial}{\partial t}$  may be substituted with  $U \frac{\partial}{\partial x}$ , Taylor's hypothesis (11)). In the initial period, inertial

effects predominate over viscous effects and the reverse is the case in the final period. According to Batchelor and Townsend the phase which may be considered the initial period of decay was characterised by the energy decay law

$$u'^2 \sim t$$

or

$$\bar{U}^2 / u'^2 = \alpha \left( \frac{x}{M} - \frac{x_0}{M} \right) \text{ where } \alpha \text{ and } x_0 \text{ are constants.}$$

By using different types of grids they attempted to relate the characteristics of turbulence to those of the grids. The grid characteristics comprise the geometry of the grid and its specific drag.

Frenkiel (14) made use of Karman Howarth equation to give a relation different from the linear decay law. He suggested the following equation,

$$\frac{u'^2}{u_0'^2} = \left[ \frac{7\nu}{\lambda_0^2} (t-t_0) + 1 \right]^{-10/7}$$

or approximately

$$\frac{u'^2}{u_0'^2} = \left( \frac{x}{x_0} \right)^{-10/7}$$

On comparison with the experimental results reported by previous investigators, he found good agreement for the decay of longitudinal turbulent energy. Later experimental values obtained by Baines and Peterson (1) agreed well with Frenkiel's equation rather than with the linear decay law.

Lin (21) put forward the decay law making assumption different from Batchelor which he claimed to be in accordance with the Kolmogoroff's concept of turbulence at high Reynolds numbers. The assumption made was that the actual deviation from the similarity of the spectrum will be limited only to small values of wave numbers and hence the effect of deviation will enter only in the calculation of energy but be neg-

ligible in the computation of the rate of energy dissipation. He suggested the following relations,

$$\begin{aligned} \frac{u'^2}{\lambda^2} &\sim t^{-1} \\ \lambda^2 &= 10\nu t \left(1 + \frac{\beta}{\alpha} t\right) && \alpha \text{ and } \beta \text{ are constants} \\ R_\lambda &= \frac{u'\lambda}{\nu} = \text{not constant} \end{aligned}$$

Goldstein (15) also derived the same law. He commented that the law does not follow from Kolmogoroff's original hypothesis. He stated that the eddies corresponding to the lower wave numbers are permanent; these eddies are not changed either by dissipation or energy transfer. But he justified the law on the assumption that the permanent eddies contain only an infinitesimal fraction of the energy and hence the eddies corresponding to all but the lowest wave numbers practically contain all the energy and are responsible for the whole of the dissipation.

Tsuji and Hamma (30) measured decay of turbulence behind a single grid and behind two grids. Lin's decay law was confirmed unless, in the two grid case, the large scale turbulence produced by the first grid was overwhelmingly predominant.

Later Tsuji (29) criticized Batchelor's linear decay law as well as Lin's decay law and found the points of self contradiction, inherent in the two laws. Tsuji derived the energy decay equation for the initial period from Karman Howarth equation,

$$V \frac{d^2 V}{dX^2} + C \left(\frac{dV}{dX}\right)^2 - E \left(\frac{dV}{dX}\right)^{3/2} = 0$$

and suggested the solution of this equation by numerical integration. In the above equation  $V = \bar{U}^2 / u'^2$ ,  $X = x/M$ ,

$$C = (7/15)G^{-2}, E = (7/3)S \sqrt{Re}/10, S = \left[ \frac{(\partial u / \partial x)^3}{(\partial u / \partial x)^2} \right]^{3/2}$$

and  $G = \frac{u^2 (\partial^2 u / \partial x^2)}{[(\partial u / \partial x)^2]^2}$  Tsuji claims that the assumptions made by him were based on the experimental findings of previous investigations.

The different assumptions made in the three decay laws can be summarized as under

	S	G	Re	S-(2G/Re)
Linear Decay Law	Const.	Const.	Const.	Const.
Lin's Decay Law	-	-	Not Const.	Const.
Tsuji's Decay Law	Const.	Const.	Not Const.	Not Const.

Deissler (12) considered correlation between fluctuation quantities at two, three and four points respectively. The set of equation, so obtained was made determinate by neglecting highest order (quintuple) correlations. The solution represented the turbulence for times between the initial and final periods. The results reproduced most of the trends observed experimentally in previous investigations. Deissler suggest that the analysis of turbulence in the initial period can be made possible by utilizing correlation equations involving a sufficient number of points in the fluid. Each times the set of equation would be made determinate by neglecting the highest order correlation involved.

Webb (37) carried out the study of the decay of turbulent energy downstream of a grid in air, argon and helium. He found that above a grid Reynolds number of about 2,000 and below a turbulence Knudsen number (Ratio of molecular mean free path to the Kolmogoroff microscale) of 0.01 an identical initial period decay law occurs independent of the

gas employed or the ambient pressure level. The rate of decay was found to be approximately linear with  $x/M$ .

Uberoi (34) reported the measurements of  $\overline{u^2}$  and  $\overline{v^2}$  in the turbulence behind a round rod square mesh grid. He found that the ratio  $u'/v'$  had a nearly constant value of 1.2 indicating that grid generated turbulence is not strictly isotropic and there is no strong tendency for it to become so further downstream. He suggested the following equation for decay

$$\begin{aligned} q^2 &\sim (x-x_0)^{-1.2} \\ \text{or } q^2 &\sim t^{-1.2} \end{aligned}$$

Uberoi and Wallis (35) attempted to obtain isotropic turbulence by passing grid turbulence through small axisymmetric contraction. It was found that while passing through contraction  $v'$  and  $u'$  tend to equalize but a clear tendency of strained isotropic turbulence to return to the precontraction anisotropic condition was observed. The same attempt was made by Comte-Bellot and Corrsin (10) and they found that the isotropy persists downstream of the small contraction. For the isotropic turbulence so obtained, they found that both  $u'$  and  $v'$  satisfied the power law of the form of equation (2.5) with an index of 1.28. For the turbulence behind square rod and round rod grids they found  $u'/v' \approx 1.05$  to 1.15 but a slow tendency to isotropy was observed. For the decay law indices varied from 1.16 to 1.33 with different grid geometries and mean velocities.

Very recently Uberoi and Wallis (36) reported the study of the effect of grid geometry on turbulence decay.

The ratio  $u'/v'$  was found to be essentially constant during decay with a value between 1.1 and 1.16 with different grids. The turbulence intensity was found to decay according to  $u'^2 \sim t^{-n}$  with  $n$  between 1.22 and 1.48 depending on the grid geometry.

## 2.2 Anisotropic Turbulence:

In 1944 MacPhail (24) obtained strong anisotropic turbulence by passing nearly isotropic grid turbulence through a distortion. He allowed the resulting anisotropic turbulence to flow through a constant area section of the wind tunnel. He observed the recovery of isotropy taking place in an oscillatory fashion.

Townsend (26) obtained anisotropic axisymmetric turbulence by passing grid turbulence through a fine mesh gauze. He measured  $\overline{u^2}$  and  $\overline{v^2}$  for few mesh lengths downstream of the mesh gauze. He observed that after a short period of comparatively rapid interchange of energy between the velocity components, the ratio of intensities become very nearly constant, and the once powerful tendency towards isotropy becomes a weak drift barely detectable. He expressed the view that while the turbulence is in the zone of influence of the gauze, its configuration is such that interchange of energy between velocity components is very rapid. According to this, the initial rapid readjustment occurs only in the zone of influence of the gauze, and the subsequent slow approach to isotropy of the energy containing eddies is typical of free anisotropic turbulence. Townsend (27)

also obtained anisotropic turbulence by passing grid turbulence through a distorted passage. Again he observed that the tendency to isotropy was very weak. From measurement of the velocity derivatives he inferred that the dissipating structure was isotropic in both of the above cases.

From Kolmogoroff's hypothesis Uberoi (33) inferred that if we deform a fluid in isotropic turbulent motion then it should become rapidly isotropic once the deformation has ceased. Kolmogoroff's hypothesis (33) may be briefly stated as follows. At sufficiently high Reynolds number the turbulence is made up of a hierarchy of eddies. It is assumed that there is a transfer of energy from larger to smaller eddies in the same way as the transfer of energy from the mean to the turbulent motion in a shear flow. The large scale eddies dissipate little energy by viscosity and pass on most of it to eddies of smaller scale, and so on to the smallest scale eddies which are responsible for most of the viscous dissipation. Uberoi produced anisotropic axisymmetric turbulence by passing grid turbulence through an axisymmetric contraction. Measurements in the uniform section after the contraction indicated a strong tendency toward isotropy. It was found that the larger components were losing more energy due to viscosity than by transfer to the smaller component. Approximately one third of the turbulent energy was left by the time  $\overline{u^2}$  and  $\overline{v^2}$  became nearly equal. It was also shown that the turbulence was becoming locally isotropic at a faster rate than the equipartition of energy was taking place.



In the course of study of large eddies of turbulent motion, Grant's (16) observations indicated very slow decrease of the anisotropy after distortion.

Tucker and Reynolds (31) observed a marked tendency towards isotropy for the turbulence in the parallel flow following the distortion similar to that used by Townsend. They concluded that the return to isotropy was rapid for highly anisotropic turbulence and slower as the turbulence approaches the isotropic condition. They presented this as one of the reasons of the discrepancy between their results and those of Townsend and of Grant.

With the exception of Uberoi's study, the above mentioned works were not carried out with prime interest in the study of the decay of anisotropic turbulence and the inferences were based on the observations for very small distances allowed for the decay in the parallel section.

### 3. THEORY

The current literature on the theoretical treatment of anisotropic turbulence does not give very clear picture about the behaviour of homogeneous anisotropic turbulence during decay. A rough idea concerning the tendency of anisotropic turbulence towards isotropy can be formed by considering the energy equation. The particular type of field considered here is an incompressible, anisotropic turbulent field under a steady unidirectional mean flow with symmetry about the direction of mean flow and homogeneity in planes normal to mean flow direction. Tensor notation is used in this chapter and the coordinate axes  $x, y, z$  are referred to here as  $x_1, x_2, x_3$  respectively, the mean velocities along the three axes are denoted by  $\bar{U}_1, \bar{U}_2, \bar{U}_3$  and the fluctuating velocities  $u, v, w$  by  $u_1, u_2, u_3$  respectively.

For incompressible flow with steady main motion and with statistical average values in steady state, the following turbulent energy equation can be obtained from the Navier Stokes equation.

$$\begin{aligned} \bar{U}_k \frac{\partial}{\partial x_k} \overline{u_i u_i} &= -2 \overline{u_k u_i} \frac{\partial \bar{U}_i}{\partial x_k} - \frac{\partial}{\partial x_k} \overline{u_i u_i u_k} - \frac{1}{\rho} u_i \frac{\partial p}{\partial x_i} + \nu \frac{\partial^2}{\partial x_1 \partial x_1} \overline{u_i u_i} \\ &\quad - 2\nu \frac{\partial u_i}{\partial x_1} \frac{\partial u_i}{\partial x_1} \end{aligned} \tag{3.1}$$

The derivation of the above equation is shown in appendix D. From the above equation we can write two different equations for  $u_1$  and  $u_2$

$$\bar{U}_k \frac{\partial \bar{u}_1^2}{\partial x_k} = -2\bar{u}_k \bar{u}_1 \frac{\partial \bar{u}_1}{\partial x_k} - \frac{\partial}{\partial x_k} \overline{u_1^2 u_k} - \frac{1}{\rho} \overline{u_1 \frac{\partial p}{\partial x_1}} + \nu \frac{\partial^2}{\partial x_1 \partial x_1} \bar{u}_1^2$$

and

$$-2\nu \frac{\partial u_1}{\partial x_1} \frac{\partial u_1}{\partial x_1}$$

$$\bar{U}_k \frac{\partial \bar{u}_2^2}{\partial x_k} = -2\bar{u}_k \bar{u}_2 \frac{\partial \bar{u}_2}{\partial x_k} - \frac{\partial}{\partial x_k} \overline{u_2^2 u_k} - \frac{1}{\rho} \overline{u_2 \frac{\partial p}{\partial x_2}} + \nu \frac{\partial^2}{\partial x_1 \partial x_1} \bar{u}_2^2 - 2\nu \frac{\partial u_2}{\partial x_1} \frac{\partial u_2}{\partial x_1}$$

For the special case with mean flow in  $x_1$  direction and homogeneity in  $x_2$  and  $x_3$  directions, the equations reduce to

$$\bar{U}_1 \frac{\partial \bar{u}_1^2}{\partial x_1} = -\frac{1}{\rho} \overline{u_1 \frac{\partial p}{\partial x_1}} - 2\nu \frac{\partial u_1}{\partial x_1} \frac{\partial u_1}{\partial x_1} + \nu \frac{\partial^2}{\partial x_1^2} \bar{u}_1^2 - \frac{\partial}{\partial x_1} \overline{u_1^3}$$

$$\text{I} \quad \bar{U}_1 \frac{\partial \bar{u}_2^2}{\partial x_1} = -\frac{1}{\rho} \overline{u_2 \frac{\partial p}{\partial x_2}} - 2\nu \frac{\partial u_2}{\partial x_1} \frac{\partial u_2}{\partial x_1} + \nu \frac{\partial^2}{\partial x_1^2} \bar{u}_2^2 - \frac{\partial}{\partial x_1} \overline{u_2^2 u_1}$$

The various terms in the above two equations can be interpreted as follows:

I represents change in turbulent energy component in the direction of main flow.

II are the correlation between the velocity fluctuation and derivative of the pressure fluctuation.

III is the viscous dissipation.

IV is the transport of energy due to viscous shear stresses.

V represents turbulent transport of component energies.

Comte-Bellot and Corrsin (10) in dealing with the energy equations have presented various points about the tendency of homogeneous turbulence towards isotropy or anisotropy. Because of their importance in the present experimental study, some of the points are reproduced here with reference to the above two equations.

The static pressure terms exchange energy among velocity directional components. It is generally believed, though possibly not theoretically deducible from the equations of motion, that they tend to transfer energy from more energetic to less energetic components. The viscous dissipation destroys component energy at a rate proportional to that energy, hence an approach toward isotropy may be present. The transport due to viscosity will be negligible compared with the turbulent transport. For isotropic turbulence  $\overline{u_1^3}$  and  $\overline{u_1 u_2^2}$  are both identically zero. However, the growth of  $\frac{\overline{u_1^3}}{(\overline{u_1^2})^{3/2}}$  has been observed in contraction studies. In a 4:1 contraction this grew to 0.08, and it returned rapidly to zero in the straight section following the contraction. The authors (Comte-Bellot and Corrsin) carried out an approximate theoretical analysis for  $\overline{u_1^3}$  due to strain, and on similar basis an approximate expression was found for  $\overline{u_1 u_2^2}$ . Then to estimate the effect of only the turbulence transport of component energies on the tendency towards isotropy, the approximate expression was obtained

$$\frac{\overline{u_{1s}^2} - \overline{u_{2s}^2}}{\overline{u_{1e}^2}} \approx \frac{u'_{1e}}{U_{1e}} \left\{ \frac{\overline{u_{1e}^3}}{(\overline{u_{1e}^2})^{3/2}} - \frac{u_{1e} u_{2e}^2}{u_{1e}^2 u_{2e}^2} \right\} \quad \text{-- (3.7)}$$

where subscript e refers to the position just after the contraction and s refers to the position where  $\overline{u_1^2}$  and  $\overline{u_2^2}$  become sensibly zero.

In the above expression

$$\frac{\overline{u_1^3}}{(\overline{u_1^2})^{3/2}} \approx 3 \frac{u'_{1p}}{U_{1p}} \left( 1 - \frac{\overline{U_{1p}^2}}{U_{1p}^2(x)} \right)$$

and

$$\frac{\overline{u_1 u_2^2}}{u'_1 \overline{u_2^2}} \approx \frac{-1}{6} \frac{\overline{u_1^3}}{(\overline{u_1^2})^{3/2}}$$

Substituting these values in equation (3.7) and making use of equation (1.1) for  $\overline{u_{1e}^2}/\overline{u_{1p}^2}$ , we obtain

$$\frac{\overline{u_{1s}^2} - \overline{u_{2s}^2}}{\overline{u_{1e}^2}} \approx \frac{10}{3} \left\{ \frac{c-1}{c} \right\} \frac{c^2}{\log 4c^3 - 1} \frac{\overline{u_{1e}^2}}{U_{1e}^2} \quad (3.8)$$

We may conclude the above discussion with the following remarks:

The velocity-pressure-gradient correlations tend to decrease the anisotropy.

The viscous dissipation of component energies is higher with the higher intensity components, this also tends to equalize the turbulent components.

A tendency towards energy inequality may be present due to turbulent transport of component energies (equation 3.8). But this effect is quite negligible in comparison to the other effects.

## 4. APPARATUS AND INSTRUMENTATION

### 4.1 Wind Tunnel:

A closed circuit low speed wind tunnel of Mechanical Engineering Department of the University of Windsor was used for the experiments. A short description of the tunnel is included here, detailed description and calibration are given in appendix A.

The dimensions of the test section were  $2\frac{1}{2}$  ft. square by 20 ft. long. Over the speed range used in the experiments, the free stream turbulence levels (without the turbulence generating grid) were of considerable magnitude. On the centreline at the upstream end of the tunnel  $u'/\bar{U}$  was found to lie between 0.20% and 0.25% and  $v'/\bar{U}$  ( $=w'/\bar{U}$ ) between 0.30% and 0.60%. At the downstream end these values were found to lie between 0.23% and 0.30% and between 0.30 and 0.65% respectively.

The coordinate system with respect to the test section is shown in figure 1.

### 4.2 Grid:

A perforated steel sheet was used as a grid for turbulence generation. The sheet was 0.03 in thick having  $11/16$  in. ( $\pm 0.0045$ ) square mesh with bars  $3/16$  in. ( $\pm 0.0025$ ) wide.

The solidity, which is defined as projected solid area per unit total area, was 0.47. This value lies in the range which is recommended for obtaining approximately homogeneous turbulence in planes parallel to the grid (11). This type of grid has not been used in studying the decay of grid turbulence by previous investigators. Tucker and Reynolds (31) have reported its use for the study of deformation effects on grid turbulence. Cheapness, light weight, and dimensional homogeneity were some of the advantages of this grid. The turbulence level obtained by this grid was nearly equal to that obtained by previous workers using square rod grids of the same solidity (11). For studying decay of isotropic turbulence the grid was inserted at the entrance of the test section. For studying decay of anisotropic axisymmetric turbulence the grid was inserted in the wind tunnel so that it was followed by a 5 3/4 :1 axisymmetric contraction leading to the test section.

Grid was made in two sizes, one to fit upstream of the contraction for anisotropic turbulence and the other to fit at the starting of the parallel section for isotropic turbulence. Because of large cross-sectional area upstream of the contraction a single manufactured grid was not available and three pieces were spot-welded together as shown in figure 2. With this, however, axisymmetry of the turbulence was slightly affected and it necessitated recording the fluctuating components of velocity  $u'$ ,  $v'$  and  $w'$ .

#### 4.3 Instrumentation:

All turbulence measurements were made with constant temperature hot wire anemometers. The following instruments were used.

DISA 55 A 01 constant temperature hot wire anemometers (two units).

DISA 55 A 06 random signal indicator and correlator.

Bruel Kjaer audio frequency spectrometer type 2112.

Bruel Kjaer random noise voltmeter type 2417.

The signal transducers were the following DISA manufactured constant temperature hot wire probes.

Type 55 A 25 miniature straight hot wire probe with wire of  $5\mu$  diameter and 1 mm length mounted normal to the probe axis.

Type 55 A 29 miniature probe with slanting wire of  $5\mu$  diameter and 1 mm length forming an angle of  $45^\circ$  with the probe axis.

Type 55 A 32 hot wire X-probe with the wire planes parallel to themselves and to the probe axis and both wires forming an angle of  $45^\circ$  with the probe axis, the diameter and length of each wire being  $5\mu$  and 1 mm respectively.

All probes were made of platinum plated tungsten wire. The magnified views of the probes are shown in fig. 37b.

The two miniature probes with 55 A 21 miniature probe support were used to measure turbulence intensities  $u'$ ,  $v'$ , and  $w'$ . For this purpose each of the probes was calibrated in the same wind tunnel using a pitot static probe



with a Wilhelm Lambrecht slanting tube micromanometer No. 655. The calibration of hot wire is described in detail in appendix B. The calibration of other instruments is reported in appendix C. For measuring turbulence energy spectra miniature straight probe was used for  $u'$  and X-probe with 55 A 30 probe support for  $v'$  and  $w'$ . Figure 35 gives the block diagrams showing the arrangements of instruments for the different measurements.

#### 4.4 Probing Technique:

Provision was made in the test section of the tunnel for inserting  $\frac{1}{4}$ " diameter steel rods in vertical position at intervals of 18" along the test section length. Each inserted rod was provided with a brass block drilled to slide on the vertical rod and having a slot to support a square bar horizontally. Each block carried two screws one to fix its own position on the vertical rod and the other to hold the supported horizontal bar. Three rods could be inserted at a time for supporting a  $\frac{1}{2}$ " square x 4 ft. long steel bar at any desired position in the central vertical plane in the test section and parallel to the direction of mean flow. (Similar arrangements were made to support the square bar horizontally in vertical planes at 6" on either side of the central vertical plane. This arrangement was made so that transverse homogeneity of turbulence could be checked in planes normal to the direction of flow at two different stations in the

test section.) The square bar was bored and slotted at one end so that the miniature probe support could be fixed in line with the bar axis, while the 55 A 30 probe support required alignment. The long bar could be given any number of  $90^\circ$  rotations because of its square section. The round ends were properly marked to enable the square bar to be supported along the centre line of the test section.

With the three vertical rods fixed at their positions, the probe could be traversed through any distance within 18" along the test section length. After every 18" traverse, out of the three vertical rods the upstream one could be removed and other vertical rod could be introduced further downstream. In this way three vertical rods could again support the horizontal bar for further 18" traverse of the probe. Figure 36 gives the schematic view of the arrangement.

The ceiling of the test section was not a plane surface, the remaining wall surfaces were approximately plane. It was estimated that the axis of the test section could be located within  $\pm 1/8$ " horizontally and  $\pm 1/4$ " vertically.

## 5. EXPERIMENTS

### 5.1 Types of Field:

The present investigation was carried out to study the decay of an anisotropic axisymmetric homogeneous field of turbulence in an incompressible steady mean flow. As mentioned previously a perforated sheet grid was used for generating the turbulence. Previous investigators have used biplane square mesh grids with round or square rods and not the perforated sheet grid used here. For the regular type of biplane grids extensive experimental research information is available for the decay of the turbulence in a constant area section behind the grid. Similar information for the perforated grid was not available. Therefore it was felt necessary to conduct experiments to obtain this information so that a comparison could be made with the turbulence produced by the more commonly used biplane grids. By this study a comparison could also be made between the nearly isotropic turbulence in a parallel section downstream of the grid and the strongly anisotropic turbulence produced by using a contraction between the grid and the parallel section. We will refer to the nearly isotropic grid turbulence and the strongly anisotropic turbulence by the terms isotropic turbulence and anisotropic turbulence respectively.

## 5.2 Properties and their measurement:

The distance downstream of the grid taken along the axis of the test section was considered to be the independent variable. The varying quantities measured along this distance were the three fluctuating components of velocity  $u'$ ,  $v'$  and  $w'$  when the mean velocity of flow was maintained constant. In the isotropic case the axisymmetry of the turbulence was confirmed within the accuracy of measurement, therefore only  $u'$  and  $v'$  were recorded. In case of anisotropic turbulence  $v'$  and  $w'$  were different, therefore all the three components were measured.

In addition to the turbulence intensities, energy spectra were obtained at two different stations at the axis of the test section downstream of the grid. Energy spectra for  $u'$ ,  $v'$  and  $w'$  were measured in both the cases of isotropic and anisotropic turbulence.

The experiments were carried out at the mean speeds of 39 ft/sec and 54 ft/sec for the anisotropic turbulence and 27 ft/sec and 36 ft/sec for the isotropic turbulence.

## 5.3 Homogeneity Check:

Homogeneity of turbulence was checked in planes normal to the working section axis. For this purpose the turbulence intensities were measured at different points covering an area of 1 foot square around the axis. (see figs. 19-21). Check of homogeneity was also carried out for free stream turbulence (see fig. 34)

5.4 Effects of acoustical and free stream turbulence  
and other inaccuracies:

From the spectrum measurements it was inferred that the waves at the frequencies above 10 kc/s were mainly due to instrument noise. Filters provided in the anemometer were used to eliminate frequencies above 10 kc/sec while recording the r.m.s. voltages of the turbulence intensities. The filters were not used for some of the spectrum readings.

For acoustical and free stream turbulence 0.1% is considered as the upper limit which can be allowed in experimental studies similar to the present one. In the wind tunnel used for the present work, as mentioned in the previous chapter, the turbulence was found to have very high values. The effect of this was more pronounced in the anisotropic field because of very low intensities of turbulence in the test section. To correct for free stream turbulence and instrument noise at any point the mean square voltages in the empty wind tunnel were subtracted from the corresponding voltages at the same operating conditions and mean velocity of flow with the grid in position. This method of correction was used in the decay study of both isotropic as well as the anisotropic turbulence. A similar method was reported by Uberoi and Wallis (36). In the measurement of energy spectra also similar type of subtraction was made by Uberoi (32). In the measurement of the energy

spectra, in the present study the same type of correction was applied for isotropic turbulence. During the measurement of spectra in anisotropic turbulence, at some of the frequencies it was noticed that the r.m.s. voltage was higher in the free stream turbulence than in the anisotropic turbulence. The exact effect of free stream turbulence spectra upon the grid turbulence spectra could not be pointed out. Therefore the energy spectra obtained for anisotropic turbulence were not corrected for free stream turbulence. It may be mentioned here that the spectrum readings were taken beyond 20 c/sec and large part of free stream turbulence was found to consist of the eddies in frequency range below 20 c/sec. (see Appendix A)

In each run, after starting the motor and fan, 15 to 20 minutes were allowed, before beginning the measurement of the turbulence quantities in order to insure low increase in temperature during these measurements. A difference of 2° to 4° F could be observed during the run, the effect of which on the anemometer readings could be neglected (11).

All of the electronic instruments were provided with the r.m.s. voltmeters and on comparison with each other some of them showed small differences (see appendix C). All of the r.m.s. readings were recorded from the random noise voltmeter to have minimum possible noise effect and to avoid discrepancies.

## 6. RESULTS AND DISCUSSION

Present experimental work was carried out mainly to study the decay of anisotropic turbulence in steady mean flow. As explained in the previous chapter nearly isotropic turbulence obtained with the same type of grid was also studied mainly for comparison. The decay results will be described under the separate headings of isotropic and anisotropic turbulence after mentioning the computation procedure and the homogeneity of the turbulence.

### 6.1 Computation:

The three fluctuating components of velocity were calculated from the hot wire data using the following equations

$$u'^2 = e_x'^2 / S_n^2$$

$$v'^2 = \frac{1}{C^2} \left\{ \left[ \frac{e_{y_1}'^2 + e_{y_2}'^2}{2S_s^2} \right] - u'^2 \right\}$$

$$w'^2 = \frac{1}{C^2} \left\{ \left[ \frac{e_{z_1}'^2 + e_{z_2}'^2}{2S_s^2} \right] - u'^2 \right\}$$

$$\text{where } S = a Y^{1/2} / 2\bar{E} (\bar{E}^2 - X)^{1-2/a}$$

values of  $a$ ,  $Y$ ,  $X$  and  $\bar{E}$  are taken for normal and for slanting wires respectively to find  $S_n$  and  $S_s$ .

$$\text{and } C = \sin Q \cos Q (1 - k^2) / (\sin^2 Q + k^2 \cos^2 Q)$$

The subscripts  $x$ ,  $y_1$ ,  $y_2$ ,  $z_1$  and  $z_2$  correspond to the diff-

erent positions of the probe which are shown in figure 37. The constants a, X and Y were determined by calibration of the hot wire probes as outlined in appendix B2. The value of the factor k, which represents the direction sensitivity of the wire, is discussed in appendix B5. The procedure for computing energy spectra is given in appendix B6. IBM 1620 II digital computer was used for major arithmetical work.

## 6.2 Homogeneity of Turbulence:

Homogeneity is one of the most important factors which affect the experimental findings in this type of turbulence. As stated by Grant and Nisbet (17), inhomogeneity is believed to be the cause of the discrepancies between various sets of measurement of energy decay in the initial period.

Of necessity decaying grid turbulence is inhomogeneous in the direction of the mean flow. According to Corrsin (11) it may be considered effectively homogeneous if the following conditions are met:

$$dL_x/dx \ll 1 \quad (a)$$

$$(L_x/\lambda)(d\lambda/dx) \ll 1 \quad (b)$$

$$-(L_x/\overline{u^2})(d\overline{u^2}/dx) \ll 1 \quad (c)$$

Approximate values of  $L_x$  could be found from the measured energy spectra as described in a later section in this chapter. To find its derivative  $L_x$  was assumed to vary



linearly with  $\sqrt{x}$  (19). Conditions (a) and (c) were approximately checked in case of the isotropic turbulence and the values of the two quantities were found to be below 0.04. Similar check was not made for anisotropic turbulence but effective homogeneity could be assumed because of the same order of turbulence energy decay as for isotropic turbulence.

To check the homogeneity in planes normal to the direction of flow the turbulence intensities were recorded at different points covering an area of one foot square around the axis of the test section. Figures 19, 20 and 21 show the location of the points and values of the fluctuating quantities in relation to the values at the centre. Table 6.1 gives the extent of homogeneity obtained in the present experiments and a comparison with other results in a nearly isotropic turbulent field. Similar measurements for anisotropic turbulence obtained in the present study are also included at the end of the table. In order to facilitate comparison, the table is based on the mean square values of fluctuating quantities, though the figures 17, 18 and 19 are based on root mean square values. Inhomogeneity in present experiments appears quite large but more clear picture is obtained when consideration is given to the area covered, the value of  $x/M$  and the grid solidity.

### 6.3 Isotropic Turbulence

#### 6.3.1 Decay Rate:

The turbulence level in a homogeneous turbulent field

is considered to be a function of time. The usual procedure for analytical treatment of experimental decay data is to fit power law of the form

$$f'^2/\bar{U}^2 \sim t^{-n}$$

where the time is measured from the virtual origin. According to Taylor's hypothesis (11)  $\frac{\partial}{\partial t}$  may be substituted with  $\bar{U} \frac{\partial}{\partial x}$ . Making use of this, the following relation for the decay of grid turbulence may be written in terms of distance downstream of the grid,

$$\frac{\bar{U}^2}{f'^2} = A \left( \frac{x}{M} - \frac{x_0}{M} \right)^n \quad (6.1)$$

We try to find the best values of A, n, and  $x_0/M$  to fit the experimental data. In the present case different values of n were assumed and values of A and  $x_0/M$  were determined by using the least square regression method. The set of values giving best correlation was selected. For the different components of turbulence the values of  $x_0/M$  were slightly different. In order to avoid complications a common value of  $(x_0/M)=5$  was considered suitable for all sets of data. After fixing the value of  $(x_0/M)=5$ , each set of readings was again analysed to find values of n and A by least square regression method. The data could be presented to fit straight line on logarithmic plot. Figures 1, 2 and 3 show such plots. The results are summarized in table 6.2. These results are quite in agreement with those obtained by several earlier investigators. Some of the previous results, most of which have been sum-

marized by Comte-Bellot and Corrsin (10) are presented in table 6.4.

### 6.3.2 Isotropy:

It is remarkable to note that  $u'/v'$  was found to lie between 1.1 and 0.9. This means that the flow was more near to isotropy than reported in most of the earlier investigations. The reasons of this may be the following

1. The grids used in previous investigations were biplane round rod or square rod periodic grids and not the perforated sheet grid which has been used in the present study.
2. The direction sensitivity of the hot wire probe affects the computation of transverse components of the fluctuating velocity. As pointed out by Champagne (8) there appears considerable disagreement as to the directional sensitivity of a hot wire and, therefore, to the accuracy of measurements made with wire oblique to the flow. This has been discussed in detail in appendix B5. Some of the previous investigators have used X-wire probe for determining transverse components of fluctuating velocity.

It should be pointed out that MacPhail (24) found  $\overline{u^2}/\overline{v^2}$  almost equal to unity for grid turbulence.

Considering the present results to be accurate the use of perforated sheet grid may be encouraged for an experimental study of isotropic turbulence.

### 6.3.3 Energy Spectra:

One dimensional  $u'^2$ ,  $v'^2$  and  $w'^2$  spectra are shown in figures 11 to 14. Measured spectra are compared with the theoretical curves. The following equations for the isotropic turbulence (19, p. 174) were used to draw theoretical curves

$$E_1(k_1, t) = \frac{2}{\pi} u'^2 \frac{L_x}{1+k_1^2 L_x^2} \quad (6.8)$$

$$E_2(k_1, t) = E_3(k_1, t) = \frac{1}{\pi} u'^2 L_x \frac{1+3k_1^2 L_x^2}{(1+k_1^2 L_x^2)^2} \quad (6.9)$$

As in the present case the turbulence was approximately isotropic,  $v'$  and  $w'$  were used in place of  $u'$  in the above equations for  $E_2$  and  $E_3$  respectively. To determine the theoretical curve the integral scale was not measured directly. From the measured values of  $E_1$  at different values of  $k_1$ ,  $L_x$  was calculated at each point using equation (6.8) and then arithmetic average was taken over the whole spectrum. That average value of  $L_x$  was used in equations (6.8) and (6.9) to plot the theoretical curves for longitudinal and lateral components of fluctuating velocity respectively. At the mean velocity of 36 ft/sec and at  $x/M = 262$  the measured spectrum was found to be considerably affected probably by the noise of fan or by unnoticed grounding of the electronic circuit. Therefore measured values of  $E_2$  and  $E_3$  were considered to calculate average  $L_x$  from equation (6.9) by trial and error. It can be seen that good agreement between the measured and the theoretical spectra is obtained except at high value numbers. At higher wave

numbers we see that the measured values lie below the theoretical line. The same tendency was observed in case of the spectra measured by A. Favre (19, p. 61), by Simmons and Salter (13) and by Dryden (13). It is worthwhile to point out that theoretical equations are based on the assumption that the coefficient of longitudinal correlation can be approximated by an exponential function.

#### 6.4 Anisotropic Turbulence

##### 6.4.1 Decay Rate:

An attempt was made to find a suitable power law of the form of equation (6.1) to fit the experimental data in anisotropic turbulence also. High scatter was observed in case of the individual components of the fluctuating velocity but good correlation could be obtained for the total turbulence kinetic energy. The results are summarized in table 6.3 and the plots are shown in figures 6, 7 and 8. It should be noticed that the exponent  $n$  for the  $q^2$  decay is nearly the same as for isotropic turbulence.

##### 6.4.2 Isotropy:

Though the correlation coefficients for the decay data were quite low for the three individual components of fluctuating velocity, it can be concluded from the best fitting curves, shown in figures 6 & 7, that a clear tendency of anisotropic turbulence towards isotropy is present. The same tendency can be seen in the plots of

the ratios  $(u'/v')$  and  $(u'/w')$  against  $x/M$ , in figure 10. This conclusion is supported by the results of Uberoi (33) and of Tucker and Reynolds (31). But the observations of Townsend (28) and those of Grant are on the contrary.

It can be seen that the ratios  $u'/v'$  and  $u'/w'$ , after being equal to unity after initial period of decay start increasing further downstream. This is in accordance with the findings of Batchelor and Stewart (5). They gave the view that close behind the grid, the system of rods parallel to  $y$  axis produces large contributions to  $\overline{u^2}$  and  $\overline{w^2}$  while the system parallel to the  $z$  axis produces large contributions to  $\overline{u^2}$  and  $\overline{v^2}$ , the net result being that the contribution to  $\overline{u^2}$  from the largest eddies is permanently greater than the contributions to  $\overline{v^2}$  and  $\overline{w^2}$ . These large eddies, according to Batchelor (3), which contain the negligible portion of the total energy in the beginning, are permanent and become dominate in the final period when the smaller eddies have decayed.

#### 6.4.3 Energy Spectra:

Measured one dimensional energy spectra for  $u'$ ,  $v'$  and  $w'$  are shown in figures 15 to 18. When  $u'$  spectra are compared with  $v'$  and  $w'$  spectra they show different trend in the energy containing range. Any significant change in the shape of the spectra is not observed with the downstream distance or with different mean velocities of flow. For the measured spectra the tendency towards different power

laws (19, p.260) in different ranges of wave number can be seen by matching the measured values with the straight lines drawn with the slopes  $-1$ ,  $-5/3$  and  $-7$  according to the power laws. Uberoi (32) measured precontraction and post contraction  $u'$  and  $v'$  energy spectra to study the effect of contraction on grid turbulence. When the present results are compared with Uberoi's post contraction results the same tendency can be seen for  $v'$  and  $w'$  spectra but  $u'$  spectra from the two results seem to have different trends. The reason may be slightly different wave number range studied in the two investigations.

Table 6.1 Homogeneity of Turbulence in Planes Parallel to the Grid

Reference	Grid type & solidity	Re <sub>M</sub>	Area or length covered normal to flow direction	x/M	quantity	Extreme variation (% of the centre line value)
<u>Nearly Isotropic Turbulence</u>						
Present Study						
Fig. 17	Perforated Steel sheet (0.47)	8,900	12 in. sq. area	52	$u^2, v^2, w^2$	22
Fig. 18	"	11,400	"	262	$u^2, v^2$	38
Uberoi & Wallis (36)	Rd. steel rod		18 in. length	95	"	10
"	Rd. wooden rod		"	95	"	23
Grant & Nisbet (17)	Rd. brass rod (0.34)		6 in. sq. area	80	"	30
"	"		6 in. length	30	$u^2$	6
Shafer & Goldrick (11)	Sq. rod (0.34)	16,000	6 in. length	40	$u^2$	14
<u>Anisotropic Turbulence</u>						
Present Study						
Fig. 19	Perforated steel sheet (0.47)	22,000	12 in. sq. area	157	$u^2, v^2, w^2$	65



Table 6.2 Decay Characteristics of Nearly Isotropic

Turbulence (ref. equ. 6.1)

$\bar{U}$ (ft/sec)	$Re_M(x10^{-3})$	quantity	n	$x_0/M$	A	Corr. coeff.	No. of exptl. pts.
35.7	12	$u'^2$	1.178	5	13.92	0.998	24
27.0	9	$u'^2$	1.230	5	12.11	0.999	28
35.7	12	$v'^2$	1.163	5	15.34	0.998	24
27.0	9	$v'^2$	1.195	5	13.59	0.998	28
35.7	12	$q^2$	1.168	5	14.84	0.999	24
27.0	9	$q^2$	1.207	5	13.07	0.999	28

Table 6.3 Decay Characteristics of Anisotropic

Turbulence (ref. equ. 6.1)

$\bar{U}$ (ft/sec)	$Re_M(x10^{-3})$	quantity	n	$x_0/M$	A	Corr. coeff.	No. of exptl. pts.
53.3	18	$u'^2$	0.485	5	$6.3 \times 10^3$	0.800	15
39.2	13	$u'^2$	0.192	5	$2.95 \times 10^4$	0.743	10
53.3	18	$v'^2$	1.52	5	16.8	0.926	15
39.2	13	$v'^2$	1.78	5	5.34	0.945	10
53.3	18	$w'^2$	1.73	5	6.8	0.950	15
39.2	13	$w'^2$	2.02	5	1.70	0.973	10
53.3	18	$q^2$	1.31	5	60.0	0.969	15
39.2	13	$q^2$	1.31	5	69.5	0.987	10

Table 6.4 Comparison of Turbulence Decay Characteristics  
for different Grids (ref. equ. 6.1)

Reference	$Re_M$ ( $\times 10^{-3}$ )	Biplane grids solidity	Rods	u' decay			v' decay		
				n	$\frac{x_0}{M}$	$\Lambda$	n	$\frac{x_0}{M}$	$\Lambda$
Corrsin (1942)	8.5	0.44	Rd.	1.30	1	20	1.22	1.5	59
	17	0.44	Rd.	1.28	3	23	1.14	2.5	62
	26	0.44	Rd.	1.35	1	17	1.16	1	58
Batchelor & Townsend (1947, 1948)	5.5	0.34	Rd.	1.13	5	70			
	11	0.34	Rd.	1.25	8	48			
Baines & Peterson (1951)	24	0.44	Sq.	1.37	3	8.5			
Tsuji & Hama. (1953)	33	0.36	Rd.	1.35	0	10			
Wyatt (1955)	11	0.34	Rd.	1.27	5	31	1.27	5	40
	22	0.34	Rd.	1.27	3.5	35	1.27	3.5	45
	44	0.34	Rd.	1.25	4	35	1.25	4	45
Kistler & Vrebalovich (1961)	2420 (p=4atm)	0.34	Rd.	1.0	9	71	1.0	7	110
Uberoi (1963)	29	0.44	Rd.	1.20	4	24	1.20	4	35
Corrsin (1966)	17	0.34	Sq.	1.33	1.5	13	1.27	1.5	20
	34	0.34	Sq.	1.26	3	17	1.20	3	25
	135	0.34	Sq.	1.18	3.5	22	1.16	3	27
	68	0.44	Rd.	1.27	2	27	1.26	2	33
Uberoi & Wallis (36)		0.23	Rd.	1.39			1.39		
		0.34	Rd.	1.22			1.22		
			(wooden grid roughened with sand grains)						

## 7. CONCLUSIONS

The conclusions which are of specific interest in the present study of anisotropic homogeneous turbulence under steady mean flow are:

1. Anisotropic turbulence shows a strong tendency towards isotropy in the initial period of decay.
2. The rate of decay of the total turbulent energy follows nearly the same power law as isotropic turbulent flow.
3. One dimensional energy spectra of longitudinal and lateral components of turbulence show considerably different trends in the energy containing range. No appreciable change with distance downstream of the grid could be noticed in the energy spectra.

On comparison with other investigators, the characteristics (transverse homogeneity, isotropy and the decay rates) of the turbulence obtained in a parallel section behind a perforated sheet grid were found comparable with those obtained by commonly used biplane grids. For the nearly isotropic grid turbulence the decay rate for the three individual components of turbulence and for the total turbulent energy was found to satisfy the commonly accepted equation.

$$\bar{U}^2 / f^2 = A \left( \frac{x}{M} - \frac{x_0}{M} \right)^n$$

with n between 1.16 and 1.23 when  $(x_0/M)=5$

It has to be pointed out that the free stream turbulence (0.2 to 0.65%) in the present wind tunnel had a pronounced effect on the results for anisotropic turbulence even though a correction was applied. This was because of low grid turbulence intensity existing after the contraction.

## BIBLIOGRAPHY

- 1 Baines, W.D. and Peterson, E.G. 1951  
An investigation of flow through screens.  
Transactions of American Society of Mechanical Engineers, vol. 73, pp. 467-480.
- 2 Batchelor, G.K. 1948  
Energy decay and self preserving correlation functions in isotropic turbulence.  
Quarterly of Applied Mathematics, vol. 6, pp. 97-116.
- 3 Batchelor, G.K. 1949  
The role of big eddies in homogeneous turbulence.  
Proceedings, Royal Society, London, A, vol. 195, pp. 513-532.
- 4 Batchelor, G.K. 1953  
The Theory of Homogeneous Turbulence.  
Cambridge University Press
- 5 Batchelor, G.K. and Stewart, R.W. 1950  
Anisotropy of the spectrum of turbulence at small wave numbers.  
Quarterly Journal of Mechanics and Applied Mathematics, vol. 3, pp. 1-8.
- 6 Batchelor, G.K. and Townsend, A.A. 1947  
Decay of vorticity in isotropic turbulence.  
Proceedings, Royal Society, London, A, vol. 190, pp. 534-550.
- 7 Batchelor, G.K. and Townsend, A.A. 1948  
Decay of isotropic turbulence in the initial period.  
Proceedings, Royal Society, London, A, vol. 193, pp. 539-558.

- 8 Champagne, F.H. 1965  
Turbulence measurements with inclined hot wires.  
Boeing Scientific Research Laboratories  
Document D1-82-0491.
- 9 Collis, D.C. and Williams, M.J. 1959  
Two dimensional convection from heated wires at low Reynolds numbers.  
Journal of Fluid Mechanics, vol. 6,  
pp. 357-384.
- 10 Comte-Bellot, G. and Corrsin, S. 1966  
The use of a contraction to improve the isotropy of grid generated turbulence.  
Journal of Fluid Mechanics, vol. 25,  
pp. 657-682.
- 11 Corrsin, S. 1963  
Turbulence: experimental methods  
Handbuch der Physik, Springer Verlag, Berlin,  
vol. VIII/2, pp. 524-590.
- 12 Deissler, R.G. 1960  
A theory of decaying homogeneous turbulence.  
Physics of Fluids, vol. 3, pp. 176-187.
- 13 Dryden, H.L. 1943  
A review of the statistical theory of turbulence.  
Quarterly of Applied Mathematics, vol. 1,  
pp. 7-42.
- 14 Frenkiel, F.N. 1948  
The decay of isotropic turbulence.  
ASME Transactions (Journal of Applied Mechanics) vol. 70, pp. 311-321.
- 15 Goldstein, S. 1951  
On the law of decay of homogeneous isotropic turbulence and the theories of the equilibrium and similarity spectra.  
Proceedings, Cambridge Philosophical Society,  
vol. 47, pp. 544-574.

- 16 Grant, H.L. 1958  
The large eddies of turbulent motion.  
Journal of Fluid Mechanics, vol. 4,  
pp. 149-190.
- 17 Grant, H.L. and Nisbet, I.C.T. 1957  
The inhomogeneity of grid turbulence.  
Journal of Fluid Mechanics, vol. 2,  
pp. 263-272.
- 18 Grant, H.P. and Kronauer, R.E. 1962  
Fundamentals of hot wire anemometry.  
ASME Symposium on measurements in un-  
steady flow, Worcester, Mass. May 21-  
23, 1962, pp. 44-53.
- 19 Hinze, J.O. 1959  
Turbulence: An Introduction to its Mech-  
anism and Theory.  
McGraw Hill Book Company, Inc.
- 20 Laufer, J. 1954  
The structure of turbulence in fully develop-  
ed pipe flow.  
National Advisory Committee for Aeronautics  
report 1174:
- 21 Lin, C.C. 1948  
Note on the law of decay of isotropic tur-  
bulence.  
Proceedings, National Academy of Sciences,  
vol. 34, pp. 540-543.
- 22 Lin, C.C. and Reid, W.H. 1963  
Turbulent flow, theoretical aspects.  
Handbuch der Physik, Springer Verlag, Berlin,  
vol. VIII/2, pp. 524-590.
- 23 MacPhail, D.C. 1940  
Turbulence changes in contracting and dis-  
torted passages.  
Royal Aircraft Establishment, Farnborough.  
Report No. Aero 1928, March 1944.

- 25 Schredl, W.H. 1968  
 Calibration of hot wire probes in known  
 turbulent shear flow.  
 B.A. Sc. paper, Deptt. of Mech. Engg.,  
 University of Windsor (unpublished).
- 26 Townsend, A.A. 1951  
 The passage of turbulence through wire  
 gauzes.  
 Quarterly Journal of Mechanics and Applied  
 Mathematics, vol. 4, pp. 308-320.
- 27 Townsend, A.A. 1954  
 The uniform distortion of homogeneous  
 turbulence.  
 Quarterly Journal of Mechanics and Applied  
 Mathematics, vol. 7, pp. 104-127.
- 28 Townsend, A.A. 1956  
 The Structure of Turbulent Shear Flow.  
 Cambridge University Press.
- 29 Tsuji, H. 1959  
 A contribution to the energy decay law of  
 isotropic turbulence in the initial period.  
 Aeronautical Research Institute, University  
 of Tokyo, Report No. 345, May 1959.
- 30 Tsuji, H. and Hama, R.F. 1953  
 Experiment on the decay of turbulence  
 behind two grids (Abstract)  
 Journal of the Aeronautical Sciences,  
 vol. 20, pp. 848-849.
- 31 Tucker, H.J. and Reynolds, A.J. 1968  
 The distortion of turbulence by irrotational  
 plain strain.  
 Journal of Fluid Mechanics, vol. 32, pp. 657-673.
- 32 Uberoi, M.S. 1956  
 Effect of wind tunnel contraction on free  
 stream turbulence.  
 Journal of the Aeronautical Sciences, vol.  
 23, pp. 754-764.



- 33 Uberoi, M.S. 1957  
Equipartition of energy and local isotropy  
in turbulent flows.  
Journal of Applied Physics, vol. 28, pp.  
1165-1170.
- 34 Uberoi, M.S. 1963  
Energy transfer in isotropic turbulence.  
The Physics of Fluids, vol. 6, pp. 1048-  
1056.
- 35 Uberoi, M.S. and Wallis, S. 1966  
Small axisymmetric contraction of grid tur-  
bulence.  
Journal of Fluid Mechanics, vol. 24, pp.  
539-543.
- 36 Uberoi, M.S. and Wallis, S. 1967  
Effect of grid geometry on turbulence decay.  
The Physics of Fluids, vol. 10, pp. 1216-  
1224.
- 37 Webb, W.H. 1962  
An experimental study of the decay of tur-  
bulent energy in several gases and at High  
and low density.  
Ph.D. thesis, Princeton University.

## APPENDICES.

	Page
A. WIND TUNNEL AND FREE STREAM TURBULENCE	48
A1. Description of the Tunnel	
A2. Mean Velocity Variation in the Test Section	50
A3. Turbulence Level	50
A4. Energy Spectra	51
A5. Homogeneity of Turbulence	52
B. HOT WIRE ANEMOMETER	53
B1. Heat Transfer Relations	53
B2. Calibration	56
B3. Equation to Compute Turbulence Quantities	61
B4. Hot Wire Anemometer with Linearizer	70
B5. Direction Sensitivity of the Slanting Hot Wire	72
B6. Measurement and Computation of One dimensional Energy Spectra	77
C. CALIBRATION	
C1. Micromanometer	79
C2. D.C. Voltmeters on Anemometers	81
C3. RMS Voltmeters	84
D. ENERGY EQUATION	87
E. SUMMARY OF ERRORS	90

## APPENDIX A

### WIND TUNNEL AND FREE STREAM TURBULENCE

#### A1. Description of the Tunnel

A closed circuit low speed wind tunnel of Mechanical Engineering Department of the University of Windsor was used for the experiments. It was designed and constructed by the Department of Civil Engineering of Colorado State University. A general view of the tunnel is given in figure 22; some of the important features are presented here.

Test section dimensions:

cross-section 30" (horizontal), 30"-31 3/4" (vertical)

length 20'

The divergence of the vertical dimension of the test section was provided to avoid axial gradient in mean speed.

Contraction upstream of test section:

length	75"
upstream dimensions	72" square
downstream dimensions	30" square
contraction ratio	5.76

Screens upstream of the contraction:

size	80" x 80"
------	-----------

square mesh	24 x 24
wire diameter	0.0075"
wire material	stainless steel
number of screens	four
spacings between screens	8"

Electric motor:

3 phase, 60 cycles, 20 h.p.  
550 volts, 19 amperes, 1760 r.p.m.

Belt driven axial flow fan:

Maximum allowable speed: 1200 r.p.m.

Maximum velocity of flow without inserting any extra screen:

80 ft/sec.

Maximum velocity of flow was reduced to about 40 ft/sec when the grid, to obtain nearly isotropic turbulence, was inserted at the entrance of the working section. The velocity was not much affected by inserting the grid upstream of the contraction to obtain strongly anisotropic turbulence; a maximum velocity of about 70 ft/sec could then be obtained.

The test section was provided with eight glass windows at each of the side walls. As the platform for the measuring instruments and for working was located on one side only, the windows on the other side were sealed to minimise infiltration of air. In studying anisotropic turbulence the intensities were low and to avoid additional turbulence due to infiltration effects the windows up-

stream of the point at which the measurement were being taken including those on the working side were properly sealed.

Various measurements of the mean velocity and the turbulence in the empty tunnel (without inserting the turbulence producing grid) will be described in the following paragraphs.

#### A2? Mean Velocity Variation in the Test Section:

Measurements of the mean velocity of flow were carried out using a pitot static probe with the Wilhelm Lambrecht slanting tube micromanometer. The mean velocity at a fixed fan speed was measured at various points along the centre line of the test section. The measurements are presented in figure 23.

#### A3? Turbulence Level:

The wind tunnel was used for the fundamental study of grid generated turbulence which is necessarily of low relative intensity. In such studies, one of the main requirements of a wind tunnel is that it should produce an air stream with turbulence negligible in comparison with the turbulence being examined. Corrsin (11) mentions that, in the study of grid turbulence, each of the three components of the root-mean square upstream turbulence velocity (plus sound) should be well under  $0.001 \bar{U}$ .

Figures 24 and 25 give the measurement of longitud-

enal and transverse component of turbulence along the test section axis at different mean velocities. The values indicated in these figures include the fan noise and the anemometer noise. Filters to eliminate frequencies above 10 kc/sec were used because, on measuring the energy spectra, these waves were found to be mainly due to noise. The same filters were used during the measurement of turbulence decay. Figures 26 and 27 indicate the free stream turbulence at different velocities in different frequency ranges. The values in these figures do not include the anemometer noise. This data was specially obtained to understand the effect of free stream turbulence on the energy spectrum measurements after inserting the grid. From figures 24 to 27 we infer that, using the 10 kc/sec filters, the maximum value of  $\frac{u'}{U}$  is 0.003 and the maximum value of  $\frac{v'}{U}$  is 0.0065. These values are high and therefore the decay measurements after inserting the grid had to be corrected for free stream turbulence as mentioned in Chapter 5.

#### A44: Energy Spectra:

Figures 28 to 33 indicate the measurement of the one dimensional energy spectra of the longitudinal and transverse components of turbulence with different mean velocities at two different points on the test section axis. It may be pointed out here that the areas under the different spectrum curves are not same because the points on the graphs do not cover the range of wave numbers which was used for measuring

the values of  $u'$ ,  $v'$  or  $w'$ . The oscillating nature of the spectrum curves after a value of  $k \approx 10$  to 12 in. indicates that the noise is predominant at higher wave numbers. The effect of noise seems to be more pronounced in  $u'$  spectra than in  $v'$  or  $w'$ . In both the longitudinal and transverse component spectra no definite change with the mean velocity of flow is observed except that the noise effect is comparatively less at higher velocities. When the spectra of longitudinal component are compared with those of transverse components, significant difference can be seen in the energy containing range.

#### A5: Homogeneity of Turbulence:

In the study of the grid turbulence homogeneity of the turbulence was checked in planes normal to the direction of flow. The same type of measurements were carried out with the free stream turbulence as well. The turbulence intensities were recorded at different points covering an area of one foot square around the axis. Figure 34 shows the location of the points and values of the fluctuating quantities in relation to the values at the centre. Figure shows that the variation in the fluctuating components is as high as  $\pm 40\%$  of the respective values at the test section axis.

## APPENDIX B

### HOT WIRE ANEMOMETER

#### B1. Heat Transfer relations:

The development of the hot wire anemometer is one of the major factors in the advancement of understanding of the behaviour of the turbulent flow. An electrically heated wire is introduced into the flow to be studied. The flowing fluid causes the temperature of the wire to drop and consequently the electric resistance of the wire diminishes. The circuit used to take care of this variation measures voltage or current which is related to the flow velocity.

The following sections deal with the various relations which are used to measure mean velocity of the flow and the three fluctuating components of turbulence.

For the hot wire placed normal to the direction of the flow the form of the heat loss relation has conventionally been assumed to be that of the empirical King's law (19, p. 79) which can be written as

$$\text{Nu} = A + B \text{Re}^{0.50} \quad (\text{B1})$$

where A and B are considered as constants. While the values of A and B reported by various authors are diverse,



they generally agree on the value of Reynolds number exponent as 0.50. The empirical relation given by Kramers (19, p.76) also agrees with King's equation when the values of A and B are taken as

$$A = 0.42 (\text{Pr})^{0.2}$$

$$B = 0.57 (\text{Pr})^{0.35}$$

For air and diatomic gases it has been assumed to be valid in the range  $0.01 < \text{Re} < 10,000$ .

A notable exception is the series of tests reported by Collis and Williams (9). They carried out the measurements in the range  $0.01 < \text{Re} < 140$ . They suggested the relation

$$\text{Nu} = A + B \text{Re}^a$$

which is the same as equation (B1) when  $a = 0.5$ . But the values of  $a$  found by Collis and Williams are different.

According to them

$$a = 0.45 \quad \text{when} \quad 0.02 < \text{Re} < 44$$

$$a = 0.51 \quad \text{when} \quad 44 < \text{Re} < 140$$

More recently Webb (37) has found different values of  $a$  to fit his experimental data in air and argon at various ambient pressures. For air at atmospheric temperature and pressure in the Reynolds number range of 0.4 to 4 he found

$$\text{Nu} = 0.3 + 0.44 \text{Re}^{0.52}$$

and under the same conditions for argon he found

$$\text{Nu} = 0.23 + 0.50 \text{Re}^{0.45}$$

As explained by Grant and Kronauer (18) the discrepancies in the values of Reynolds number exponent may be due to different values of length to diameter ratio of the wires used by different investigators.

In the hot wire anemometry, as pointed out earlier, proper electronic circuits are used to enable measurement of heat transfer rate in terms of electric current or voltage. Hinze (19, p.76) has derived the following relation from Kramer's equation

$$\frac{I^2 R_w}{R_w - R_g} = A + B U^{0.50} \quad (B3)$$

For the present investigation, constant temperature (which means  $R_w = \text{constant}$ ) hot wire anemometer has been used in a flow at nearly room temperature.  $R_g$  could be assumed constant because of very small variation of temperature of the air during a run as mentioned in Chapter 4. Moreover equation B3 can be written with voltage and velocity as the variables since the anemometer, which is used for present work, measures voltage and not current corresponding to the heat transfer rate. In view of the divergence of opinion over the proper value of the exponent of velocity, a more general equation has to be considered.

Therefore instead of equation (B3) we can write

$$E^2 = X + Y U^a \quad (B4)$$

In the above equation  $X$ ,  $Y$  and  $a$  are to be determined by calibration.

If the wire is inclined to the direction of velocity by an angle  $Q$  then, in the above equation,  $U$  can be replaced by the effective velocity (19, p.103) which is defined as

$$U_{\text{eff}} = U^2 (\sin^2 Q + k^2 \cos^2 Q) \quad (\text{B2})$$

where  $k$  is a factor depending on direction sensitivity of the wire. In other words for inclined wire we can write the equation as

$$E^2 = X_1 + Y_1 (U_{\text{eff}})^a \quad (\text{B5})$$

$$\text{or } E^2 = X + Y U^a$$

where  $Y = Y_1 (\sin^2 Q + k \cos^2 Q)^{1/2}$  and  $X = X_1$

Calibration of the hot wire anemometer with different probes to determine the voltage-velocity curves and the discussion and experimentation for the value of  $k$  will be reported in different sections.

## B2. Calibration of the Hot Wire Anemometer:

DISA constant temperature hot wire anemometer 55 A 01 was used in the present study. The DC voltmeter incorporated in the anemometer had an accuracy of  $\pm 1\%$ . For the calibration purposes a pitot static probe with Wilhelm Lambrecht micromanometer was used as reference. The DC voltmeters and RMS voltmeters on both of the anemometers in use were precalibrated against other instruments as reported in Appendix C.

The hot wire probe was exposed to the flow in the same wind tunnel which was used for the main experimental work. It was mounted such that the probe axis was parallel to the direction of mean flow as shown in figure 36. A pitot static probe was stationed close ( $3/4''$ ) to the hot wire. Flow velocity was varied with the fan regulator and the anemometer DC voltages and the corresponding manometer readings were recorded simultaneously at various velocities. Mean velocities were calculated from the manometer readings.

In equation (B4) various values of 'a' were assumed in the range 0.20 to 0.60 with an interval of 0.01. For each value of a, X and Y were determined to fit the experimental data. Least square regression method was used for curve fitting. The set of values of a, X and Y giving highest correlation coefficient (or least RMS error) was selected to represent the best fitting curve to the experimental data. This analysis was carried out for the experimental points in the range of interest only that is nearly 15 ft/sec to about 60 ft/sec. To be more clear the voltmeter reading with the wire unexposed to flow, referred to as  $E_0$ , was not included for determining the best fitting curve. A value of  $a = 0.35$  (or slightly different) was found to give the best correlation with each hot wire probe. But this value was very low when compared to the values recommended by previous investig-

ators. But the same value was found to be the most appropriate even on repeating the experiments with some of the probes. Such a clear contradiction with previous investigators compelled the present author to try the above method of curve fitting after including  $E_0$  as one of the experimental points. And it was found that the best fitting curve was obtained with  $a = 0.50$  (or slightly different) which was in accordance with the conventional King's law. Though the correlation coefficient in this case was not as high as obtained on excluding  $E_0$ , but it was high enough from the statistical point of view. On the other hand very small but a systematic deviation of experimental data from the best fitting straight line could be appreciated. Same type of deviation was observed in a typical calibration curve supplied by DISA, the manufacturers. Therefore  $a = 0.35$  and hence the use of the curve fitting in the range of interest was considered to be more suitable for computing turbulence quantities. The calibration curves can be seen in figures 38 and 39. The detail of the probes and the calibration constants is as under.

	Right Angle Probe		Slanting Probe		X-Probe
	No. 1	No. 2	No. 1	No. 2	(two wires)
Type specified by DISA	55A25	55A25	55A29	55A29	55A32
Material	Platinum plated tungsten for all				
Wire diameter (micron)	5	5	5	5	5,5
Wire length (mm)	1	1	1	1	1,1
Cold resistance at the temperature indicated (ohm)	3.49 (82°F)	3.30 (77°F)	3.53 (84°F)	3.31 (78°F)	3.36, 3.47 (85°F)
Operating resistance (ohm)	6.40	6.40	6.40	6.40	6.40, 6.40
Velocity range for calibration (ft/sec)	7-50	11-60	7-50	11-60	
Barometric pressure (in. mercury)	29.53	29.67	29.57	29.42	
Calibration constants (excluding E <sub>0</sub> )					
a	0.35	0.35	0.35	0.35	
X	21.5569	21.9211	20.0074	21.2872	
Y	13.9339	13.0812	11.4625	11.5825	
Calibration constants (including E <sub>0</sub> )					
a	0.50	0.50	0.50	0.50	
X	33.9571	33.4865	30.1121	32.4955	
Y	6.0528	5.6635	4.9982	4.8584	

The following table will give an idea about the sensitivity of equation (B4) towards the value of  $a$ .

Analysis of experimental data disregarding the value of  $E_0$

	$a$	X	Y	RMS error (inE)	Corr. coeff.	No. of exptl. points
Right Angle Probe						
No. 1	0.36	22.6767	13.1338	0.0813	0.99995	14
	0.35	21.5569	13.9339	0.0750	0.99996	
	0.34	20.3715	14.7943	0.0753	0.99995	
No. 2	0.36	23.1004	12.2915	0.1050	0.99990	14
	0.35	21.9211	13.0812	0.1036	0.99990	
	0.34	20.6722	13.9326	0.1050	0.99989	
Slanting Probe						
No. 1	0.36	20.9286	10.8043	0.1210	0.99983	16
	0.35	20.0074	11.4625	0.1129	0.99985	
	0.32	16.8989	13.7545	0.1031	0.99988	
	0.31	15.7292	14.6427	0.1054	0.99987	
No. 2	0.36	22.3255	10.8847	0.1065	0.99987	13
	0.35	21.2872	11.5825	0.1047	0.99987	
	0.34	20.1877	12.3349	0.1050	0.99987	

Analysis of experimental data including the value of  $E_0$

Right Angle Probe						
No. 1	0.51	34.2220	5.8008	0.3628	0.99945	15
	0.50	33.9571	6.0528	0.3560	0.99947	
	0.49	33.6911	6.3152	0.3785	0.99941	
No. 2	0.51	33.7370	5.4182	0.5003	0.99899	15
	0.50	33.4865	5.6635	0.4121	0.99931	
	0.47	32.7374	6.4644	0.2203	0.99981	
	0.46	32.4895	6.7544	0.2282	0.99979	
Slanting Probe						
No. 1	0.51	30.3348	4.7888	0.3262	0.99931	17
	0.50	30.1121	4.9982	0.3131	0.99937	
	0.49	29.8882	5.2166	0.3203	0.99934	
No. 2	0.51	32.6937	4.6499	0.2697	0.99963	14
	0.50	32.6955	4.8584	0.2421	0.99970	
	0.49	32.2976	5.0758	0.2443	0.99969	

### B3. Equations to Compute Turbulence Quantities

The equations obtained for turbulence quantities are based on the assumption that fluctuating components of velocity are very small compared to the mean velocity, i.e.

$$\frac{u'}{\bar{U}} \ll 1, \quad \frac{v'}{\bar{U}} \ll 1, \quad \frac{w'}{\bar{U}} \ll 1 \quad \text{and therefore} \quad \frac{e'}{\bar{E}} \ll 1.$$

Figure 37 shows a calibration curve and various positions of the hot wire probe with respect to the flow.

Let us start from equation (B4) which reads

$$E^2 = X + Y U^a \quad (\text{B4})$$

where  $U = \bar{U} + u$

and  $E = \bar{E} + e$

We can use mean quantities in place of total quantities (19, p.81) in equation (B4), hence we can write

$$\bar{E}^2 = X + Y \bar{U}^a \quad (\text{B5})$$

Substituting the values of U and E in equation (B4), we get, for a probe at right angles to the direction of flow

$$(\bar{E} + e)^2 = X + Y (\bar{U} + u)^a$$

$$\text{or} \quad \bar{E} + 2e\bar{E} + e^2 = X + Y \bar{U} \left( 1 + a\frac{u}{\bar{U}} + \frac{a(a-1)}{2!} \left(\frac{u}{\bar{U}}\right)^2 + \dots \right)$$

$$\text{or} \quad 1 + \frac{2e}{\bar{E}} = \frac{1}{\bar{E}^2} \left[ X + Y \bar{U}^a \left( 1 + a\frac{u}{\bar{U}} + \frac{a(a-1)}{2} \left(\frac{u}{\bar{U}}\right)^2 + \dots \right) - \left(\frac{e}{\bar{E}}\right)^2 \right]$$

as  $\frac{u}{\bar{U}} \ll 1$  and  $\frac{e}{\bar{E}} \ll 1$ , the quantities  $\left(\frac{e}{\bar{E}}\right)^2$  and  $\left(\frac{u}{\bar{U}}\right)^2$

and higher order terms can be neglected.



$$\therefore 1 + 2 \frac{e}{\bar{E}} = \frac{1}{\bar{E}^2} \left[ X + Y \bar{U}^a + Y a \frac{u}{\bar{U}} \bar{U}^a \right]$$

Substituting the value of  $\bar{E}^2$  from equation (B6), we get

$$1 + 2 \frac{e}{\bar{E}} = 1 + \frac{1}{\bar{E}^2} Y a \frac{u}{\bar{U}} \bar{U}^a$$

$$\text{or } e = \frac{Y a \bar{U}^a}{2 \bar{E}} \frac{u}{\bar{U}}$$

$$\text{or } e = S u$$

where  $S = \text{sensitivity}$

$$= \frac{Y a \bar{U}^{(a-1)}}{2 \bar{E}}$$

Again making use of equation (B4a), we get

$$\bar{U}^{(a-1)} = \left( \frac{\bar{E}^2 - X}{Y} \right)^{(a-1)/a}$$

$$\bar{S} = \frac{(a/2) Y}{\bar{E} (\bar{E} - X)^{1/a}} (1-a)/a \quad (B27)$$

where  $a$ ,  $X$ ,  $Y$  are determined from the calibration curve and  $\bar{E} = \text{dc voltage reading from the anemometer}$

$$\therefore e = S u$$

$$\text{or } e^2 = S^2 u^2$$

$$\text{or } \overline{e^2} = S^2 \overline{u^2} \quad (B7)$$

where  $\overline{e^2} = e'^2$  and

$e' = \text{RMS voltmeter reading with the right}$

angle probe.

Now take the case of the slanting probe (refer to figure 37 for the explanation of various quantities in use).

Rewrite equations (B4) and (B6)

$$E^2 = X + Y U^a \quad (B4)$$

$$\bar{E}^2 = X + Y \bar{U}^a \quad (B6)$$

Using effective velocity for the slanting probe in the above equations, we get

$$E^2 = X_1 + Y_1 (U_{\text{eff}})^a \quad (B8)$$

$$\bar{E}^2 = X_1 + Y_1 (\bar{U}_{\text{eff}})^a \quad (B9)$$

where

$$\begin{aligned} U_{\text{eff}}^2 &= U^2 \sin^2 Q + k^2 U^2 \cos^2 Q \\ &= U_n^2 + k^2 U_t^2 \end{aligned}$$

and therefore

$$Y_1 = \text{slope} = Y_1 (\sin^2 Q + k^2 \cos^2 Q)^{a/2} \quad (B10)$$

Now  $U_t = (\bar{U} + u) \cos Q - v \sin Q$

$$U_n = (\bar{U} + u) \sin Q + v \cos Q$$

$$\begin{aligned} U_{\text{eff}}^2 &= [(\bar{U}+u) \sin Q + v \cos Q]^2 + k^2 [(\bar{U}+u) \cos Q - v \sin Q]^2 \\ &= (\bar{U}+u)^2 \sin^2 Q + v^2 \cos^2 Q + 2v(\bar{U}+u) \sin Q \cos Q \\ &= +k^2 (\bar{U}+u)^2 \cos^2 Q + k^2 v^2 \sin^2 Q - k^2 2v(\bar{U}+u) \sin Q \cos Q \\ &= (\bar{U}+u)^2 (\sin^2 Q + k^2 \cos^2 Q) + v^2 (\cos^2 Q + k^2 \sin^2 Q) \\ &\quad + 2v(\bar{U}+u) \sin Q \cos Q (1-k^2) \end{aligned}$$

or

$$\begin{aligned} U_{\text{eff}}^2 &= \bar{U}^2 (\sin^2 Q + k^2 \cos^2 Q) + 2u\bar{U} (\sin^2 Q + k^2 \cos^2 Q) \\ &\quad + 2v\bar{U} \sin Q \cos Q (1-k^2) + u^2 (\sin^2 Q + k^2 \cos^2 Q) \\ &\quad + v^2 (\cos^2 Q + k^2 \sin^2 Q) + 2uv \sin Q \cos Q (1-k^2) \\ &= \bar{U}^2 (\sin^2 Q + k^2 \cos^2 Q) \left[ 1 + \frac{2u}{\bar{U}} + \frac{2v}{\bar{U}} \frac{\sin Q \cos Q (1-k^2)}{\sin^2 Q + k^2 \cos^2 Q} \right. \\ &\quad \left. + \left( \frac{u}{\bar{U}} \right)^2 + \left( \frac{v}{\bar{U}} \right)^2 \frac{\cos^2 Q + k^2 \sin^2 Q}{\sin^2 Q + k^2 \cos^2 Q} + \frac{2uv}{\bar{U}^2} \frac{\sin Q \cos Q (1-k^2)}{\sin^2 Q + k^2 \cos^2 Q} \right] \end{aligned}$$

$$\begin{aligned}
U_{\text{eff}}^a &= (\bar{U} \sqrt{\sin^2 Q + k^2 \cos^2 Q})^a \left[ 1 + 2 \frac{u}{\bar{U}} + \frac{2v}{\bar{U}} \frac{\sin Q \cos Q (1-k^2)}{\sin^2 Q + k^2 \cos^2 Q} \right. \\
&+ \frac{u^2}{\bar{U}^2} + \left( \frac{v}{\bar{U}} \right)^2 \frac{\cos^2 Q + k^2 \sin^2 Q}{\sin^2 Q + k^2 \cos^2 Q} + \frac{2uv}{\bar{U}^2} \frac{\sin Q \cos Q (1-k^2)}{\sin^2 Q + k^2 \cos^2 Q} \quad (B11) \\
&= (\bar{U} \sqrt{\sin^2 Q + k^2 \cos^2 Q})^a \left[ 1 + \frac{a}{2} \left\{ \frac{2u}{\bar{U}} + \frac{2v}{\bar{U}} \frac{\sin Q \cos Q (1-k^2)}{\sin^2 Q + k^2 \cos^2 Q} \right. \right. \\
&+ \left. \left. \left( \frac{u}{\bar{U}} \right)^2 + \left( \frac{v}{\bar{U}} \right)^2 \frac{\cos^2 Q + k^2 \sin^2 Q}{\sin^2 Q + k^2 \cos^2 Q} + \frac{2uv}{\bar{U}^2} \frac{\sin Q \cos Q (1-k^2)}{\sin^2 Q + k^2 \cos^2 Q} \right\} \right. \\
&+ \frac{a}{2} \left( \frac{a}{2} - 1 \right) \left\{ \frac{2u}{\bar{U}} + \frac{2v}{\bar{U}} \frac{\sin Q \cos Q (1-k^2)}{\sin^2 Q + k^2 \cos^2 Q} + \left( \frac{u}{\bar{U}} \right)^2 \right. \\
&+ \left. \left. \left( \frac{v}{\bar{U}} \right)^2 \frac{\cos^2 Q + k^2 \sin^2 Q}{\sin^2 Q + k^2 \cos^2 Q} + \frac{2uv}{\bar{U}^2} \frac{\sin Q \cos Q (1-k^2)}{\sin^2 Q + k^2 \cos^2 Q} \right\}^2 \right. \\
&+ \left. \left. \text{cubic and higher order terms} \right] \right.
\end{aligned}$$

$$\begin{aligned}
\text{or } U_{\text{eff}}^a &= (\bar{U} \sqrt{\sin^2 Q + k^2 \cos^2 Q})^a \left[ 1 + a \frac{u}{\bar{U}} + a \frac{\sin Q \cos Q (1-k^2)}{\sin^2 Q + k^2 \cos^2 Q} \frac{v}{\bar{U}} \right. \\
&+ \frac{a(a-1)}{2} \left( \frac{u}{\bar{U}} \right)^2 + \frac{a}{2} \left\{ \frac{(a-1) \sin^2 Q \cos^2 Q (1-k^2)^2 + k^2}{(\sin^2 Q + k^2 \cos^2 Q)^2} \right\} \left( \frac{v}{\bar{U}} \right)^2 \\
&+ \left. \left. a(a-1) \left\{ \frac{\sin Q \cos Q (1-k^2)}{\sin^2 Q + k^2 \cos^2 Q} \frac{uv}{\bar{U}^2} \right\} + \text{cubic and higher order terms.} \right] \right.
\end{aligned}$$

Neglecting the terms associated with

$$\left( \frac{u}{\bar{U}} \right)^2, \left( \frac{v}{\bar{U}} \right)^2 \text{ and } \left( \frac{uv}{\bar{U}^2} \right)^2, \text{ we get}$$

$$U_{\text{eff}}^a = (\bar{U} \sqrt{\sin^2 Q + k^2 \cos^2 Q})^a \left[ 1 + a \frac{u}{\bar{U}} + a \frac{\sin Q \cos Q (1-k^2)}{\sin^2 Q + k^2 \cos^2 Q} \frac{v}{\bar{U}} \right] \quad (B12)$$

Rewrite equations (B8) and (B9)

$$E^2 = X_1 + Y_1 (U_{\text{eff}})^a \quad (\text{B8})$$

$$\bar{E}^2 = X_1 + Y_1 (\bar{U}_{\text{eff}})^a \quad (\text{B9})$$

Substituting  $E = \bar{E} + e$  in (B8), we get

$$(\bar{E} + e)^2 = X_1 + Y_1 (U_{\text{eff}})^a$$

$$\text{or } \bar{E}^2 + 2e\bar{E} + e^2 = X_1 + Y_1 (U_{\text{eff}})^a$$

Substituting the value of  $(U_{\text{eff}})^a$  from above and dividing the equation by  $\bar{E}^2$ , we get

$$1 + \frac{2e}{\bar{E}} + \left(\frac{e}{\bar{E}}\right)^2 = \frac{1}{\bar{E}^2} \left[ X_1 + Y_1 (\bar{U} \sqrt{\sin^2 Q + k^2 \cos^2 Q})^a + Y_1 a (\bar{U} \sqrt{\sin^2 Q + k^2 \cos^2 Q})^{a-1} \left( \frac{u}{\bar{U}} + \frac{\sin Q \cos Q (1-k^2)}{\sin^2 Q + k^2 \cos^2 Q} \frac{v}{\bar{U}} \right) \right]$$

But from equation (B10)

$$Y = Y_1 (\sqrt{\sin^2 Q + k^2 \cos^2 Q})^a$$

$$\text{and } X = X_1$$

we get

$$1 + \frac{2e}{\bar{E}} + \left(\frac{e}{\bar{E}}\right)^2 = \frac{1}{\bar{E}^2} \left[ X + Y \bar{U}^a + Y a \frac{\bar{U}^{a-1}}{\bar{U}} \left( u + \frac{\sin Q \cos Q (1-k^2)}{\sin^2 Q + k^2 \cos^2 Q} \cdot v \right) \right]$$

Substituting  $X + Y \bar{U}^a = \bar{E}^2$  according to equation (B6) and neglecting  $\left(\frac{e}{\bar{E}}\right)^2$ , we get

$$1 + 2 \frac{e}{\bar{E}} = 1 + \frac{Y a \bar{U}^{(a-1)}}{\bar{E}^2} \left( u + \frac{\sin Q \cos Q (1-k^2)}{\sin^2 Q + k^2 \cos^2 Q} v \right)$$

Again from equation (B6), we get

$$\bar{U}^{(a-1)} = \left( \frac{\bar{E}^2 - X}{Y} \right)^{(a-1)/a}$$

$$e = \frac{a Y^{1/a}}{2 \bar{E} (\bar{E}^2 - X)^{(1-a)/a}} \left( u + \frac{\sin Q \cos Q (1-k^2)}{\sin^2 Q + k^2 \cos^2 Q} v \right)$$

$$\text{or } e = (S_1)_y u + (S_2)_y v$$

$$\text{or } e^2 = (S_1)_y^2 u^2 + 2(S_1)_y (S_2)_y uv + (S_2)_y^2 v^2$$

$$\text{or } \overline{e^2} = (S_1)_y^2 \overline{u^2} + 2(S_1)_y (S_2)_y \overline{uv} + (S_2)_y^2 \overline{v^2} \quad (\text{B13})$$

where

$$(S_1)_y = \frac{a Y^{1/a}}{2 \bar{E} (\bar{E}^2 - X)^{(1-a)/a}}$$

and

$$(S_2)_y = \frac{\sin Q \cos Q (1-k^2)}{\sin^2 Q + k^2 \cos^2 Q} (S_1)_y = C (S_1)_y$$

$$\text{where } C = (\sin Q \cos Q (1-k^2)) / (\sin^2 Q + k^2 \cos^2 Q)$$

After deriving equations (B7) and (B13), we can write the following equations for different positions of the probes as shown in figure 37b

$$\text{x position: } e_x^2 = S_x^2 u_x^2$$

$$y_1 \text{ position: } e'_{y_1}{}^2 = (S_1)_{y_1}^2 u'^2 + (S_2)_{y_1}^2 v'^2 + 2(S_1 S_2)_{y_1} \overline{uv}$$

$$y_2 \text{ position: } e'_{y_2}{}^2 = (S_1)_{y_2}^2 u'^2 + (S_2)_{y_2}^2 v'^2 + 2(S_1 S_2)_{y_2} \overline{uv}$$

$$z_1 \text{ position: } e'_{z_1}{}^2 = (S_1)_{z_1}^2 u'^2 + (S_2)_{z_1}^2 w'^2 + 2(S_1 S_2)_{z_1} \overline{uw}$$

$$z_2 \text{ position: } e'_{z_2}{}^2 = (S_1)_{z_2}^2 u'^2 + (S_2)_{z_2}^2 w'^2 + 2(S_1 S_2)_{z_2} \overline{uw}$$

As the values of  $a$ ,  $X$ ,  $Y$  and  $\bar{E}$  for the slanting probe are same in the four positions, we have

$(S_1)_{y_1} = (S_1)_{y_2} = (S_1)_{z_1} = (S_1)_{z_2} = S_s$ , where subscript  $s$  represents slanting probe.

For convenience, let us use  $S_n$  for  $S_x$  where  $n$  stands for normal (or right angle) probe.

Now, we have

$$Q \text{ in } y_2 \text{ position} = 180^\circ - Q \text{ in } y_1 \text{ position.}$$

$$(\sin Q)_{y_2} = (\sin Q)_{y_1}$$

$$\text{and } (\cos Q)_{y_2} = -(\cos Q)_{y_1}$$

$$\text{But } (S_2)_y = \frac{\sin Q \cos Q (1-k^2)}{\sin^2 Q + k^2 \cos^2 Q} S_1$$

$$\therefore (S_2)_{y_1} = \left( \frac{\sin Q \cos Q (1-k^2)}{\sin^2 Q + k^2 \cos^2 Q} \right)_{y_1} (S_1)_{y_1}$$

$$\text{and } (S_2)_{y_2} = \left( \frac{\sin Q \cos Q (1-k^2)}{\sin^2 Q + k^2 \cos^2 Q} \right)_{y_2} (S_1)_{y_2}$$

$$= - \left( \frac{\sin Q \cos Q (1-k^2)}{\sin^2 Q + k^2 \cos^2 Q} \right)_{y_1} (S_1)_{y_2}$$

$$= - \left( \frac{\sin Q \cos Q (1-k^2)}{\sin^2 Q + k^2 \cos^2 Q} \right)_{y_1} (S_1)_{y_1}$$

$$\therefore (S_2)_{y2} = -(S_2)_{y1}$$

which means

$$(S_2)_{y2}^2 = (S_2)_{y1}^2$$

Similarly it can be shown that

$$(S_2)_{z2}^2 = (S_2)_{z1}^2$$

But  $(Q)_{y1} = (Q)_{z1}$

$$\therefore (S_2)_{y1}^2 = (S_2)_{y2}^2 = (S_2)_{z1}^2 = (S_2)_{z2}^2 = S_{S2}^2 = C^2 S_S^2$$

Now, write the equations for x, y<sub>1</sub> and y<sub>2</sub> positions

$$e'_x{}^2 = S_n^2 u'^2 \quad (B14)$$

$$e'_{y1}{}^2 = S_S^2 u'^2 + C^2 S_S^2 v'^2 + 2 C S_S \overline{uv} \quad (B15)$$

$$e'_{y2}{}^2 = S_S^2 u'^2 + C^2 S_S^2 v'^2 - 2 C S_S \overline{uv} \quad (B16)$$

Solution of these equations gives

$$u'^2 = e'_x{}^2 / S_n^2 \quad (B17)$$

$$v'^2 = \frac{1}{C^2} \left[ \left\{ (e'_{y1}{}^2 + e'_{y2}{}^2) / 2 S_S^2 \right\} - u'^2 \right] \quad (B18)$$

$$\overline{uv} = \left\{ (e'_{y1}{}^2 - e'_{y2}{}^2) \right\} / 4 C S_S^2 \quad (B20)$$

Similarly, making use of the equations for the x, z<sub>1</sub> and z<sub>2</sub> positions, we will get

$$w'^2 = \frac{1}{C^2} \left[ \left\{ (e'_{z1})^2 + (e'_{z2})^2 \right\} / 2S_s^2 - u'^2 \right] \quad (B19)$$

$$\overline{uw} = \left\{ (e')_{z1}^2 - (e')_{z2}^2 \right\} / 4C S_s^2 \quad (B21)$$

$$\text{where } C = \frac{\sin Q \cos Q (1-k^2)}{\sin^2 Q + k^2 \cos^2 Q} = \frac{1-k^2}{1+k^2} \quad \text{when } Q = 45^\circ$$

as in the present case. (B26)

This may be mentioned that the above expressions for the turbulence quantities are considerably simpler than the ones obtained by Champagne (8), and on comparison of some numerical values the results were found to agree up to three significant figures.



B4. Hot wire Anemometer with Linearizer:

As we have seen the output voltage of constant temperature anemometer is non linear function of the flow velocity under measurement. An electric circuit can be used which gives output voltage linearly related to velocity. The use of linearizer is preferred in the measurement of high degrees of turbulence. In the course of present investigation, experimentation was carried out with known turbulent shear flow in a pipe. This was done in an attempt to find an appropriate value of the direction sensitivity of slanting hot wire probe. DISA type 55D10 linearizer was used with DISA constant temperature hot wire anemometer. Only the slanting hot wire probe was needed in this study. The probe was calibrated without linearizer, it had to be recalibrated with the linearizer assuming an appropriate value of the velocity exponent 'a' in equation (B4). Being influenced by the experimental findings of Collis and Williams (9) to take  $a = 0.45$  and by the calibration without linearizer in the present investigation which gave  $a = 0.35$ , two values of a that is 0.45 and 0.40 were tried first.  $a = 0.45$  gave higher correlation coefficient than the one obtained with  $a = 0.40$ . For the linear relation

$$E_{11} = X_{11} + Y_{11}U \quad (B22)$$

$$E_1 = X_1 + Y_1 U_{\text{eff}} \quad (B23)$$

the following values of constants were obtained to fit

the experimental data with the two values of the index a

a	X <sub>11</sub>	Y <sub>11</sub>	RMS error	Corr. Coeff.	No. of exptl. pts.
1/2.5(.40)	-2.0702	0.2162	0.0451	0.9997	13
1/2.22(.45)	-1.0313	0.1867	0.0206	0.9999	13

Before carrying out this calibration, it was not realized that a = 0.50 gives best results with the non linearized circuit when the voltage reading (E<sub>0</sub>) at zero velocity is included in the analysis, as it is pointed out in the previous section on calibration. Therefore a = 0.45 was selected as the best value with linearizer, otherwise a = 0.50 could also be tried. The calibration curve obtained with a = 0.45 has been shown in figure 40.

The expressions for the turbulence quantities will be different in this case than the ones obtained with a non linear relation between voltage output and the velocity.

From equation (B11), we can write

$$U_{\text{eff}} = \bar{U} \sqrt{\sin^2 Q + k^2 \cos^2 Q} \left[ 1 + 2 \frac{u}{\bar{U}} + 2 \frac{v}{\bar{U}} \frac{\sin Q \cos Q (1 - k^2)}{\sin^2 Q + k^2 \cos^2 Q} + \left( \frac{u}{\bar{U}} \right)^2 + \left( \frac{v}{\bar{U}} \right)^2 \frac{\cos^2 Q + k^2 \sin^2 Q}{\sin^2 Q + k^2 \cos^2 Q} + 2 \frac{uv}{\bar{U}^2} \frac{\sin Q \cos Q (1 - k^2)}{\sin^2 Q + k^2 \cos^2 Q} \right]^{\frac{1}{2}}$$

As equation (B12) was obtained from equation (B11), we can obtain the following approximate expression for U<sub>eff</sub>

$$U_{\text{eff}} = \bar{U} \sqrt{\sin^2 Q + k^2 \cos^2 Q} \left[ 1 + \frac{u}{\bar{U}} + \frac{\sin Q \cos Q (1-k^2)}{\sin^2 Q + k^2 \cos^2 Q} \frac{v}{\bar{U}} \right]$$

Now  $E_1 = X_1 + Y_1 U_{\text{eff}}$

$$= X_1 + Y_1 \bar{U} \sqrt{\sin^2 Q + k^2 \cos^2 Q} \left[ 1 + \frac{u}{\bar{U}} + \frac{\sin Q \cos Q (1-k^2)}{\sin^2 Q + k^2 \cos^2 Q} \frac{v}{\bar{U}} \right]$$

But  $\bar{E}_1 = X_1 + Y_1 \bar{U} \sqrt{\sin^2 Q + k^2 \cos^2 Q}$

where

$$E_1 = \bar{E}_1 + e_1$$

$$e_1 = Y_1 \bar{U} \sqrt{\sin^2 Q + k^2 \cos^2 Q} \left[ \frac{u}{\bar{U}} + \frac{\sin Q \cos Q (1-k^2)}{\sin^2 Q + k^2 \cos^2 Q} \frac{v}{\bar{U}} \right]$$

$$= Y_1 \sqrt{\sin^2 Q + k^2 \cos^2 Q} \left[ u + \frac{\sin Q \cos Q (1-k^2)}{\sin^2 Q + k^2 \cos^2 Q} v \right]$$

or  $e_1 = S_{11} u + S_{12} v$

where

$$S_{11} = Y_1 \sqrt{\sin^2 Q + k^2 \cos^2 Q}$$

and

$$S_{12} = \frac{\sin Q \cos Q (1-k^2)}{\sin^2 Q + k^2 \cos^2 Q} S_{11} = C S_{11}$$

where

$$C = \frac{\sin Q \cos Q (1-k^2)}{\sin^2 Q + k^2 \cos^2 Q} = \frac{1-k^2}{1+k^2} \quad \text{when } Q = 45^\circ \text{ as in the present case.}$$

Referring to equation (B20), for  $y_1$  and  $y_2$  positions of the probe in figure 37a, we can write

$$\overline{uv} = (e'_1)_{y_1}^2 - (e'_1)_{y_2}^2 / 4C S_{11}^2 \quad (\text{B24})$$

This equation was used in Reynolds shear stress calculations as appearing in the preceding section.

B5. Direction Sensitivity of the slanting hot wire:

If a hot wire is placed so that it makes an angle  $Q$  with respect to the mean flow direction as shown in figure 37a then the output voltage is given by

$$E^2 = X_1 + Y_1 U_{\text{eff}}^a \quad (B5)$$

$$\text{where } U_{\text{eff}}^2 = U^2 \sin^2 Q + k^2 U^2 \cos^2 Q. \quad (B2)$$

This is based on the assumption that the cooling of the wire is accomplished essentially by the component of the velocity which is normal to the wire that is  $U \sin Q$ . In the above expression  $k^2 U^2 \cos^2 Q$  indicates that the tangential component of the incident velocity also have some effect on cooling. In this connection the literature review presented by Champagne (8) can be summarized as follows.

Prandtl, Struminsky, Jones and Sears established for infinitely long cylinder that the heat loss rate per unit length depends only on the normal velocity components. Schubauer and Klebanoff concluded from their experimental study that  $k \approx 0$  for finite wires when  $90^\circ > Q > 20^\circ$ . Newman and Leary concluded that

$$U_{\text{eff}}^{1/2} = U^{1/2} (\cos Q)^n \quad \text{with } n = 0.457$$

although Sandborn and Laurence found that  $n$  varied with each wire tested. Kronauer's experimental results indicate that the direction sensitivity of the wire is dependent on the length to diameter ratio of the wire and

substantially independent of the Reynolds number. He expressed his results in the form

$$U_{\text{eff}} = U \cos Q + 1.2 \left(\frac{d}{l}\right)^{\frac{1}{2}} \sin^2 Q$$

Hinze gave the factor  $k$ , in equation B2, a value between 0.1 and 0.3 depending upon the magnitude of the velocity ( $k$  increasing with decreasing velocity). Webster determined  $k$  to be 0.20. Delleur stated that for  $90^\circ > Q > 20^\circ$ ,  $k \approx 0$  but for  $Q < 20^\circ$  he recommended  $k = 0.14$ .

According to Champagne (8), for the wires with finite length the non uniform wire temperature indicates that the tangential component of velocity has considerable effect on the heat transfer from the wire and it must be taken into account. He carried out measurements of heat transfer from wires inclined and normal to the flow. He found that the value of  $k$  depends primarily upon the length to diameter ratio ( $l/d$ ) of the wire. He determined that for platinum wires  $k \approx 0.20$  for  $l/d = 200$ , decreases with increasing  $l/d$ , and becomes effectively zero at  $l/d = 600$ .

Tucker and Reynolds (31) reported the measurement of turbulence quantities with a slanting hot wire probe. They used  $k = 0$  and in justification they presented the measurements of shear stress in pipe flow and found good agreement with theory. Same type of shear stress measurements were carried out by Schredl (25) in an attempt to predict  $k$  for the slanting hot wire probes which were

used in the turbulence decay study. He used DISA constant temperature hot wire anemometer without linearizer. His results indicate that  $0.20 < k < 0.35$  would give the values of shear stress as predicted by theory. The present author used the same experimental facilities as reported by Schredl (25) but DISA type 55D10 linearizer was included in the measuring equipment.

The probe which has been referred to as slanting probe No. 1 in the previous sections was used in this study of pipe flow. The calibration of the probe with and without linearizer is presented in Appendix B2 and B4 and figures 38, 39 and 40.

For an incompressible fully developed turbulent pipe flow the theoretical relation as derived by Laufer (20) is

$$\overline{uv} = \nu \frac{d\bar{U}}{dr} + \frac{r}{a} U_*^2 \quad (B25)$$

where  $U_*^2 = \frac{\tau_0}{\rho_{air}}$

and  $2 \pi a L \tau_0 = \pi a^2 (p_1 - p_2) / g_0$

where  $L$  = length of the pipe between the points for which static pressure difference  $p_1 - p_2$  was measured.

and  $a$  = radius of the pipe.

The experiment was carried out at a Reynolds number

(based on centre line velocity) of 88,700. The experimental procedure may be summarized as under.  $\overline{uv}$  and  $\overline{U}$  were determined from the hot wire readings at a number of points along the radius of the pipe. At each point the slanting wire was placed in two positions  $y_1$  and  $y_2$  as shown in figure 37 and corresponding d.c. voltages ( $\overline{E}_{11}$ ) and r.m.s. voltages ( $e_{1y1}$  and  $e_{1y2}$ ) were recorded.  $\overline{U}$  was calculated from equation (B22) and  $\overline{uv}$  from equation (B24). For  $U_*^2$ , static pressure drop was measured for 10 ft. length of pipe using wall taps leading to the micromanometer.

The theoretical curve in figure 42 was drawn according to equation (B25) in which the quantities at right hand side were found experimentally. The experimental points were obtained using equation (B24) for  $\overline{uv}$  and assuming different values of  $k$ . The values of  $k$  which would give the values of shear stress in exact agreement with equation B25 were also found from the same experimental data. For this purpose the value of  $\overline{uv}$  in equation B24 can be substituted from equation B25 and the combination gives the following equation with  $k$  as the only unknown

$$\left\{ (e'_{1y1})^2 - (e'_{1y2})^2 \right\} / 4C S_{11}^2 = \nu \frac{d\overline{U}}{dr} + \frac{r}{a} U_*^2$$

$$C = \left\{ (e'_{1y1})^2 - (e'_{1y2})^2 \right\} / \left\{ 4S_{11}^2 \left( \nu \frac{d\overline{U}}{dr} + \frac{r}{a} U_*^2 \right) \right\}$$

In this equation all the quantities on RHS were known

from the experiment.

$$\text{Now } C = \frac{\sin Q \cos Q (1-k^2)}{\sin^2 Q + k^2 \cos^2 Q} = \frac{1-k^2}{1+k^2} \text{ when } Q = 45^\circ \text{ as in the}$$

present case.

$$\therefore k = \sqrt{(1-C)/(1+C)}$$

The values of  $k$  determined in this way are presented in figure 41. Figures 41 and 42 indicate that  $k$  lies between 0.2 and 0.4. After the experimentation the probe holder was examined for its axial movement by observing a magnified projection. It was found that, while rotating the probe through  $180^\circ$ , it experienced a shift from its original point. Therefore the values of  $k$  obtained from the above experiment were not used in turbulence calculation. As the wires had a length to diameter ratio of 200,  $k = 0.2$  was assumed, as suggested by Champagne (8).



B6. Measurement and Computation of one dimensional Energy Spectra:

Consider, for instance, the component  $u$  of the turbulence fluctuation of velocity in a fixed point of the flow field. We assume that this field is quasi steady so that it is statistically homogeneous with respect to time. There then exists a constant average value of  $u^2$  which can be considered to consist of the sum of the contributions of all the frequencies  $n$ . Let  $E_1(n) dn$  be the contribution to  $\overline{u^2}$  of the frequencies between  $n$  and  $n + dn$ , the distribution function  $E_1(n)$  then has to satisfy the condition (19, p.54)

$$\int_0^{\infty} dn E_1(n) = \overline{u^2}$$

It is the general practice to consider the wave number  $k_1 = 2\pi n/\bar{U}$  instead of  $n$  and to use the energy spectrum function  $E_1(k_1)$  instead of  $E_1(n)$ , so that  $E_1(k_1)$  will be defined as (19, p.166)

$$E_1(k_1) = E_1(n) \bar{U}/2\pi$$

and therefore  $\int_0^{\infty} dk_1 E_1(k_1) = \overline{u^2}$

Similarly  $\int_0^{\infty} dk_1 E_2(k_1) = \overline{v^2}$

and  $\int_0^{\infty} dk_1 E_3(k_1) = \overline{w^2}$

We can write

$$d u^2 = dk_1 E_1(k_1)$$

$$\text{but } dk_1 = 2\pi dn / \bar{U}$$

$$\therefore d u^2 = E_1(k_1) \cdot 2\pi dn / \bar{U}$$

$$\therefore E_1(k_1) / \bar{u}^2 = \bar{U} du^2 / \bar{u}^2 \cdot 2\pi dn$$

$$\text{where } du^2 / \bar{u}^2 = de^2 / \bar{e}^2$$

$$= \frac{\text{RMS voltage at frequency } n \text{ for a band } dn}{\text{total RMS voltage}}$$

The spectrum curves are plotted with  $E_1(k_1) / \bar{u}^2$ ,

$E_2(k_1) / \bar{v}^2$  and  $E_3(k_1) / \bar{w}^2$  against  $k_1$  for  $u'$ ,  $v'$  and  $w'$

respectively.

## APPENDIX C

### CALIBRATION OF THE INSTRUMENTS

#### C1. Micromanometer:

Wilhelm Lambrecht slanting tube micromanometer No. 655 with pitot static probe was used for measuring the dynamic pressure to give the mean velocity of flow to calibrate the hot wire anemometer. The micromanometer was filled with normal butyl alcohol the specific gravity of which was given to be 0.81 at normal temperature and pressure. The micromanometer tube was graduated from 0 to 200 mm with divisions of 1 mm each. The tube could be fixed in four slanting positions with the slopes of 1:2, 1:5, 1:10 and 1:25. With the graduated tube at 1:10 and at 1:25 this micromanometer was calibrated against Flow Corporation model MM3 micromanometer. Flow Corporation micromanometer was filled with normal butyl alcohol. The alcohol was supplied by Flow Corporation and, according to them, in the temperature range 50°F to 100°F, its density could be given to 0.03% by

$$\text{density (gm/cc)} = 0.8176 - 0.0004(t^{\circ}\text{F} - 50)$$

The micromanometer could be read to  $\pm 0.0002$ " of the liquid column over a 2" range.

For calibration purposes both of the manometers were connected to the same pitot static probe. The pitot static probe was exposed to the flow in the wind tunnel. The flow velocity could be controlled by regulating the wind tunnel fan. The readings of the two meters were recorded simultaneously at a number of velocities. The dynamic pressure in inches of water was calculated from Flow Corporation manometer readings and it was plotted against the Wilhelm Lambrecht micromanometer readings in mm. The calibration data is plotted in figure 43. The best fitting lines were determined by least square regression method.

C2. D.C. Voltmeters on the hot wire anemometers:

Two sets of DISA Constant temperature hot wire anemometers (numbered as MEC97 and MEC116) were used in the experimentation. The d.c. voltmeters on these anemometers were accurate to  $\pm 1\%$ . These voltmeters were calibrated against Hewlett Packard digital voltmeter 3440A which could read the d.c. voltage upto 4 significant figures in various ranges from 100 mV to 1000 volts. For calibration, connections were provided between anemometer and the digital voltmeter so that both of them could simultaneously receive the signal from the hot wire probe exposed to the regulated flow in the wind tunnel. The two anemometer voltmeters were calibrated seperately. Because of observable fluctuations in the digital voltmeter readings, lowest and highest observed values were recorded from that against a mean value on anemometer voltmeter. The following tables give some of the readings obtained for calibration.

DC Volts from Anemometer	DC Volts from digital voltmeter		$\frac{(B+C)/2 - A}{A} \times 100$
(A)	highest (B)	lowest (C)	

Anemometer MEC116

5.53	5.679	5.675	2.66
5.86	6.022	6.011	2.67
6.44	6.626	6.604	2.72
6.79	6.980	6.967	2.70
7.05	7.234	7.227	2.56
7.19	7.374	7.358	2.45
7.30	7.494	7.464	2.45
7.50	7.704	7.686	2.60
7.68	7.868	7.851	2.34

Anemometer MEC97

5.41	5.577	5.566	2.99
5.51	5.698	5.666	3.12
5.97	6.187	6.143	3.27
6.24	6.444	6.406	2.96
6.49	6.704	6.661	2.97
6.70	6.906	6.855	2.69
6.82	7.051	7.013	3.11
7.12	7.345	7.321	2.99

The above tables show that both of the anemometer voltmeters were showing lower values when compared to the digital voltmeter which was considered to be more accurate and reliable. From the tables it could also be inferred that both of the anemometer voltmeters were quite in agreement with each other. Therefore the digital voltmeter was checked with the other available meters. This checking could be made in lower ranges than that used in the above tables. The digital voltmeter was

found to give higher readings upto 2%. Therefore the readings on anemometer voltmeters were directly used for determining various quantities.

C3. RMS Voltmeters on various instruments:

As mentioned in the section on instrumentation, the following instruments were needed for the measurement of various turbulence quantities.

DISA constant temperature hot wire anemometer  
55 A 01 (two sets numbered as MEC97 and MEC116)

DISA random signal indicator and correlator  
55 A 06

Bruel and Kjaer audio frequency spectrometer  
Type 2112

Every one of the above instruments was provided with RMS voltmeters which could be used in various ranges with an accuracy of  $\pm 1\%$  at full scale deflection.

All RMS voltmeters were checked with each other and with Bruel and Kjaer random noise voltmeter type 2417. Some of the calibration readings are being presented here.



RMS mV from Anemometer (B)	RMS mV from random noise voltmeter (A)	$\frac{B-A}{A} \times 100$
<u>Anemometer MEC116</u>		
7.2	7.0	2.86
9.5	9.6	-1.04
14.3	14.4	-0.69
20.9	20.9	0.00
24.8	24.9	-0.40
30.0	30.5	-1.16
34.2	34.6	-1.16

Anemometer MEC97

11.0	14.0	-21.43
14.0	17.0	-17.65
15.9	19.3	-17.62
18.1	21.7	-16.59
21.2	25.8	-17.83
23.0	29.5	-22.03
26.0	32.1	-19.00
28.4	35.5	-25.00

RMS mV from Correlator (B)	RMS mV from Anemometer MEC116 (A)	$\frac{B-A}{A} \times 100$
8.8	8.8	0.00
10.7	10.6	0.94

RMS mV from Spectrometer (B)	RMS mV from Anemometer MEC116 (A)	$\frac{B-A}{A} \times 100$
4.10	3.72	10.22
4.20	3.95	6.33
4.90	4.40	11.36

From the above values we can infer that the readings given by the random noise voltmeter, the anemometer MEC116 and the correlator are in agreement. The anemometer MEC97 and

the spectrometer give considerably different values. To avoid the discrepancies and because of high fluctuations in RMS milli volts, especially in the spectrometer, all RMS signals were measured on the random noise voltmeter in which sufficient damping could be achieved.

APPENDIX D

ENERGY EQUATION

The Navier Stokes equation of an incompressible fluid for the case of steady main motion (19, p.250) reads

$$\frac{\partial u_i}{\partial t} + (\bar{U}_k + u_k) \frac{\partial}{\partial x_k} (\bar{U}_i + u_i) = -\frac{1}{\rho} \frac{\partial \bar{P}}{\partial x_i} - \frac{1}{\rho} \frac{\partial p}{\partial x_i} + \nu \frac{\partial^2}{\partial x_1 \partial x_1} (\bar{U}_i + u_i) \quad (3.1)$$

The equation of continuity for incompressible flow reads

$$\frac{\partial U_k}{\partial x_k} = 0 \quad (3.2)$$

But 
$$\frac{\partial U_k}{\partial x_k} = \frac{\partial \bar{U}_k}{\partial x_k} + \frac{\partial u_k}{\partial x_k} = \frac{\partial u_k}{\partial x_k}$$

Adding  $u_i \frac{\partial u_k}{\partial x_k} = 0$  to the left-hand side of equation

(3.1), we get

$$\begin{aligned} \frac{\partial u_i}{\partial t} + u_k \frac{\partial \bar{U}_i}{\partial x_k} + \bar{U}_k \frac{\partial u_i}{\partial x_k} + \frac{\partial}{\partial x_k} u_i u_k \\ = -\frac{1}{\rho} \frac{\partial \bar{P}}{\partial x_i} - \frac{1}{\rho} \frac{\partial p}{\partial x_i} + \nu \frac{\partial^2}{\partial x_1 \partial x_1} (\bar{U}_i + u_i) \end{aligned}$$

Subtracting from this its average value, we obtain

$$\begin{aligned} \frac{\partial u_i}{\partial t} + u_k \frac{\partial \bar{u}_i}{\partial x_k} + \bar{u}_k \frac{\partial u_i}{\partial x_k} + \frac{\partial}{\partial x_k} (u_i u_k - \bar{u}_i \bar{u}_k) \\ = -\frac{1}{\rho} \frac{\partial p}{\partial x_i} + \nu \frac{\partial^2 u_i}{\partial x_1 \partial x_1} \end{aligned} \quad (3.3)$$

For the velocity component  $u_j$ , we can write the similar equation

$$\begin{aligned} \frac{\partial u_j}{\partial t} + u_k \frac{\partial \bar{u}_j}{\partial x_k} + \bar{u}_k \frac{\partial u_j}{\partial x_k} + \frac{\partial}{\partial x_k} (u_j u_k - \bar{u}_j \bar{u}_k) \\ = -\frac{1}{\rho} \frac{\partial p}{\partial x_j} + \nu \frac{\partial^2 u_j}{\partial x_1 \partial x_1} \end{aligned} \quad (3.4)$$

Multiplying (3.3) by  $u_j$  and (3.4) by  $u_i$  and adding the two equations, we get

$$\begin{aligned} \frac{\partial}{\partial t} u_i u_j + u_k u_j \frac{\partial \bar{u}_i}{\partial x_k} + u_k u_i \frac{\partial \bar{u}_j}{\partial x_k} + \bar{u}_k \frac{\partial u_i u_j}{\partial x_k} + \frac{\partial u_i u_j u_k}{\partial x_k} \\ - u_j \frac{\partial}{\partial x_k} u_i u_k - u_i \frac{\partial}{\partial x_k} \bar{u}_j u_k = -\frac{1}{\rho} \left\{ u_j \frac{\partial p}{\partial x_i} + u_i \frac{\partial p}{\partial x_j} \right\} \\ + \nu \frac{\partial^2}{\partial x_1 \partial x_1} \bar{u}_i \bar{u}_j - 2\nu \frac{\partial u_i \partial u_j}{\partial x_1 \partial x_1} \end{aligned}$$

After averaging all the quantities, we obtain

$$\begin{aligned} \frac{\partial}{\partial t} \overline{u_i u_j} + \overline{u_k u_j} \frac{\partial \bar{U}_i}{\partial x_k} + \overline{u_k u_i} \frac{\partial \bar{U}_j}{\partial x_k} + \bar{U}_k \frac{\partial}{\partial x_k} \overline{u_i u_j} + \frac{\partial}{\partial x_k} \overline{u_i u_j u_k} \\ = -\frac{1}{\rho} \left( u_j \frac{\partial p}{\partial x_i} + u_i \frac{\partial p}{\partial x_j} \right) + \nu \frac{\partial^2}{\partial x_1 \partial x_1} \overline{u_i u_j} - 2\nu \frac{\partial u_i}{\partial x_1} \frac{\partial u_j}{\partial x_1} \end{aligned}$$

A contraction gives

$$\begin{aligned} \frac{\partial}{\partial t} \overline{u_i u_i} + 2\overline{u_k u_i} \frac{\partial \bar{U}_i}{\partial x_k} + \bar{U}_k \frac{\partial}{\partial x_k} \overline{u_i u_i} + \frac{\partial}{\partial x_k} \overline{u_i u_i u_k} \\ = -\frac{1}{\rho} u_i \frac{\partial p}{\partial x_i} + \nu \frac{\partial^2}{\partial x_1 \partial x_1} \overline{u_i u_i} - 2\nu \frac{\partial u_i}{\partial x_1} \frac{\partial u_i}{\partial x_1} \end{aligned}$$

The statistical average values are assumed to be in steady state, therefore

$$\begin{aligned} \bar{U}_k \frac{\partial}{\partial x_k} \overline{u_i u_i} = -2 \overline{u_k u_i} \frac{\partial \bar{U}_i}{\partial x_k} - \frac{\partial}{\partial x_k} \overline{u_i u_i u_k} - \frac{1}{\rho} \overline{u_i \partial p} \\ + \nu \frac{\partial^2}{\partial x_1 \partial x_1} \overline{u_i u_i} - 2\nu \frac{\partial u_i}{\partial x_1} \frac{\partial u_i}{\partial x_1} \end{aligned}$$

## APPENDIX E

### SUMMARY OF ERRORS

The following lines give an account of the analysis of the appreciable errors in the measurement of mean velocity and the turbulence intensities.

(i) Mean Velocity: The accuracies of the instruments were as follows:

Wilhelm Lambrecht slanting tube micromanometer,  
 $\pm 0.5\text{mm} = dh$

D.C. voltmeter with the hot wire anemometer,  
 $\pm 1\% = d\bar{E}/\bar{E}$

The relation used to find the velocity from the manometer readings was

$$\frac{1}{2} \rho_{\text{air}} U^2 = \Delta P$$

for a given temperature and pressure

$$U = a \text{ constant } x \sqrt{h}$$

$$dU/U = (\text{constant}/2) (dh/U^2)$$

Assuming  $h$  as the readings in mm. with the manometer tube having a slope of 1:5, at a temperature of  $80^{\circ}\text{F}$  and a pressure of 29.9 in. mercury,

constant  $\approx 5.4$

$$dU/U = 2.7 dh/U^2$$

In the experiments  $U > 25$  ft/sec

$$\therefore dU/U < 0.0028 \text{ or } 0.28\%$$

Hot wire response is given by the equation (B6)

$$\bar{E}^2 = X + Y \bar{U}^a$$

$$d\bar{U}/\bar{U} = d\bar{E}^2/a(\bar{E}^2 - X).$$

To find the mean velocity by hot wire,  $\bar{E}$  was measured by the anemometer and then the above equation (obtained by calibration) was used to find  $\bar{U}$ . Therefore maximum error in  $\bar{U}$  is given by

$$|d\bar{U}/\bar{U}| = \left\{ \left| d\bar{E}^2_{\text{reading}} \right| + \left| d\bar{E}^2_{\text{calibration}} \right| \right\} / a(\bar{E}^2 - X)$$

In calibration of the four hot wire probes used in experiments the r.m.s. error in  $\bar{E}^2 < 0.105$ , Y had values between 11.4 and 14.0, X between 20 and 22 and  $a = 0.35$ . Considering a value of  $\bar{E} = 8$  volts which correspond to  $\bar{U} \approx 25$  ft/sec, error in reading is given by

$$d\bar{E}^2 = 2\bar{E}^2 |d\bar{E}/\bar{E}| = 128 \times 0.01 = 1.28$$

$$\therefore |d\bar{U}/\bar{U}| < (1.28 + 0.105) / \{0.35(64 - 22)\} < 0.0942, \text{ say } \pm 10\%$$

Similarly considering a value of  $\bar{E} = 9$  volts which correspond to  $\bar{U} \approx 60$  ft/sec, we get

$$|d\bar{U}/\bar{U}| < 0.089, \text{ say } \pm 9\%$$

(ii) Longitudinal Component of Fluctuating Velocity:

The accuracy of the r.m.s. voltmeter was  $\pm 1\%$  at full scale deflection. Assume a value of  $\pm 4\%$  as the accuracy for normal deflections and to take into account the effect of fluctuations during observations.

$$de'^2/e'^2 = \pm 0.08$$

Consider the equation (ref. eqn. B17 and B27)

$$u'^2/\bar{U}^2 = e'_x{}^2/(S_n^2 \cdot \bar{U}^2)$$

$$d(u'^2/\bar{U}^2)/(u'^2/\bar{U}^2) = (de'_x{}^2/e'_x{}^2) - d(S_n^2 \cdot \bar{U}^2)/S_n^2 \bar{U}^2$$

Now  $S_n = aY^{1/a} / 2\bar{E}(\bar{E}^2 - X)^{(1-a)/a}$

and  $\bar{U}^2 = \left\{ (\bar{E}^2 - X) / .Y \right\}^{2/a}$

$$S_n^2 \bar{U}^2 = (a^2/4) \left\{ (\bar{E}^2 - X)^2 / \bar{E}^2 \right\}$$

$\therefore$  error in  $S_n^2 \bar{U}^2$  is given by

$$\begin{aligned} d(S_n^2 \bar{U}^2) / S_n^2 \bar{U}^2 &= (a^2/4) \left\{ \left| d(\bar{E}^2 - X)^2 / (\bar{E}^2 - X)^2 \right| + \left| d\bar{E}^2 / \bar{E}^2 \right| \right\} \\ &= (0.35^2/4) \left\{ \left| d\bar{E}^2 / (\bar{E}^2 - X)^2 \right| + 0.02 \right\} \end{aligned}$$



Considering a value of  $\bar{E} = 8$  volts, and taking  $X = 22$ , the above expression is negligible.

$$\left| d(u'^2/\bar{U}^2)/(u'^2/\bar{U}^2) \right| = \left| d e'_x{}^2/e'_x{}^2 \right|$$

(iii) Lateral Components of Fluctuating Velocity: Considering equations (B18), (B19) and (B27) we can see that

$$\begin{aligned} \left| d(v'^2/\bar{U}^2)/(v'^2/\bar{U}^2) \right| &= \left| d(v'^2/\bar{U}^2)/(w'^2/\bar{U}^2) \right| \\ &= 2 \left| d(u'^2/\bar{U}^2)/(u'^2/\bar{U}^2) \right| = 0.16 \text{ or } 16\% \end{aligned}$$

when C is assumed to be without any error.

The grid turbulence was corrected for the free stream turbulence as mentioned in chapter 5. In free stream turbulence the intensity values were less than 20% of the values in nearly isotropic grid turbulence and less than 50% of the values in strongly anisotropic grid turbulence. Therefore in isotropic grid turbulence

$$\begin{aligned} \left| d(u'^2/\bar{U}^2)/(u'^2/\bar{U}^2) \right| &= 0.08 + (0.08 \times 20/100) \\ &= 0.096, \text{ say } 10\% \end{aligned}$$

similarly  $\left| d(v'^2/\bar{U}^2)/(v'^2/\bar{U}^2) \right| = 0.192, \text{ say } 20\%$

In the same way for strongly anisotropic turbulence, the above values will be 12% and 24% respectively.

(iv) Effect of the Value of k on Measurement of  $v'^2$ :

A value of  $k = 0.20$  was used for the slanting hot wire in the present study as mentioned in Appendix B5. Assuming that k has got a value between 0.15 and 0.25, let us find the effect on the value of C.

$$C = \frac{\sin Q \cos Q (1 - k^2)}{\sin^2 Q + k^2 \cos^2 Q}$$

$$= (1 - k^2) / (1 + k^2) \text{ as } Q = 45^\circ \text{ in the present case}$$

$$\left| \frac{dC}{C} \right| = \left| \frac{dk^2}{(1 - k^2)} \right| + \left| \frac{dk^2}{(1 + k^2)} \right|$$

$$= (0.02/0.96) + (0.02/1.04)$$

$$\approx 0.04$$

$$\left| \frac{dC^2}{C^2} \right| \approx 0.08 \text{ or } 8\%$$

In the equations (B18) and (B19) we can see that  $v'^2$  and  $w'^2$  will have an error of  $\pm 8\%$  due to uncertainty in the value of k by  $\pm 25\%$ .

(v) Effect of inaccuracy in the angle Q: The slanting hot wire was inclined to the mean flow by an angle,  $Q = 45^\circ$ . Assuming that  $Q = 45^\circ \pm \frac{1}{2}^\circ$  let us find the effect on C

$$C = \frac{\sin Q \cos Q (1 - k^2)}{(\sin^2 Q + k^2 \cos^2 Q)}$$

$$\left| \frac{dC}{C} \right|_{\#} = d \sin Q / \sin Q + d \cos Q / \cos Q + \frac{d (\sin^2 Q + k^2 \cos^2 Q)}{(\sin^2 Q + k^2 \cos^2 Q)}$$

In the present case  $Q = 45^\circ$

$$\therefore \frac{dC}{C} \approx 4 d \sin Q / \sin Q = 4 (\sin 45.25^\circ - \sin 44.75^\circ) / \sin 45^\circ$$

$$\approx 0.0308 \text{ or } 3.1\%$$

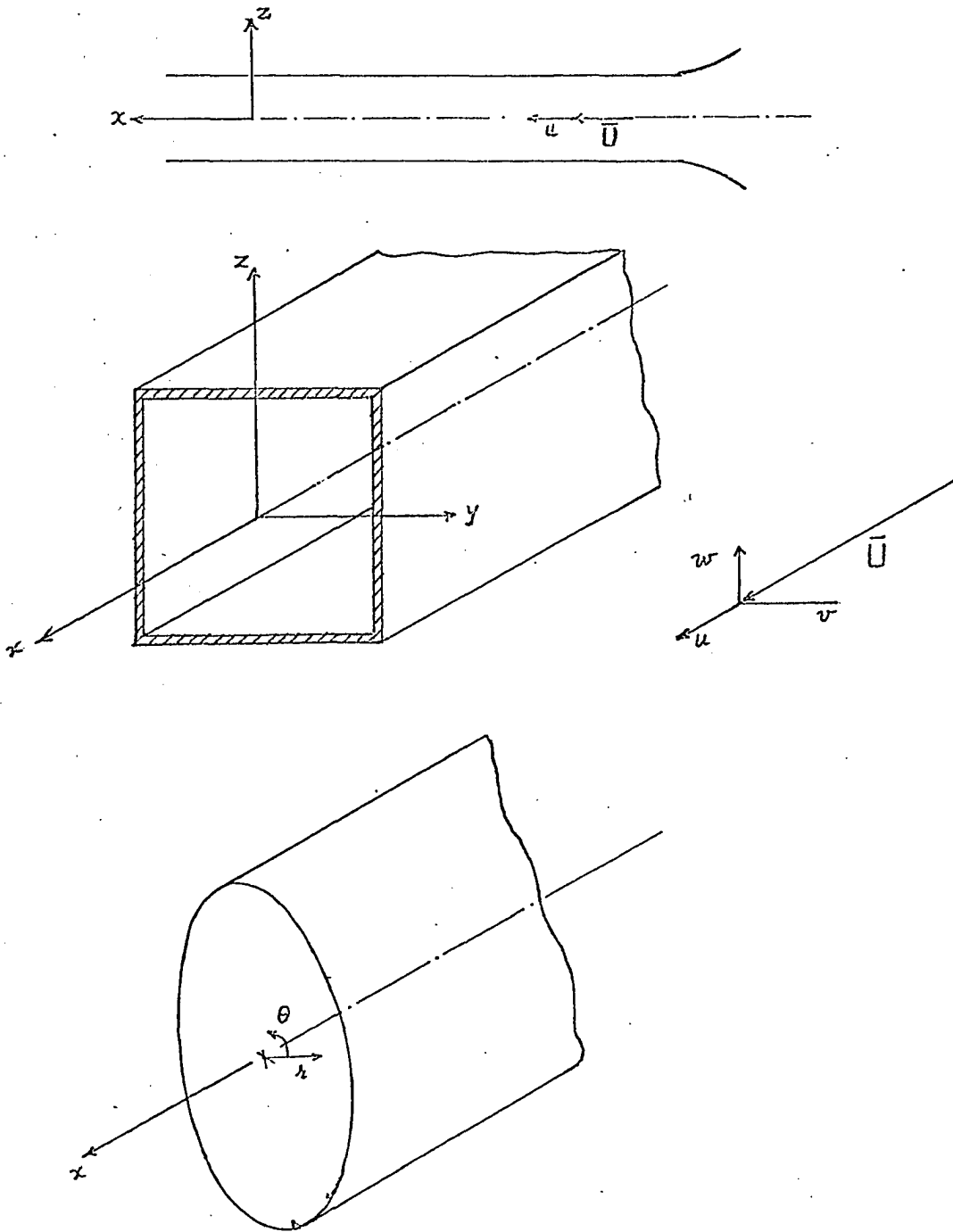
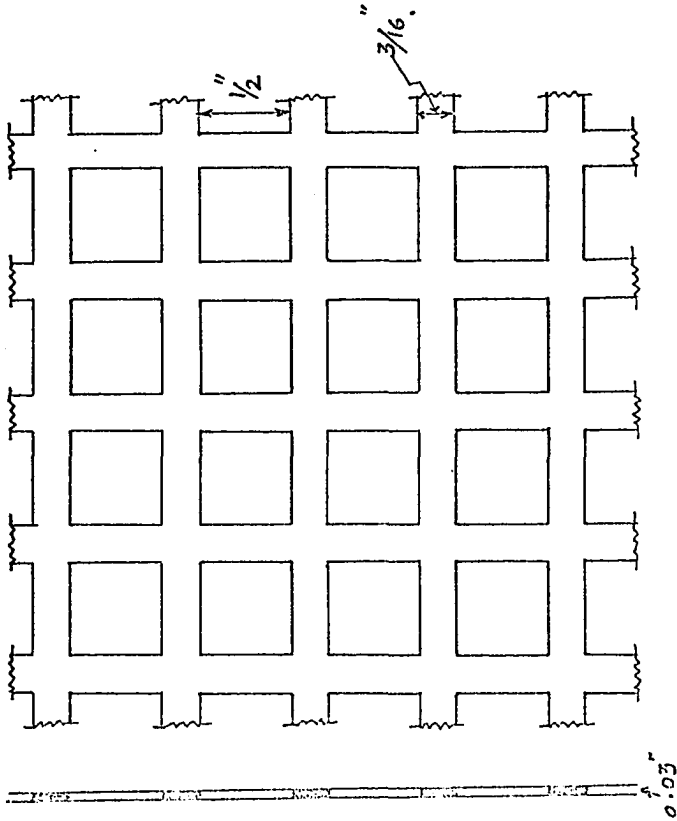
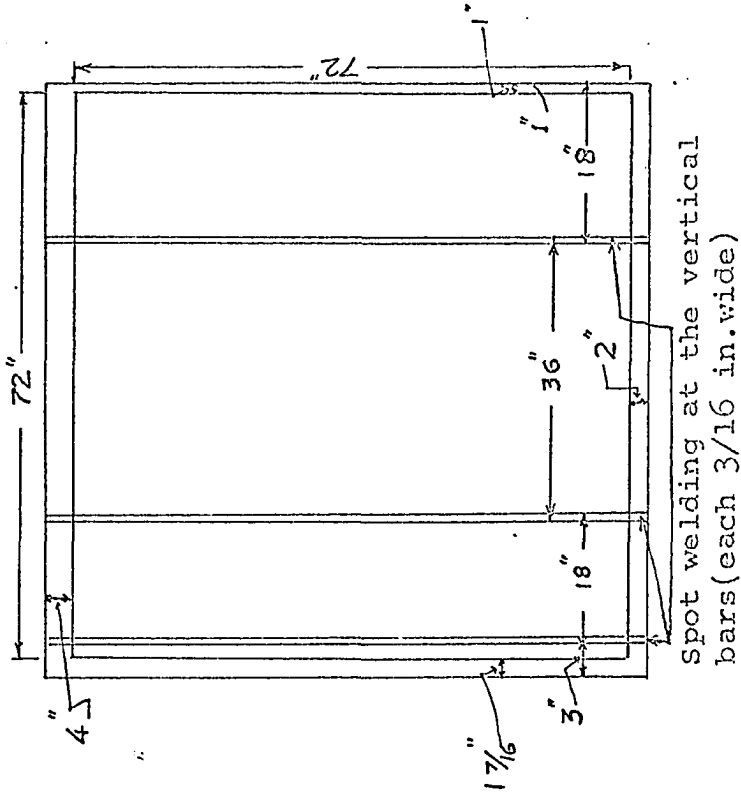


Fig.1 Coordinate system w.r.t. the wind tunnel test section and the pipe.



(i) Small section of perforated sheet grid used in present experiments.



(ii) Dimensions of the grid used at the beginning of the contraction for anisotropic turbulence.

Fig.2a

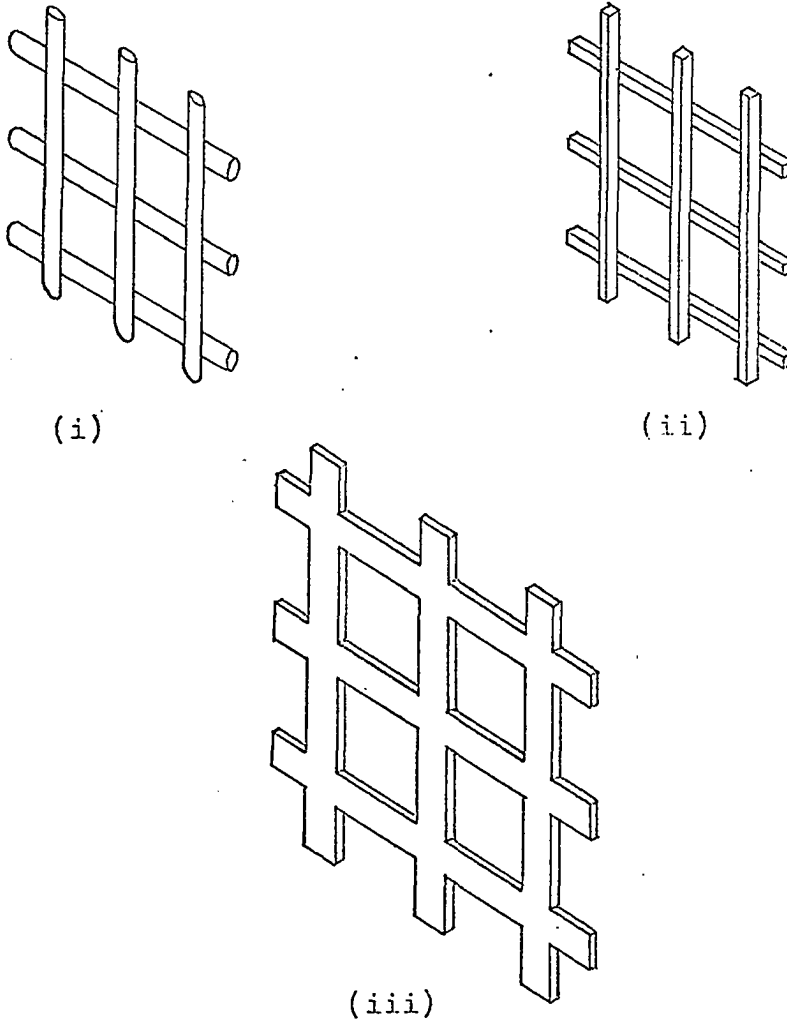


Fig.2b Typical grids for generating approximately isotropic turbulence  
(i) Commonly used round rod bi-plane grid  
(ii) Commonly used square rod bi-plane grid  
(iii) Perforated sheet grid used in present experiments.

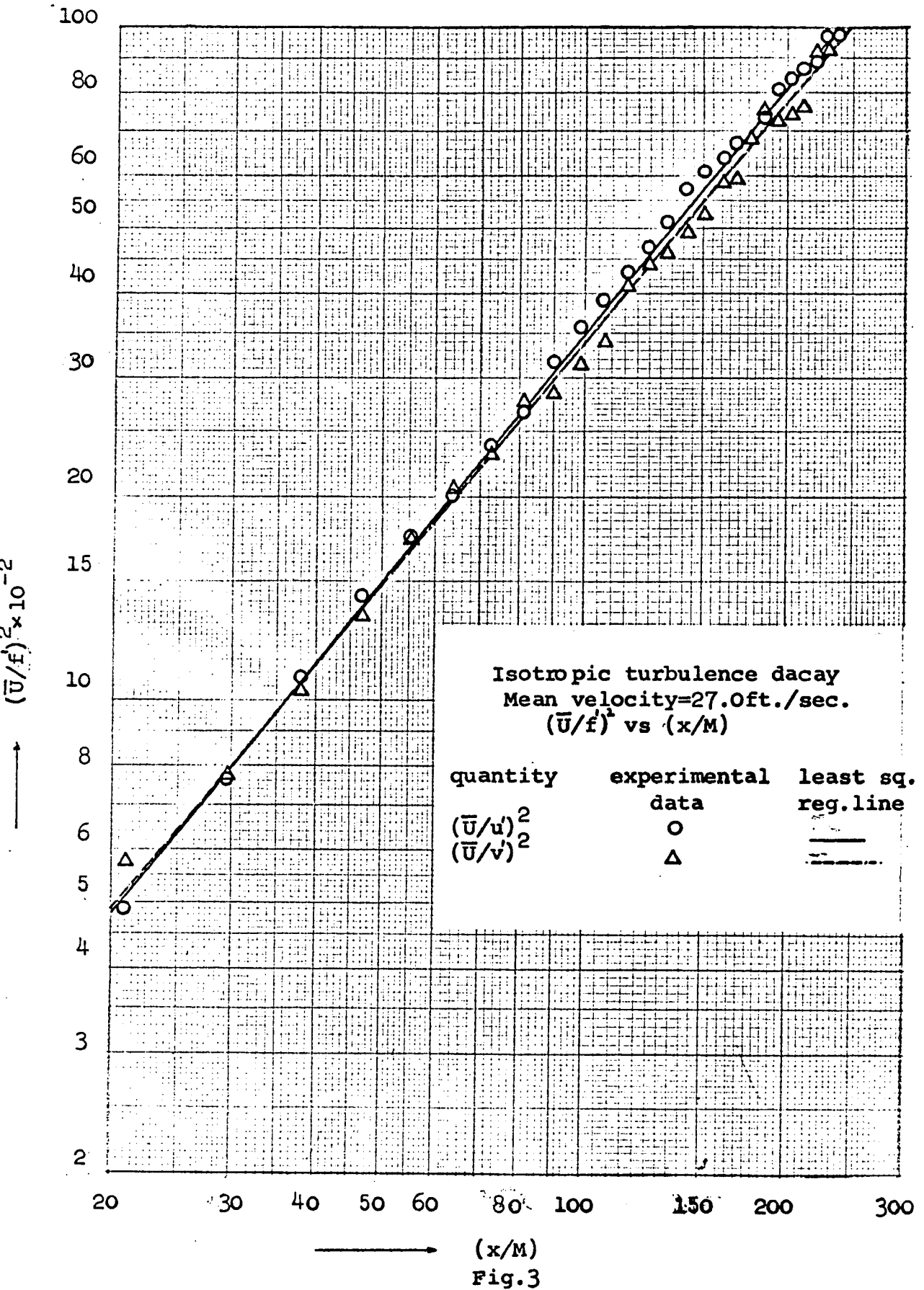


Fig.3

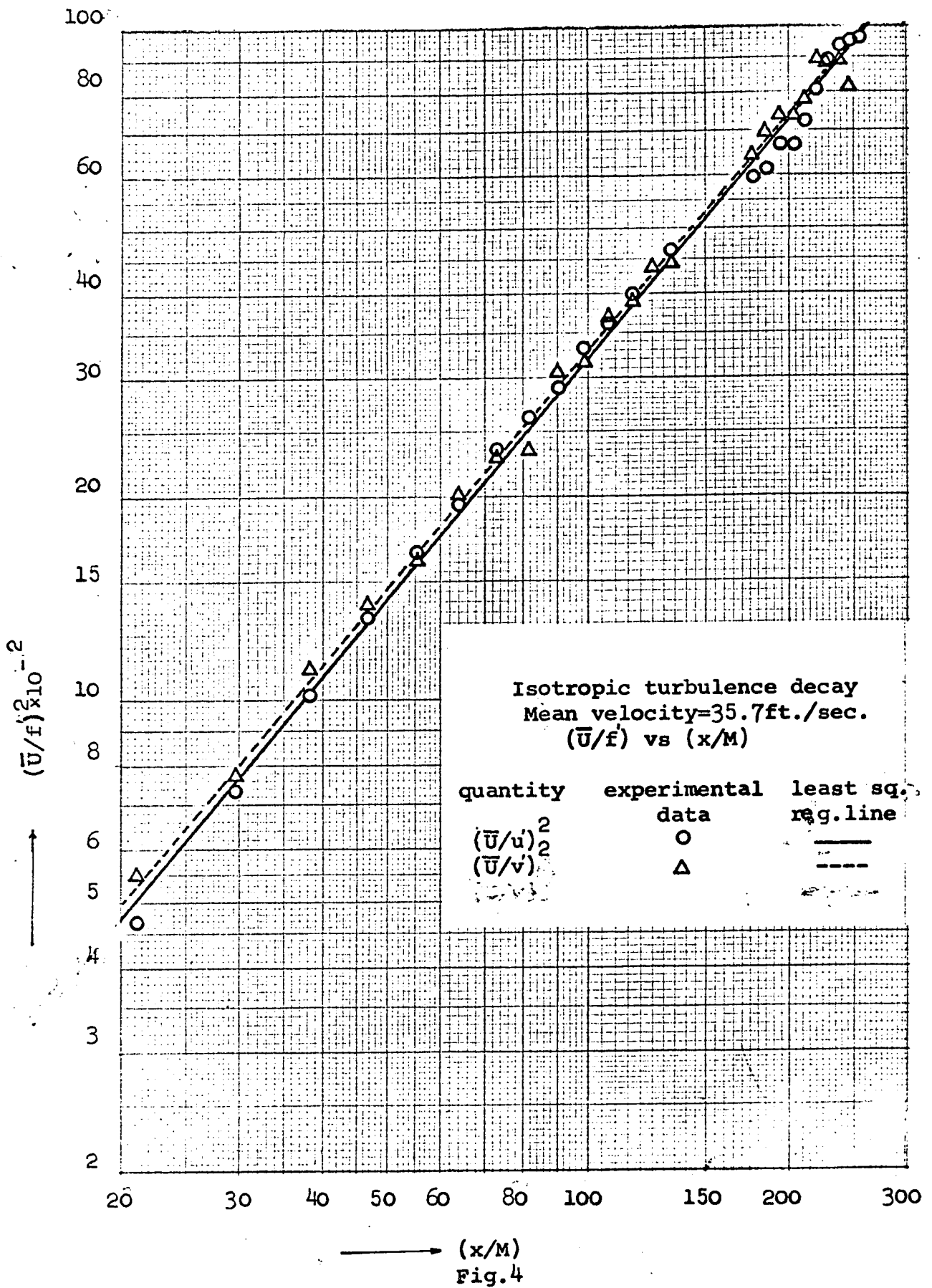


Fig.4

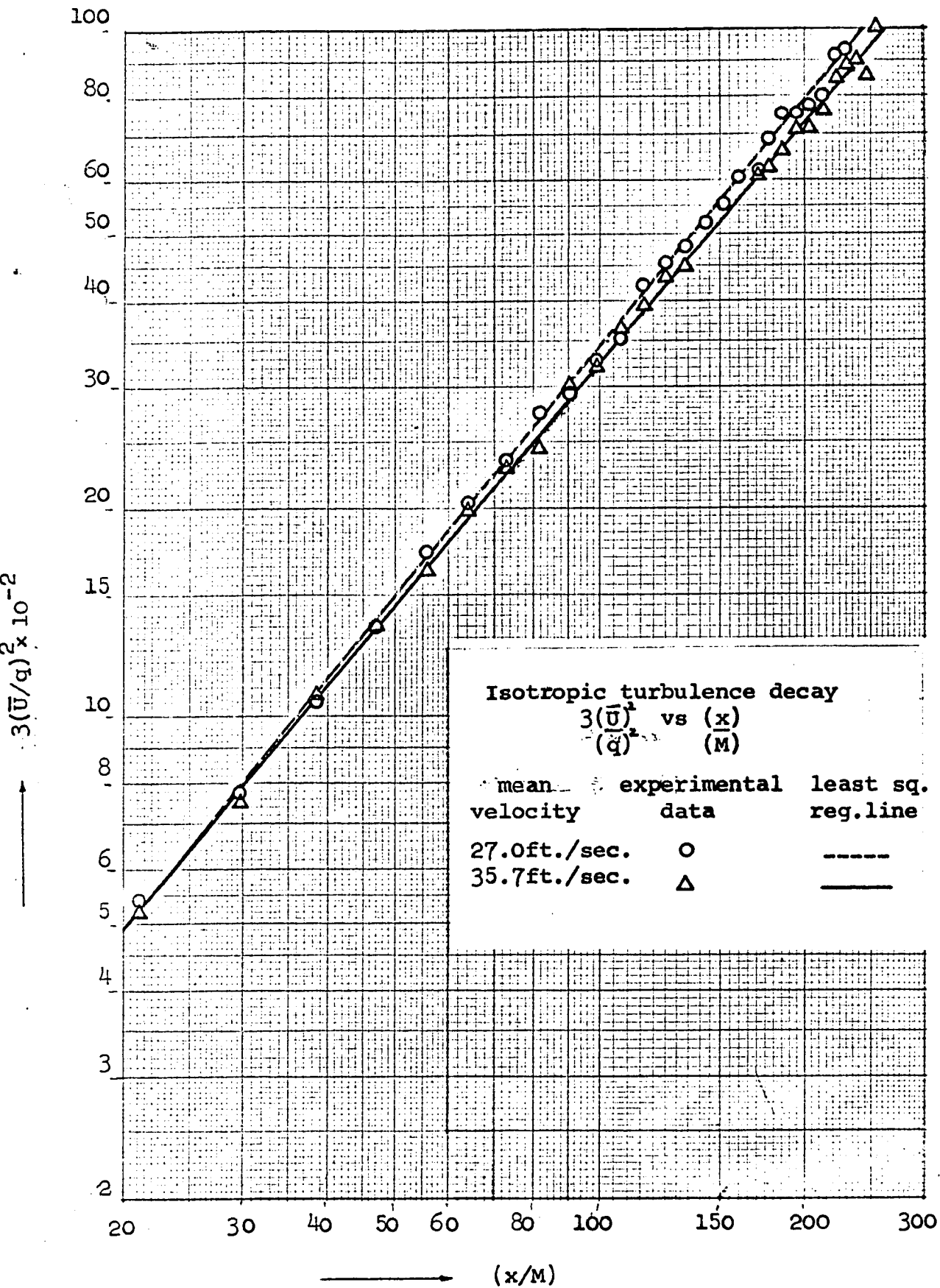
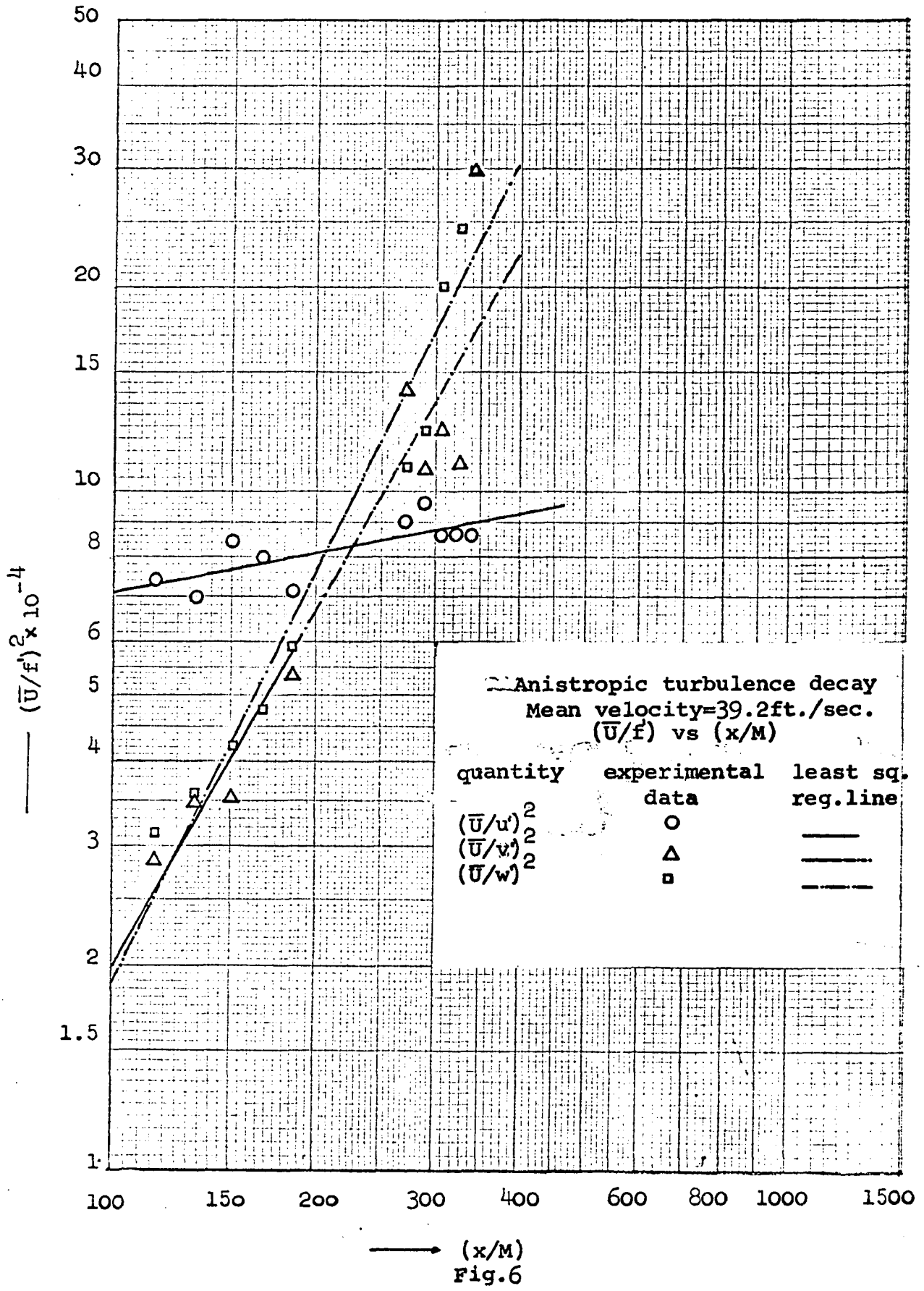


Fig.5





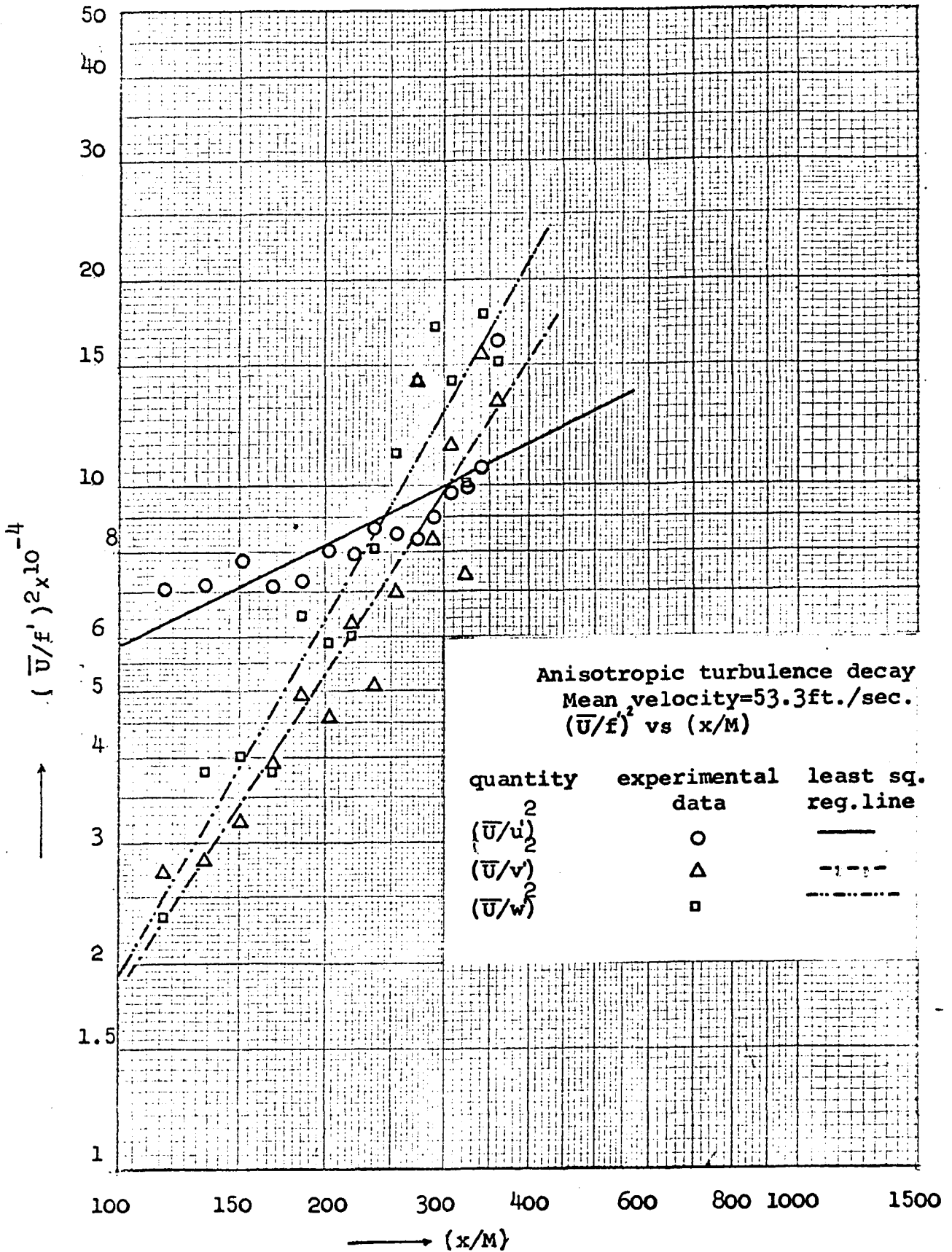


Fig.7

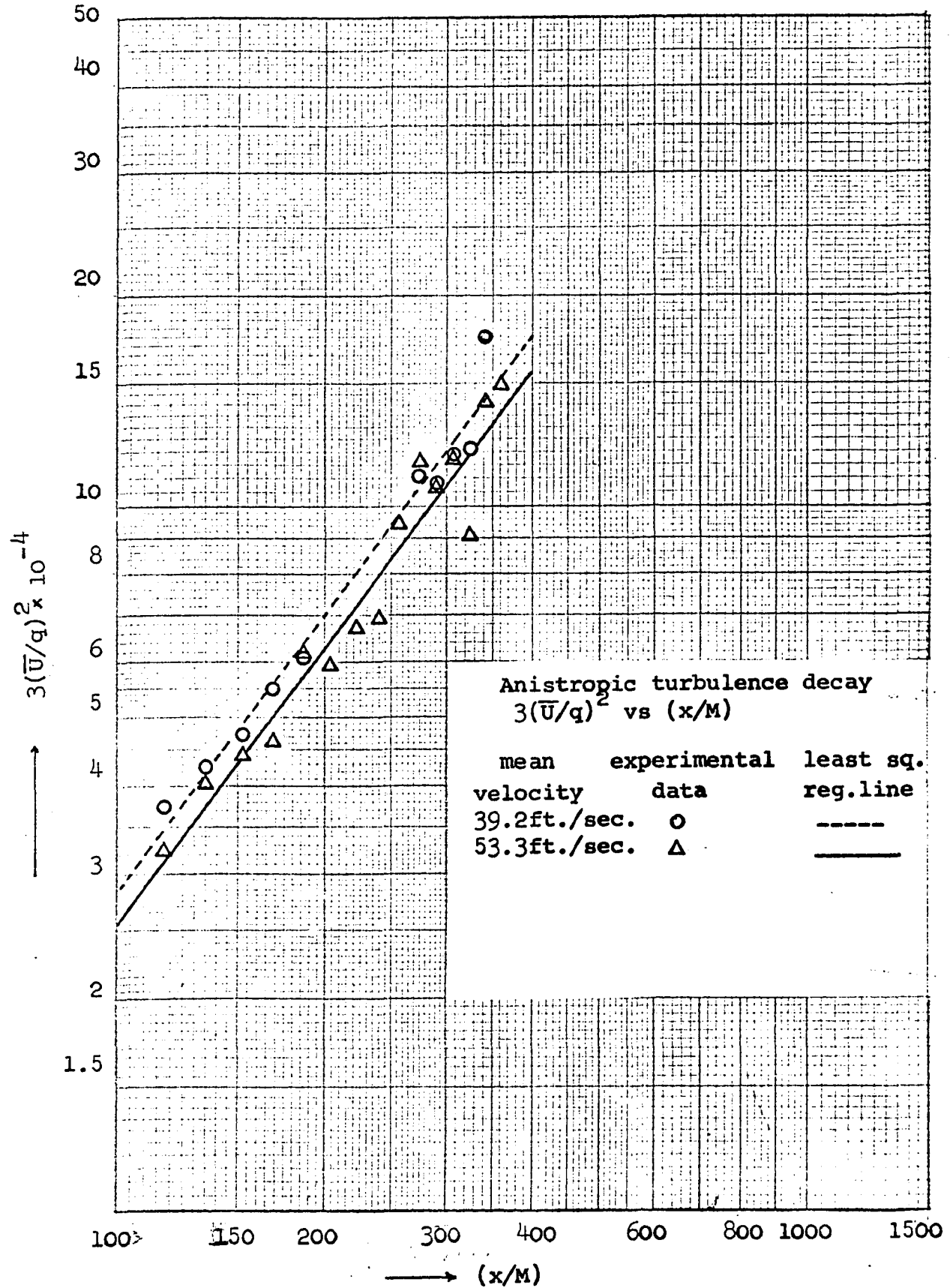


Fig.8

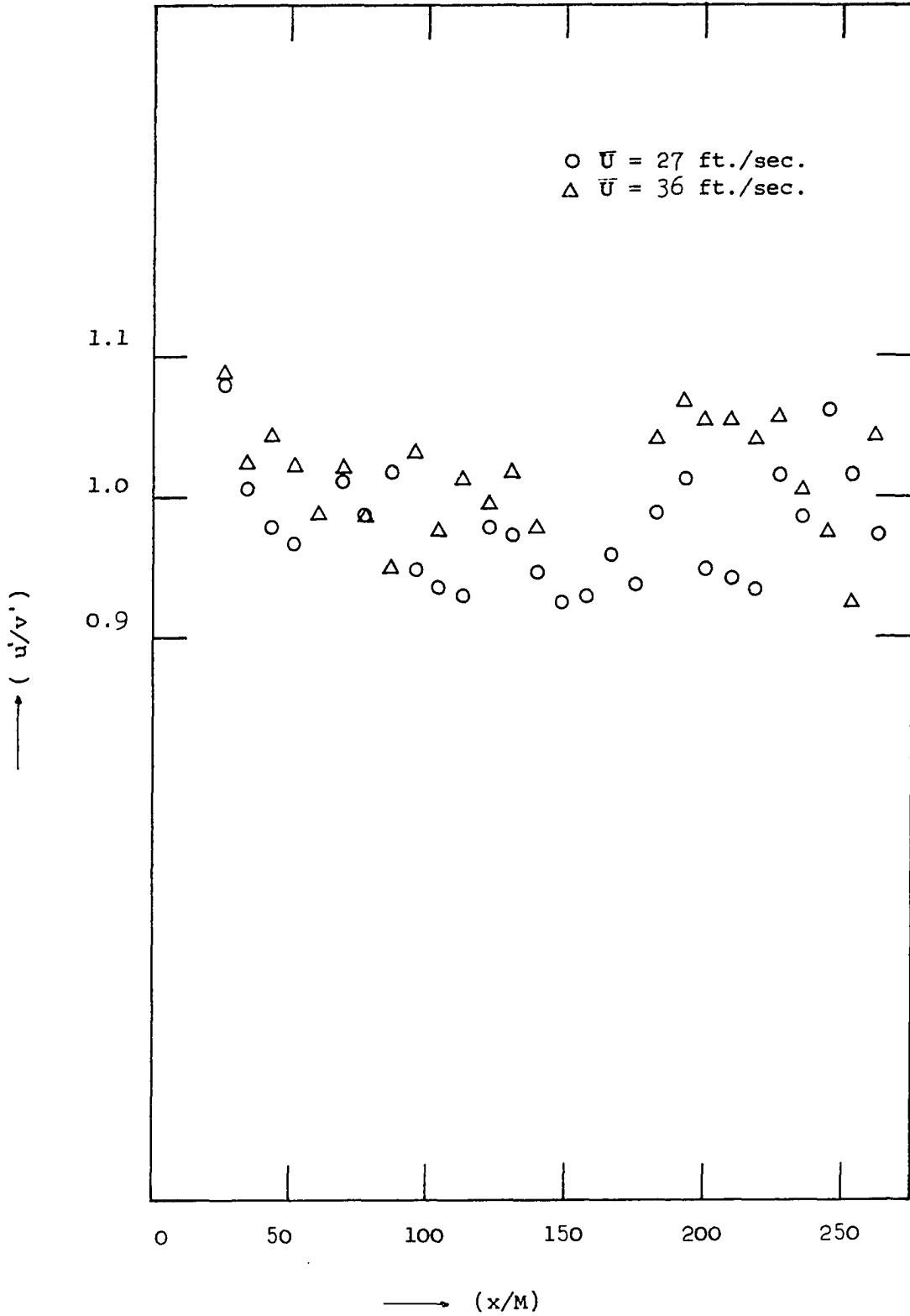


Fig.9 Change in  $u'/v'$  in nearly isotropic turbulence during decay.

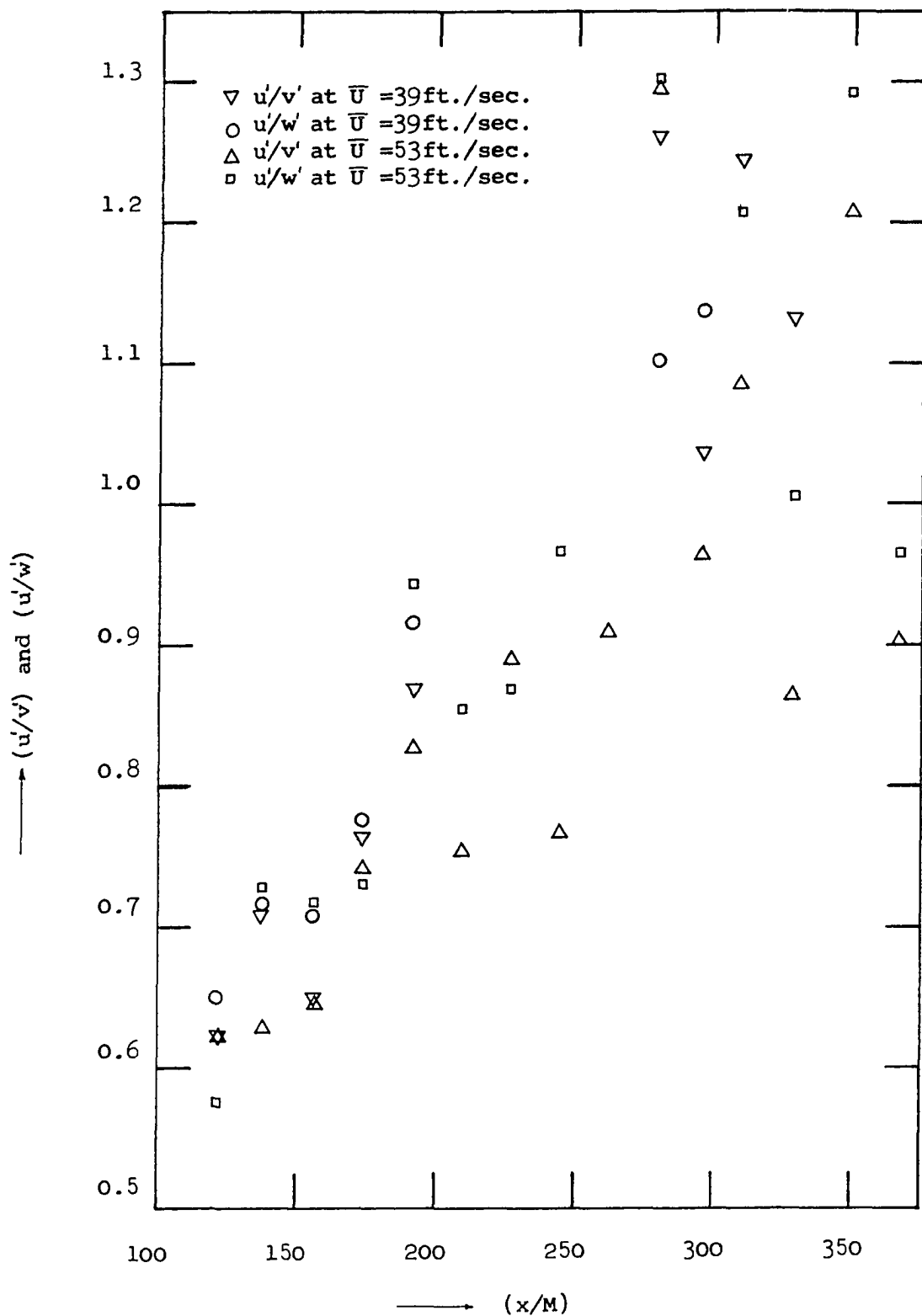


Fig.10 Change in  $u'/v'$  and  $u'/w'$  in anisotropic Turbulence during decay.

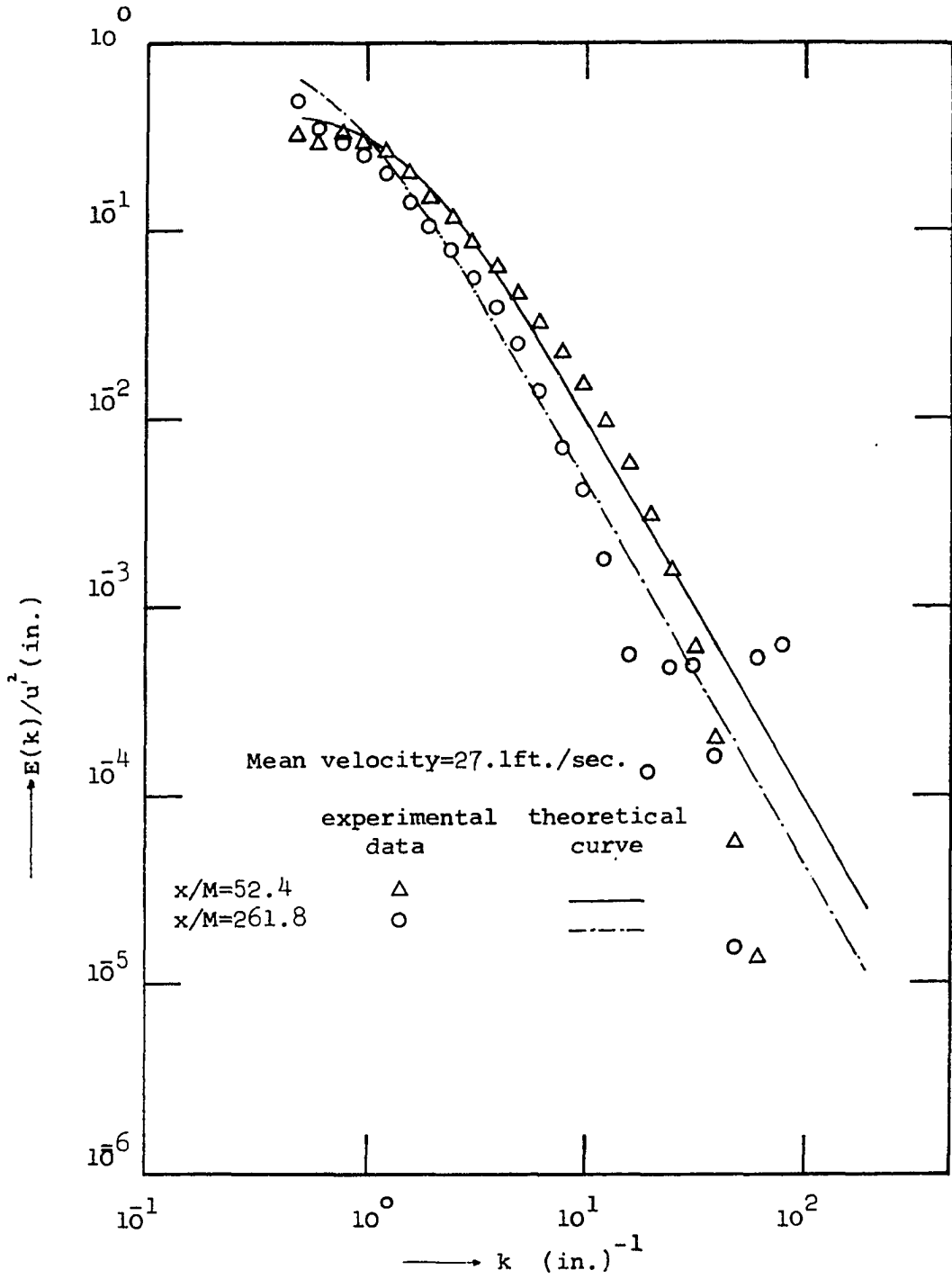


Fig.11 Spectra of  $u'$  in nearly isotropic turbulence.

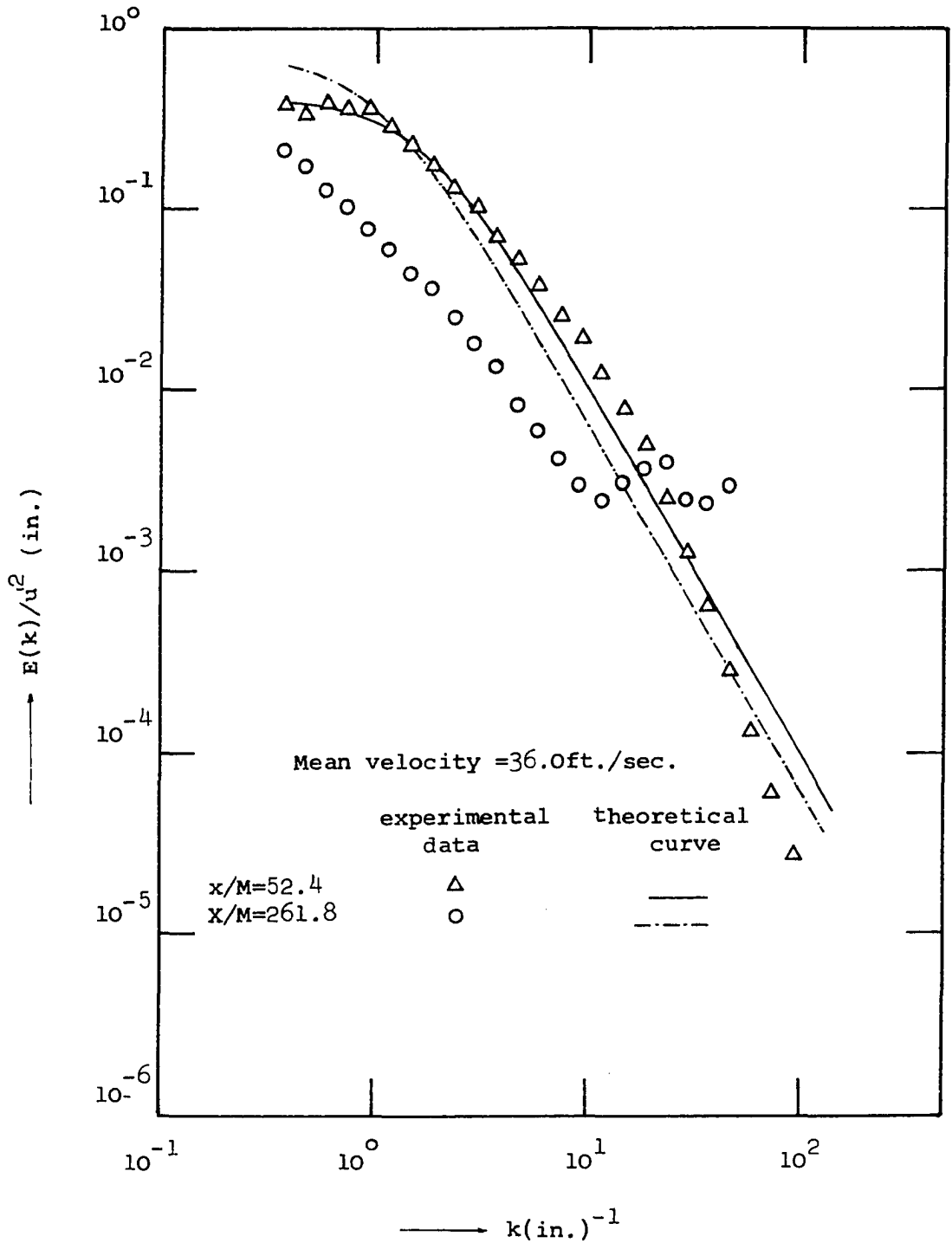


Fig.12 Energy spectra of  $u'$  in isotropic turbulence

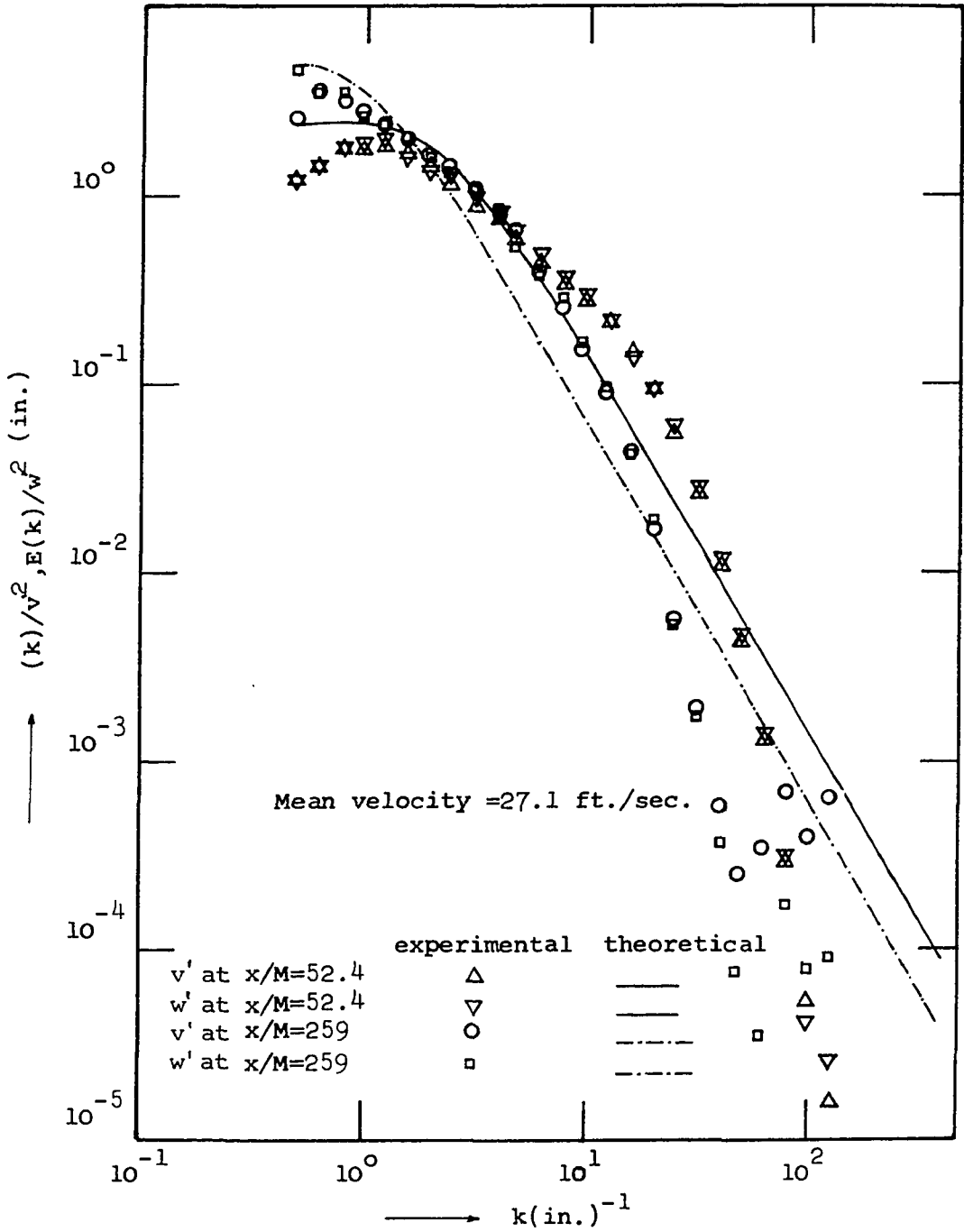


Fig.13 Energy spectra of  $v'$  and  $w'$  in nearly isotropic turbulence.



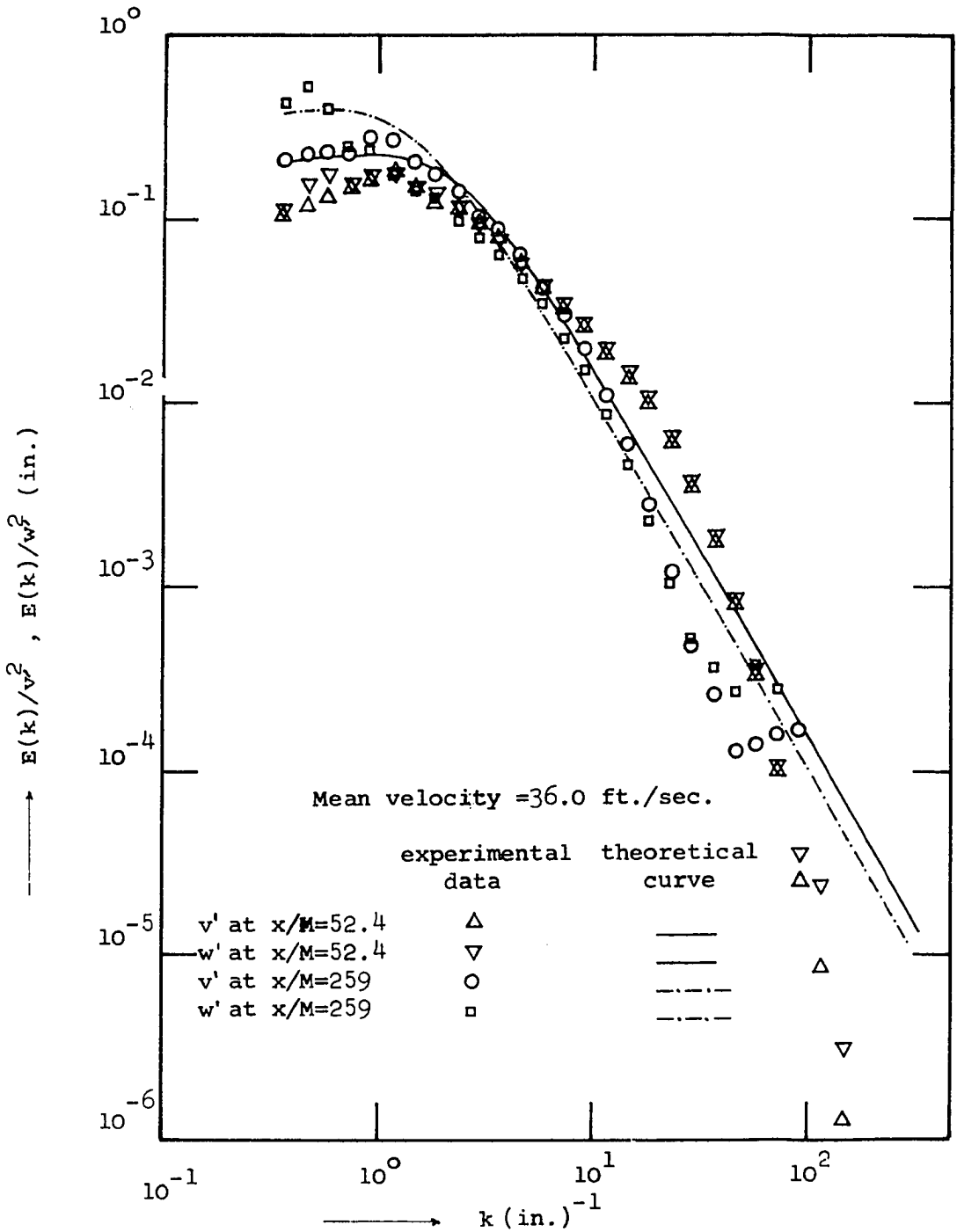


Fig.14 Energy spectra of  $v$  and  $w$  in nearly isotropic turbulence.

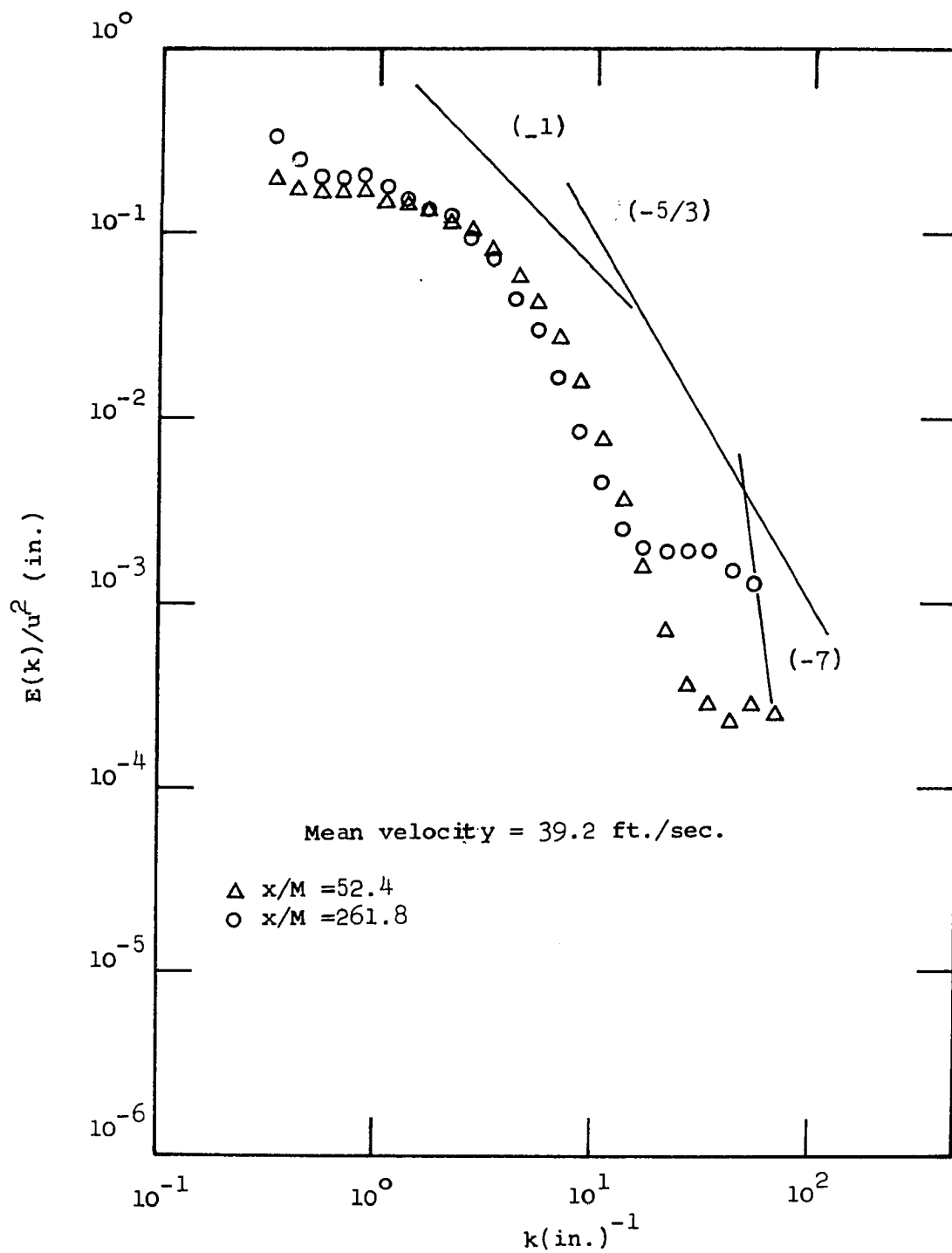


Fig.15 Energy spectra of  $u'$  in anisotropic turbulence

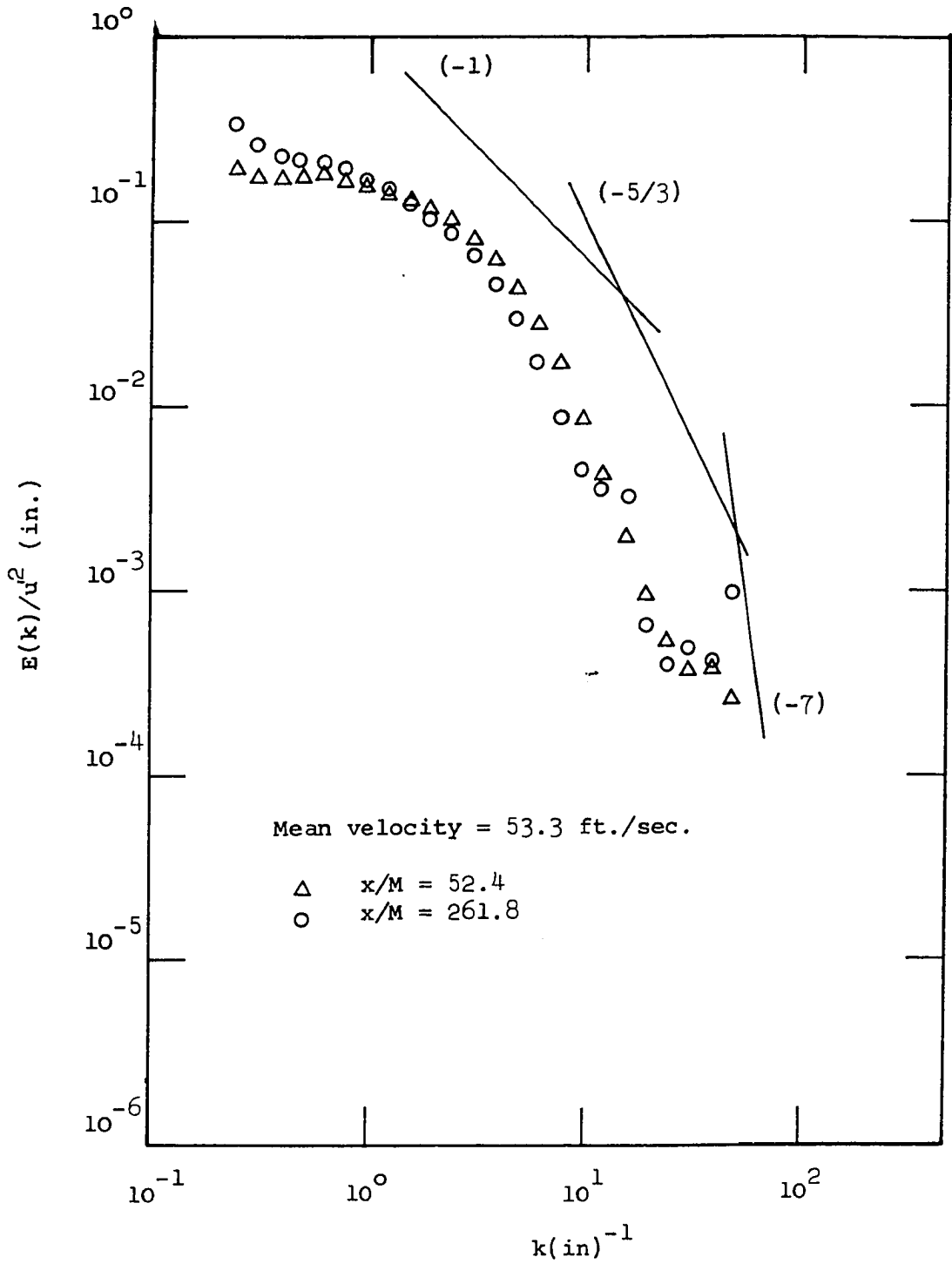


Fig.16 Energy spectra of  $u'$  in anisotropic turbulence.

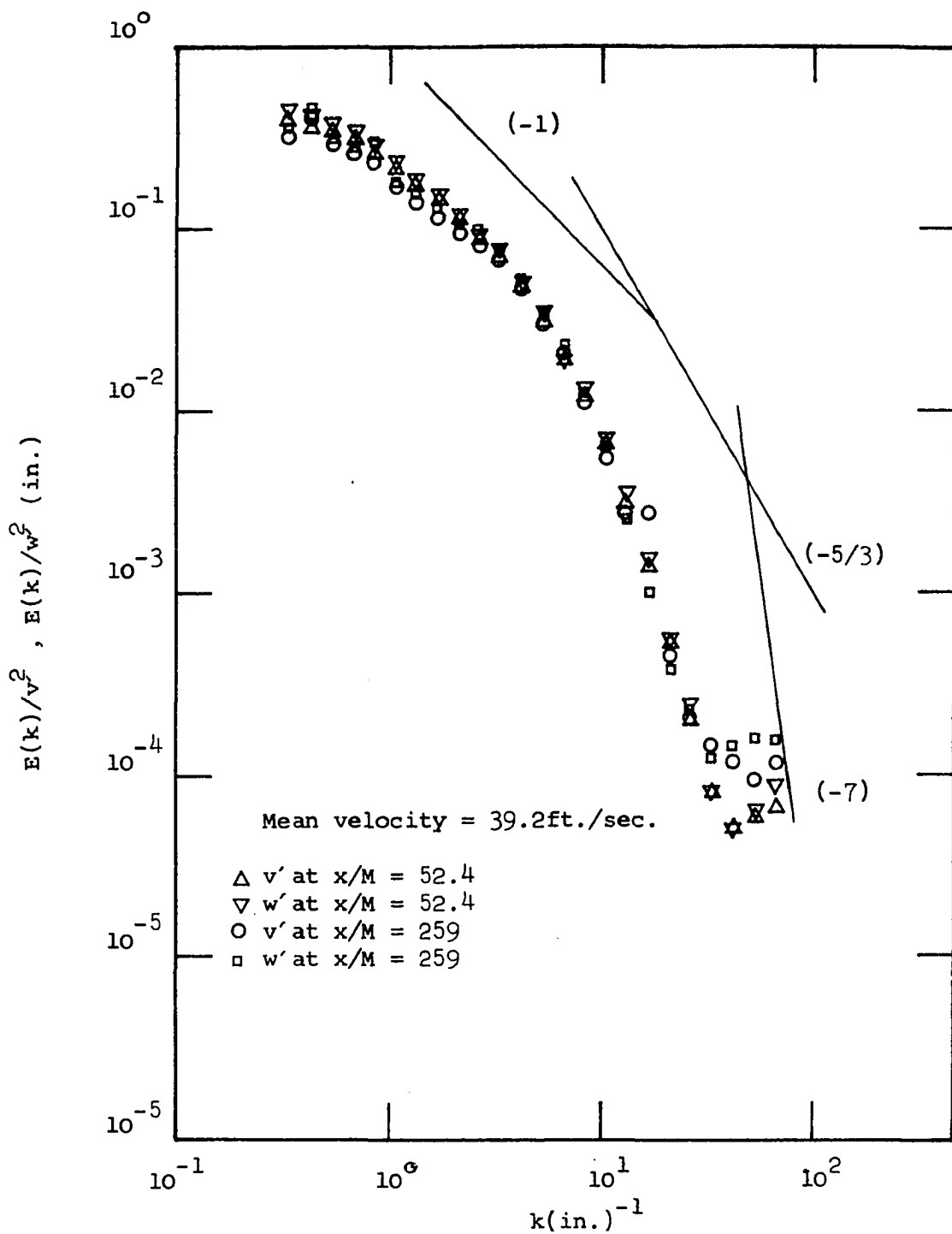


Fig.17 Energy spectra of  $v'$  and  $w'$  in anisotropic turbulence

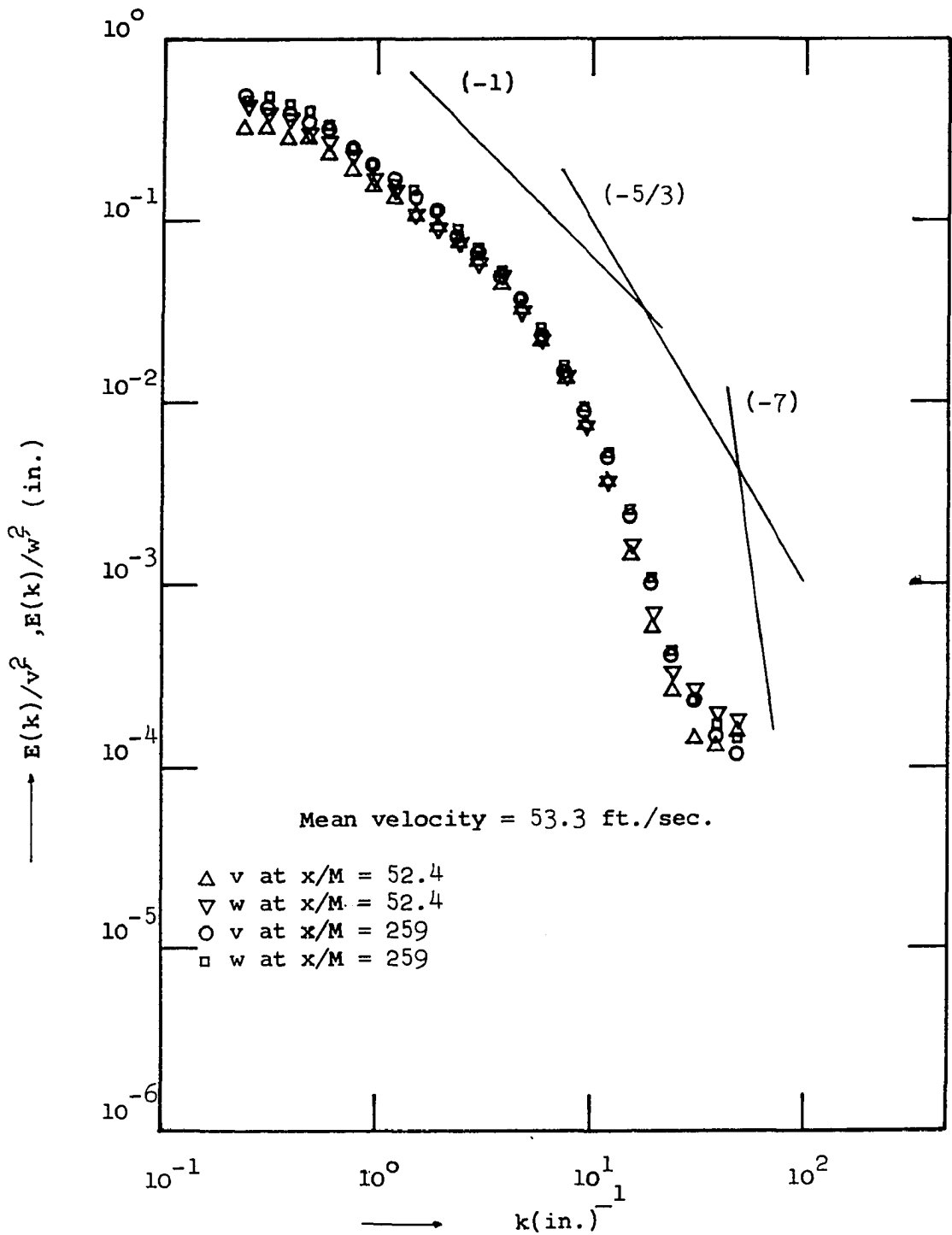


Fig.18 Energy spectra of  $v'$  and  $w'$  in anisotropic turbulence.

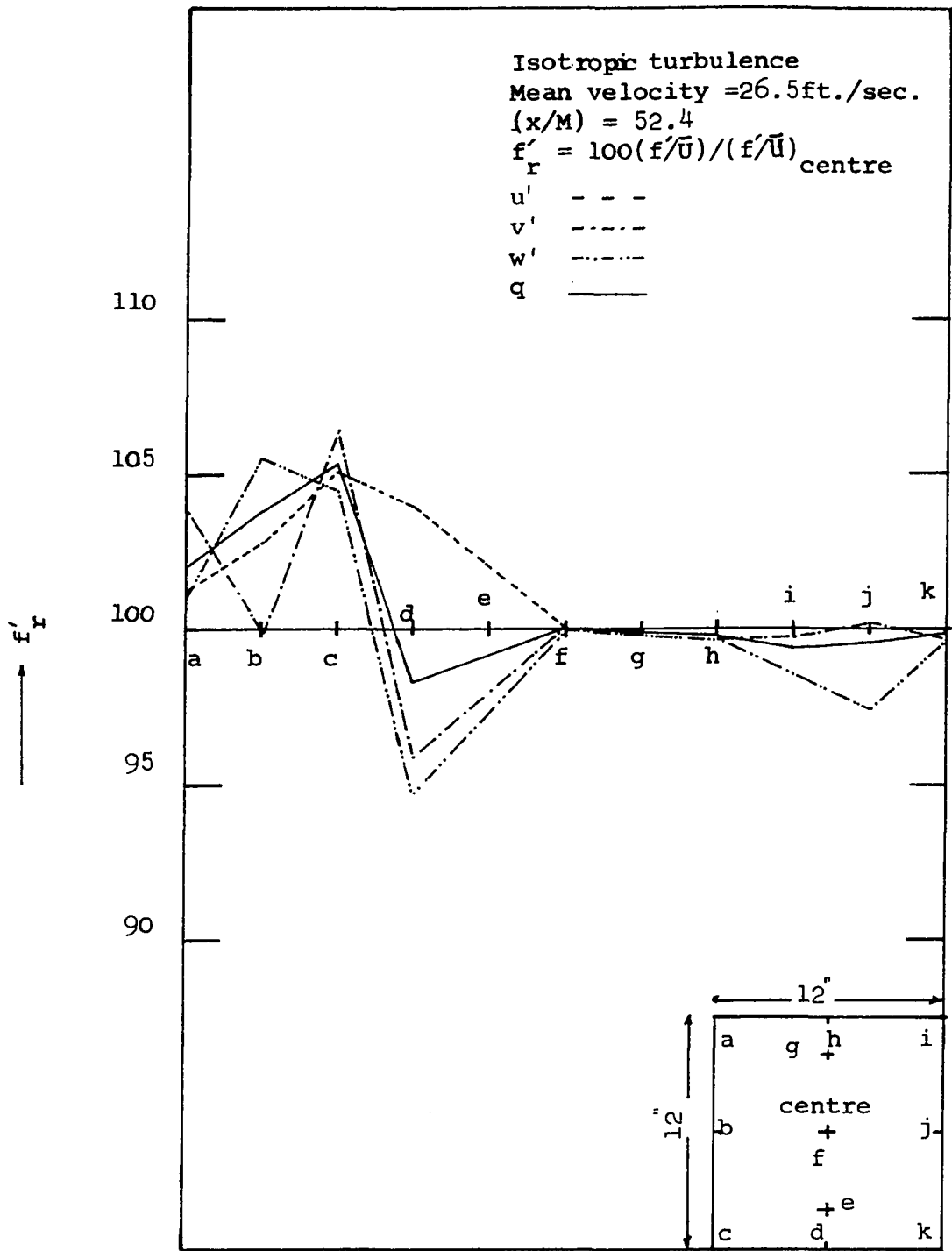


Fig.19 Homogeneity of turbulence in a plane normal to the direction of flow.

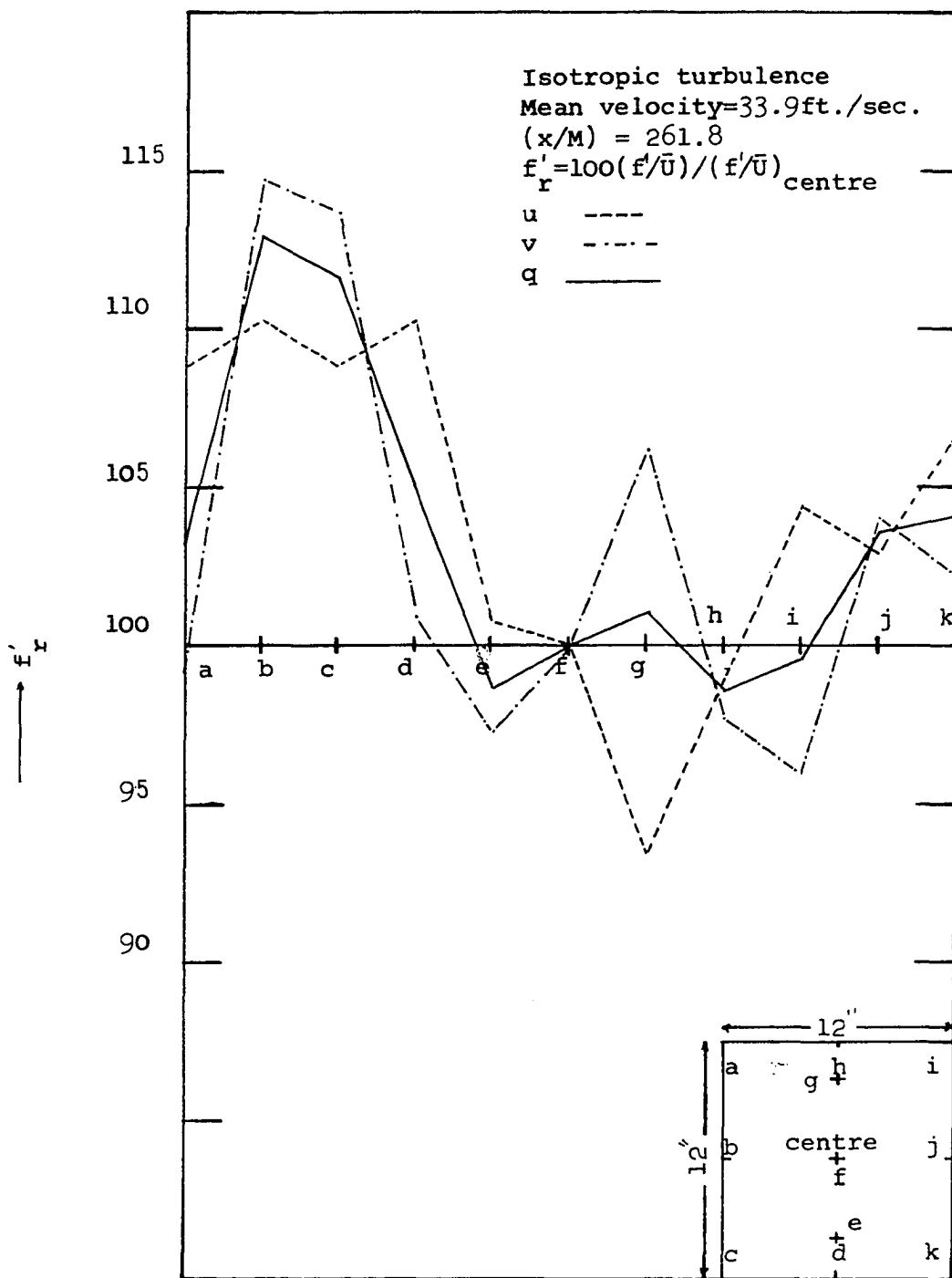


Fig.20 Homogeneity of turbulence in a plane normal to the direction of flow.

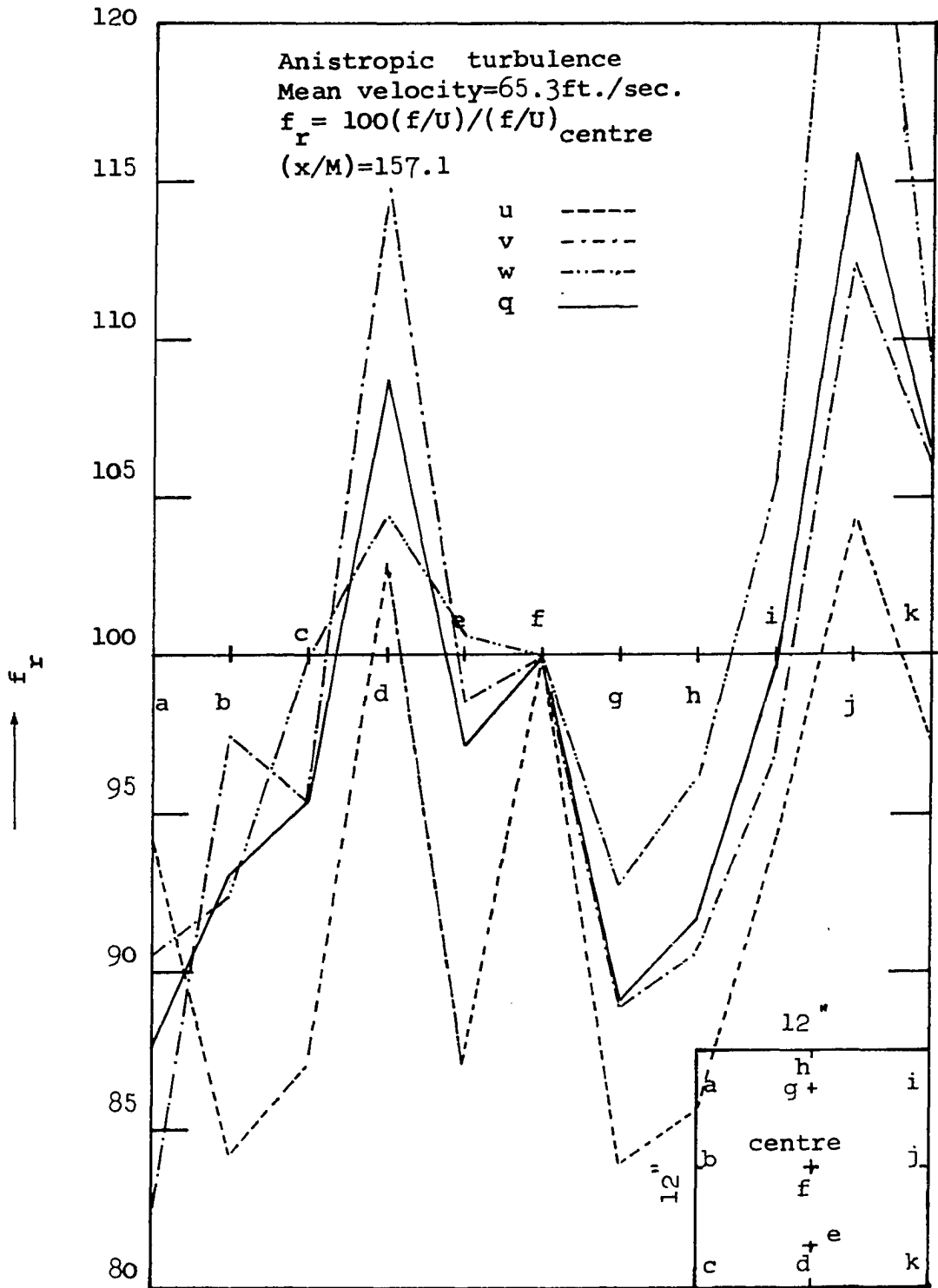


Fig.21 Homogeneity of turbulence in a plane normal to the direction of flow.



- 1 TEST SECTION
- 2 SMALL BEND
- 3 TRANSITION SQUARE TO ROUND
- 4 CIRCULAR BEND
- 5 MOTOR
- 6 DRIVING PULLEY FOR FAN
- 7a RETURN DUCT TRANSITION ROUND TO SQUARE
- 7b RETURN DUCT DIVERGING SECTION

- 8a LARGE BEND: BOTTOM
- 8b LARGE BEND: TOP
- 9 SCREENS
- 10 CONTRACTION LEADING TO TEST SECTION
- 11 PLATFORM
- 61 GRID POSITION TO GET NEARLY ISOTROPIC TURBULENCE
- 62 GRID POSITION TO GET STRONGLY ANISOTROPIC TURBULENCE

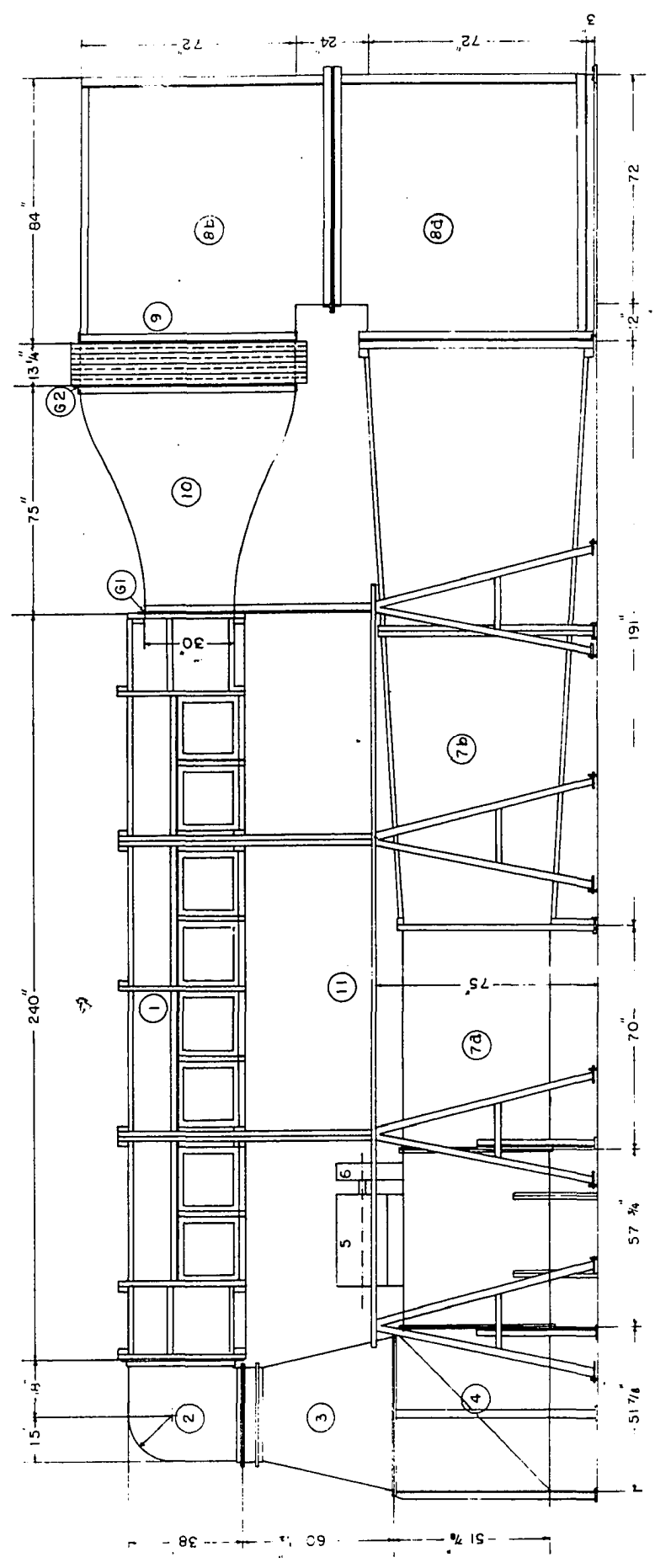


FIG.22 GENERAL VIEW OF THE WIND TUNNEL

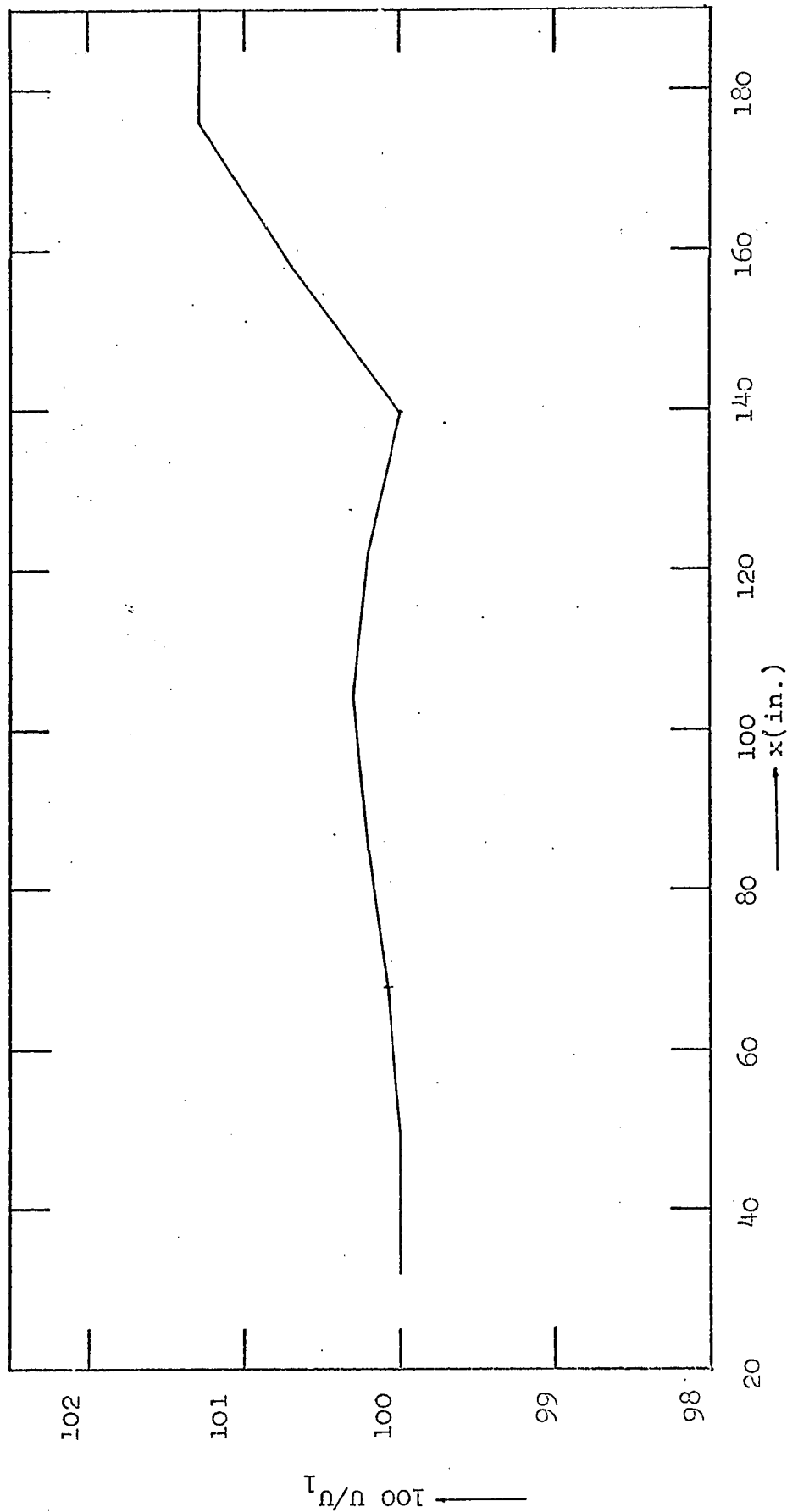


Fig.23 Mean velocity variation of flow along the centre line of the test section  
 ( $U_1$  = velocity at the starting point.)

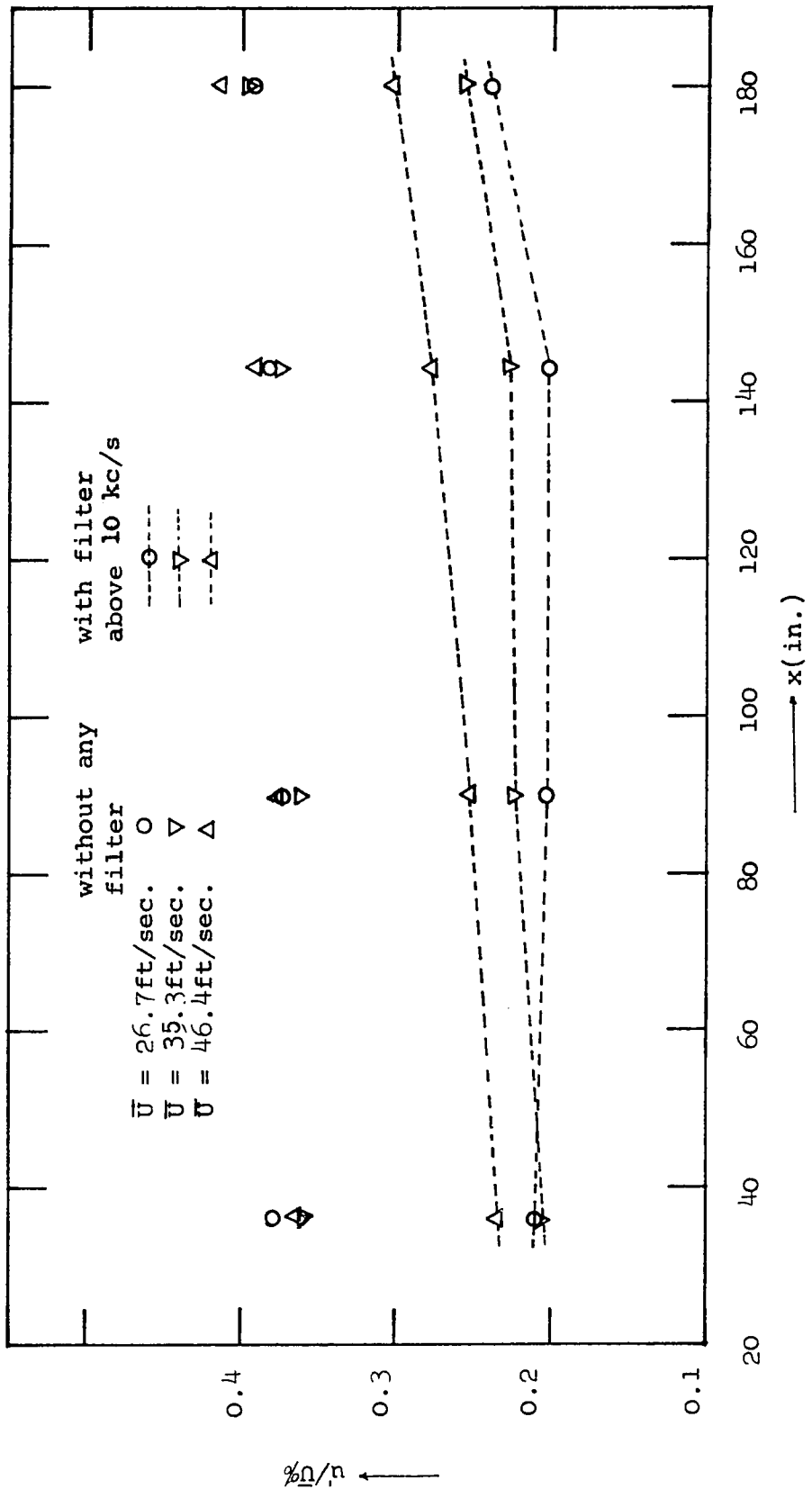


Fig.24 Longitudinal component of free stream turbulence( plus instrument noise ) at different velocities and frequency ranges.

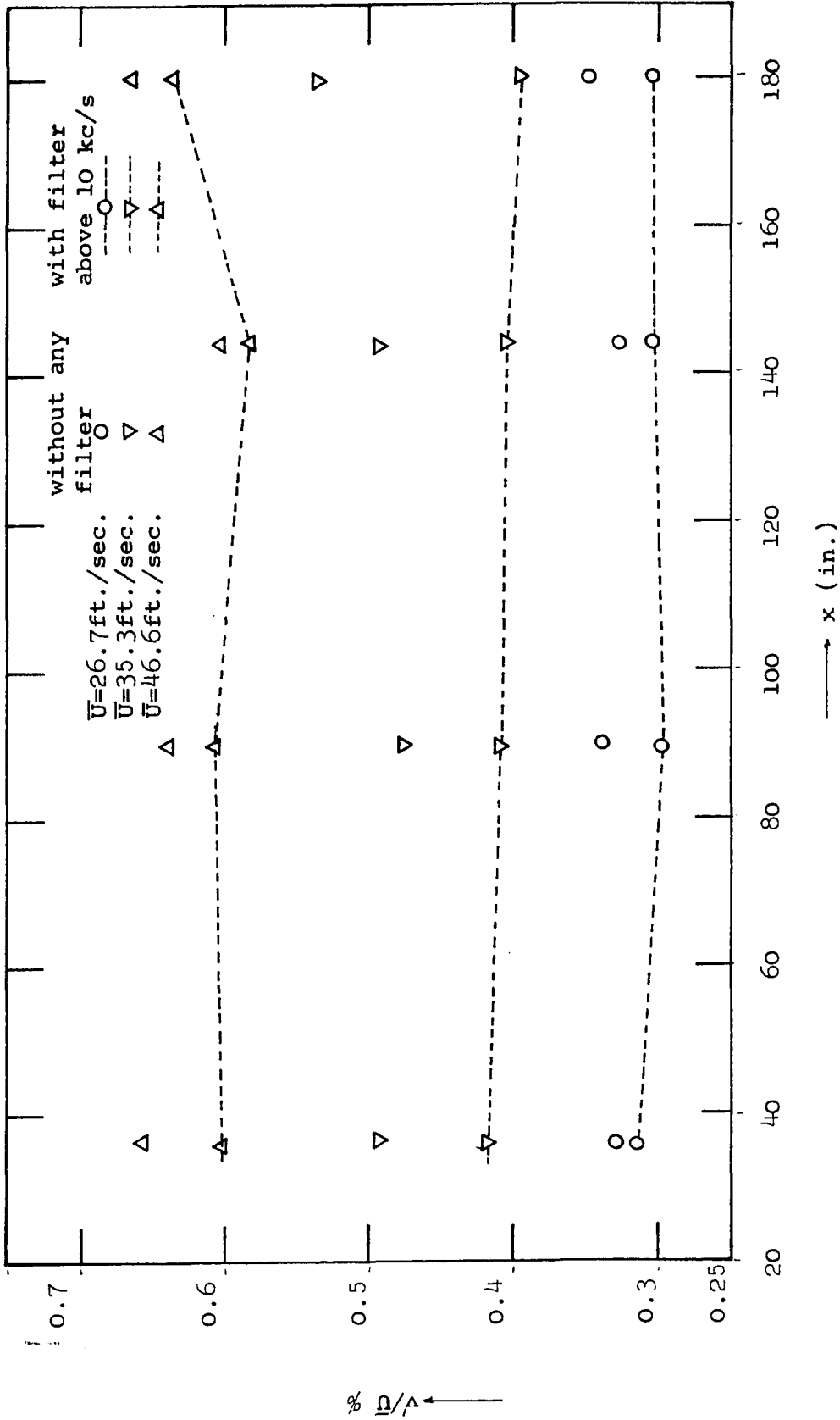


Fig.25 Transverse component of free stream turbulence ( plus instrument noise ) at different velocities and frequency ranges.

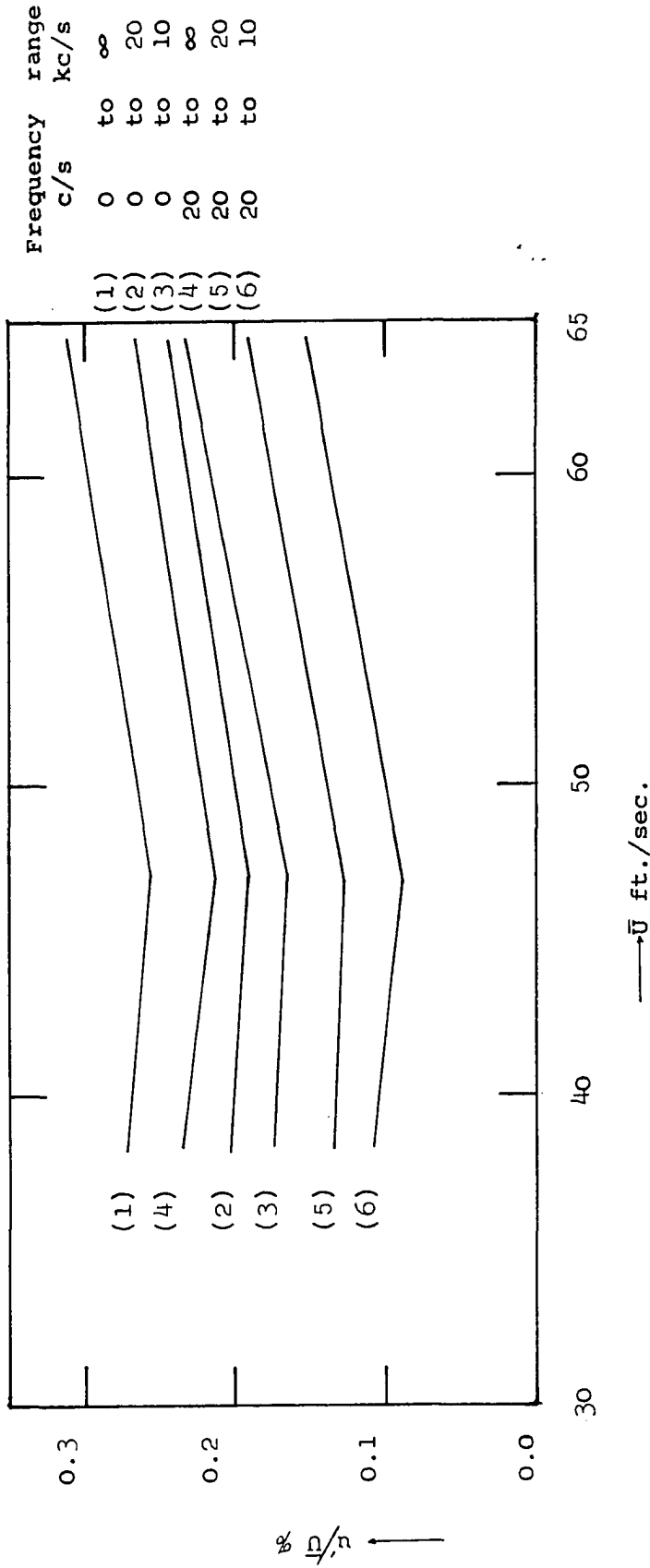


Fig.26 Longitudinal component of free stream turbulence in the wind tunnel in different frequency ranges measured at the centre line of the test section at  $x = 36$  in.

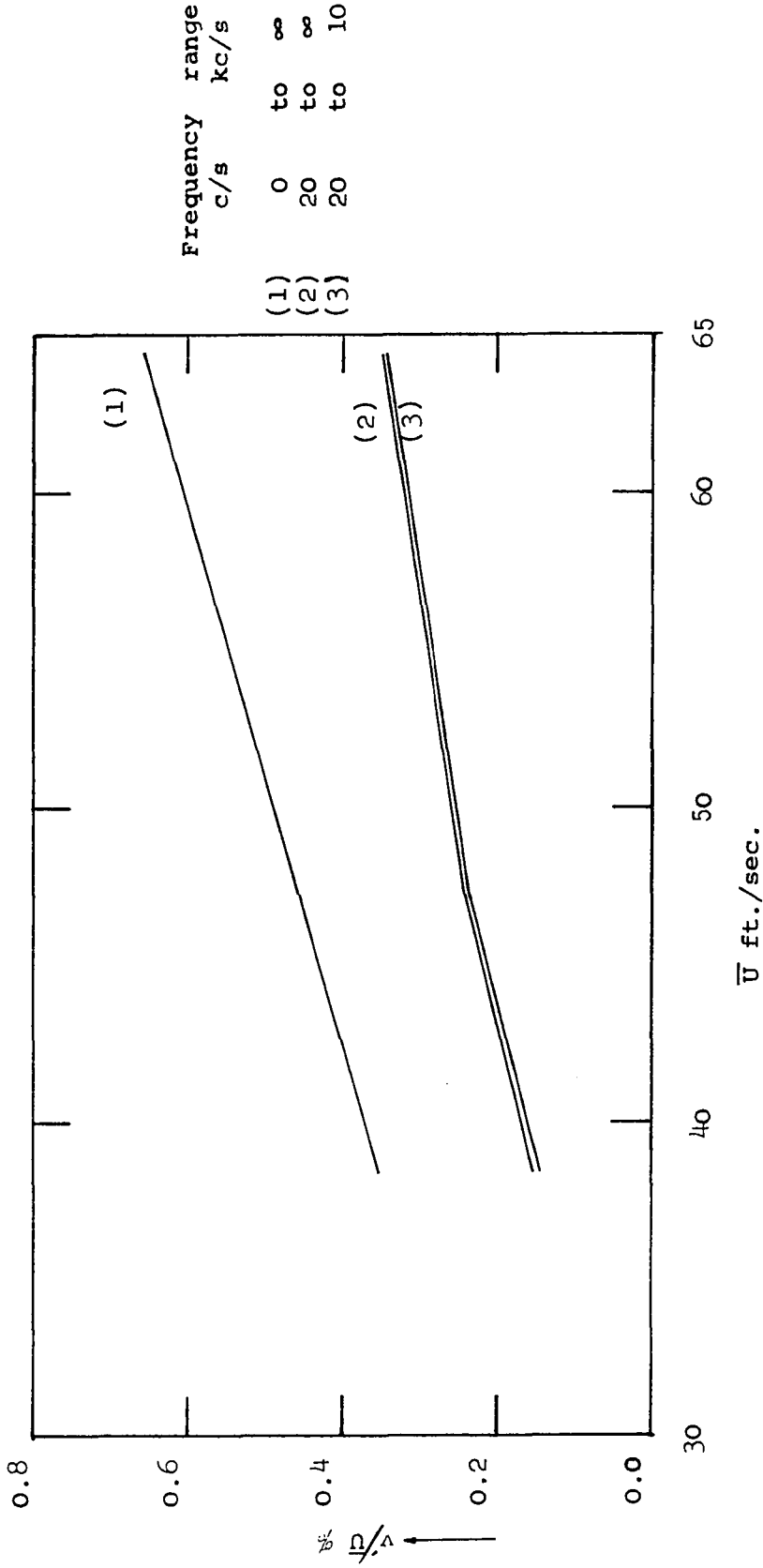


Fig.27 Transverse component of free stream turbulence in the wind tunnel in different frequency ranges measured at the centre line of the test section at  $x = 36$  in.

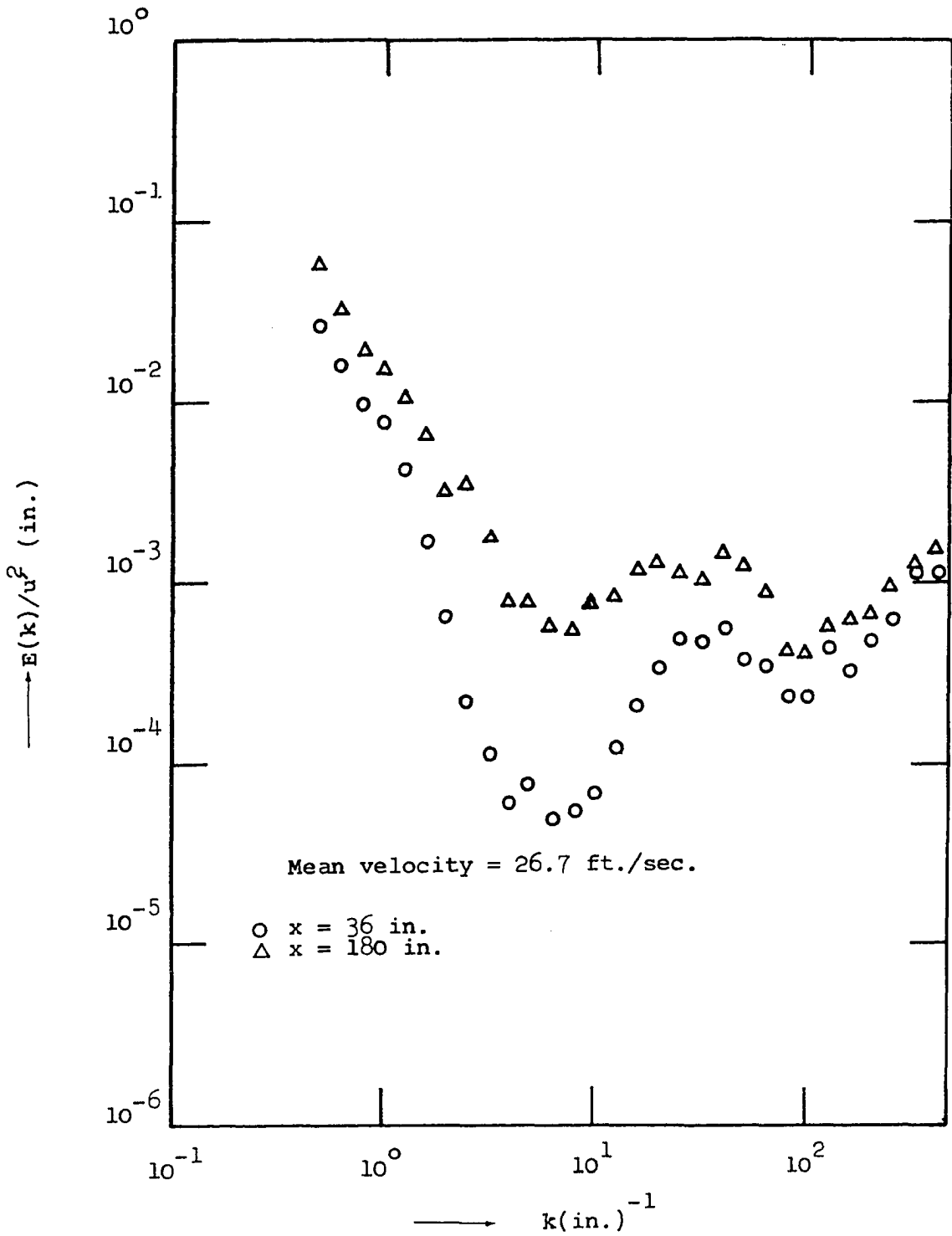


Fig.28 Energy spectra of  $u'$  in free stream turbulence in the wind tunnel.

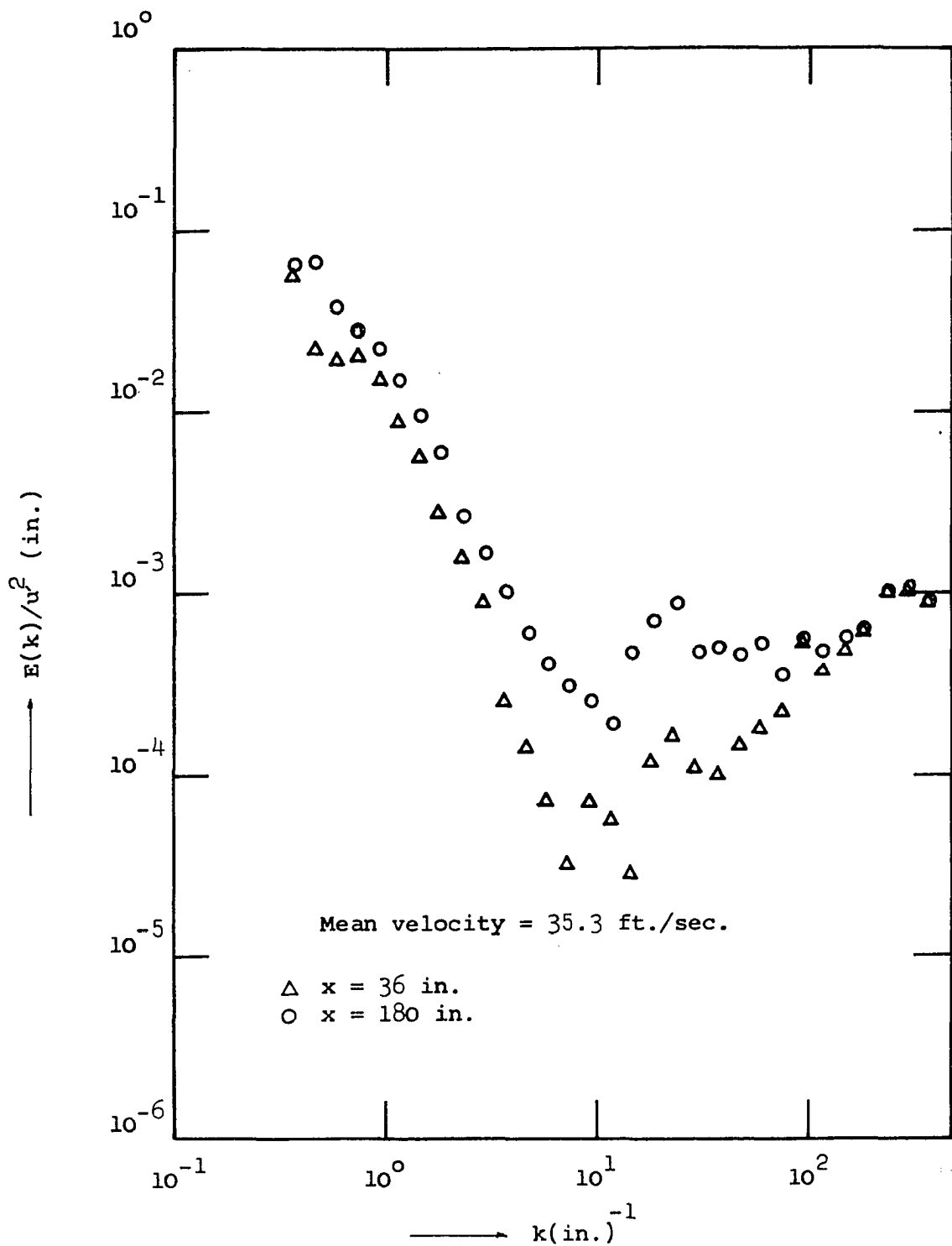


Fig. 29 Energy spectra of  $u'$  in free stream turbulence in the wind tunnel.



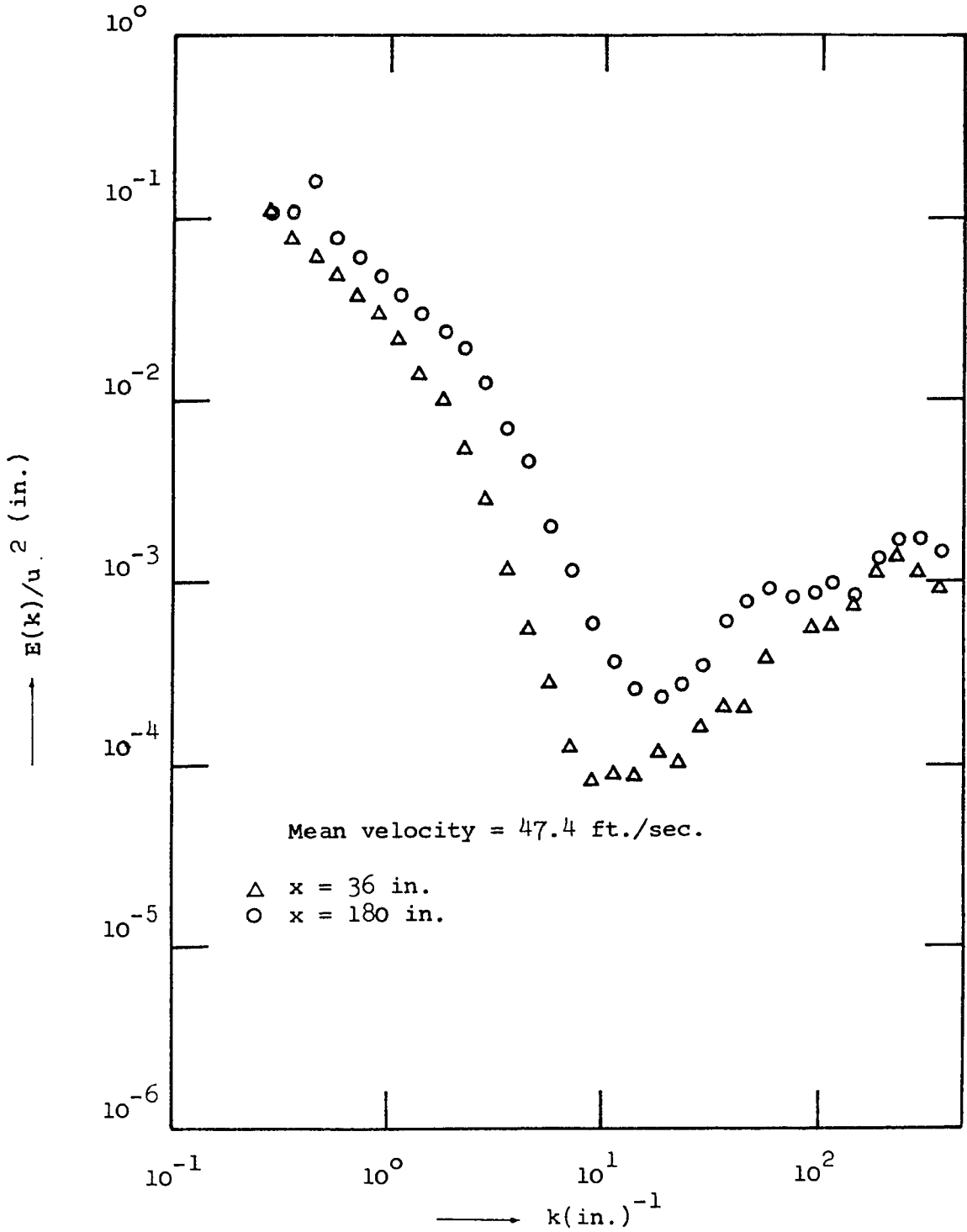


Fig.30 Energy spectra of  $u'$  in free stream turbulence in the wind tunnel.

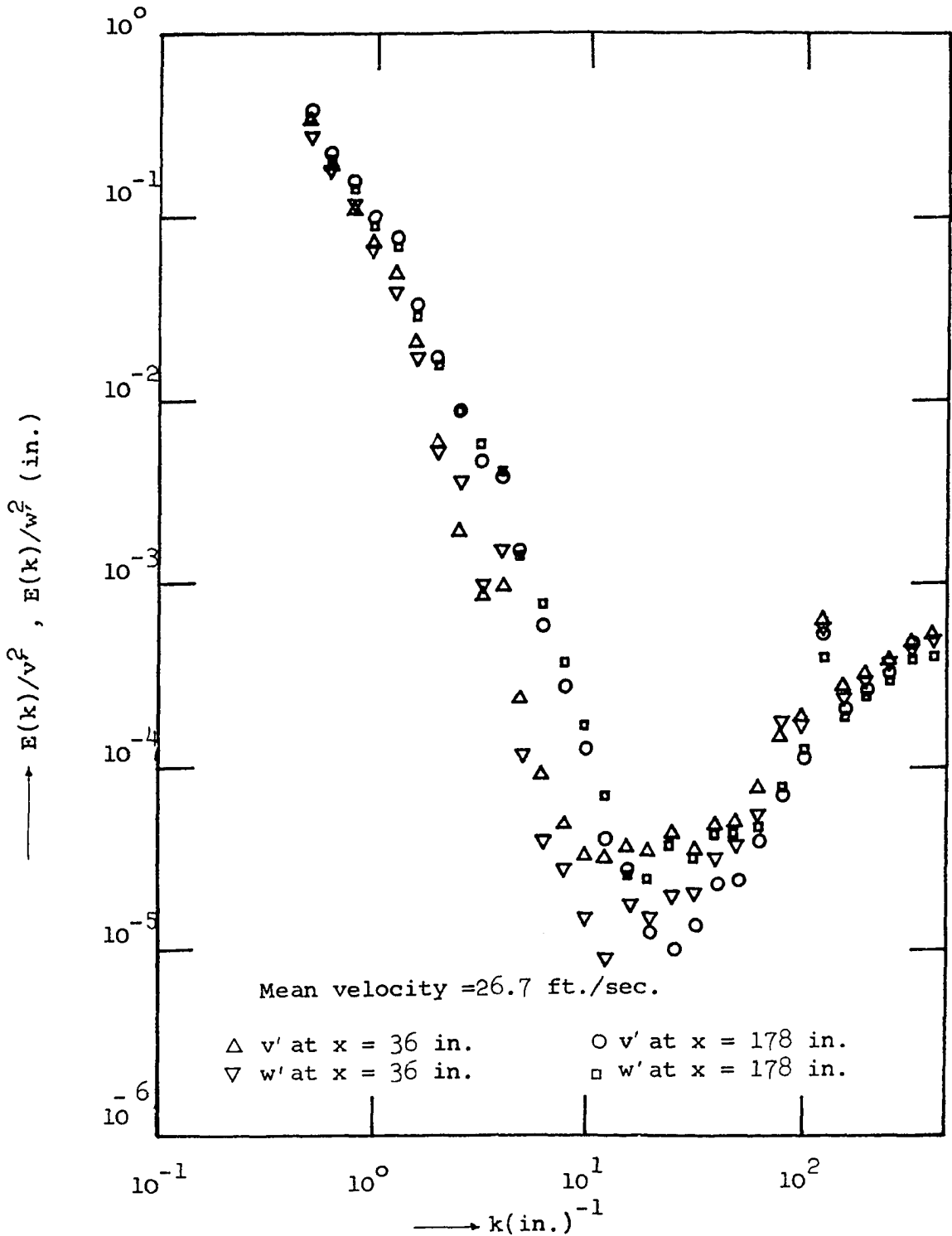


Fig.31 Energy spectra of  $v$  and  $w$  in free stream turbulence in the wind tunnel.

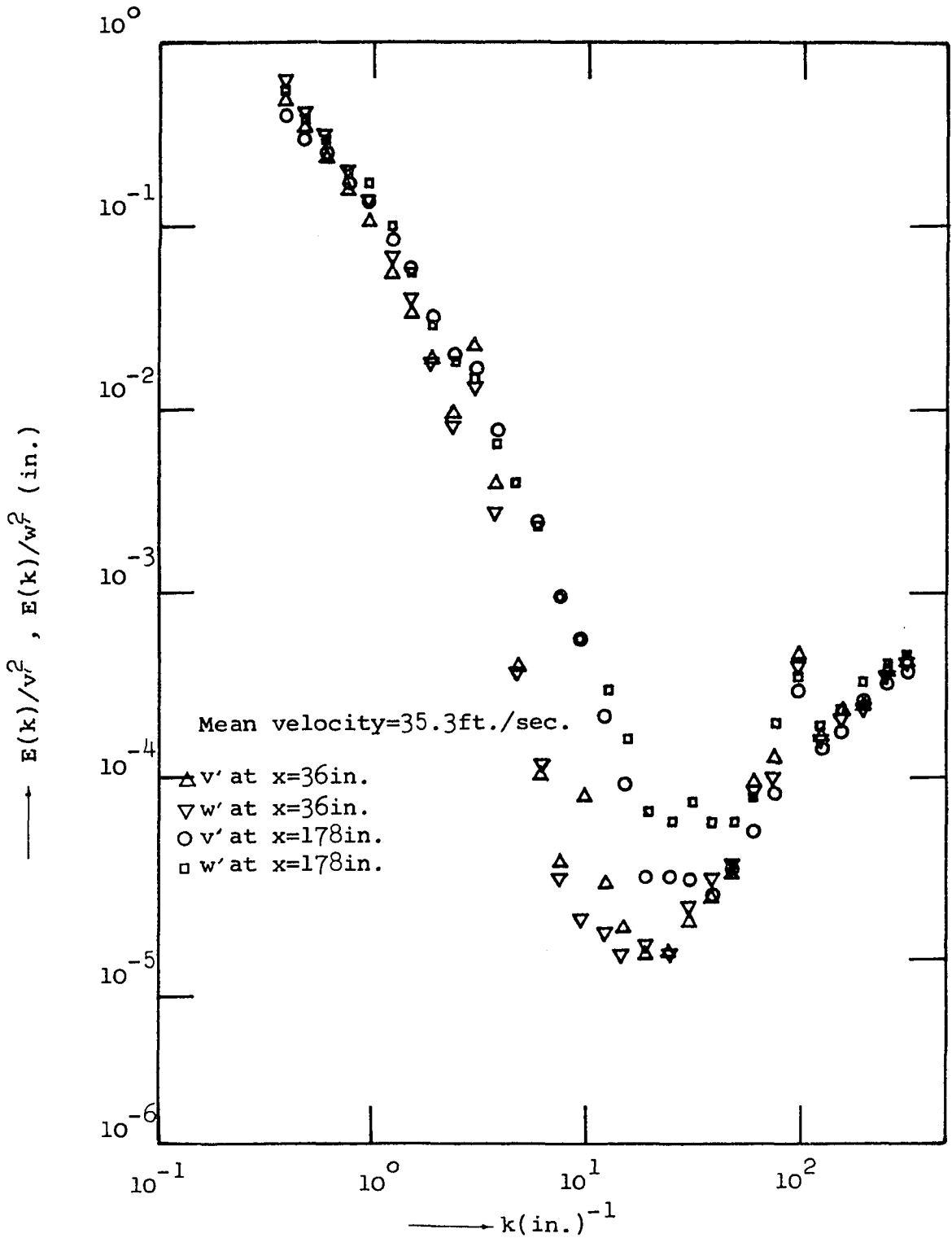


Fig.32 Energy spectra of v and w in free stream turbulence in the wind tunnel.

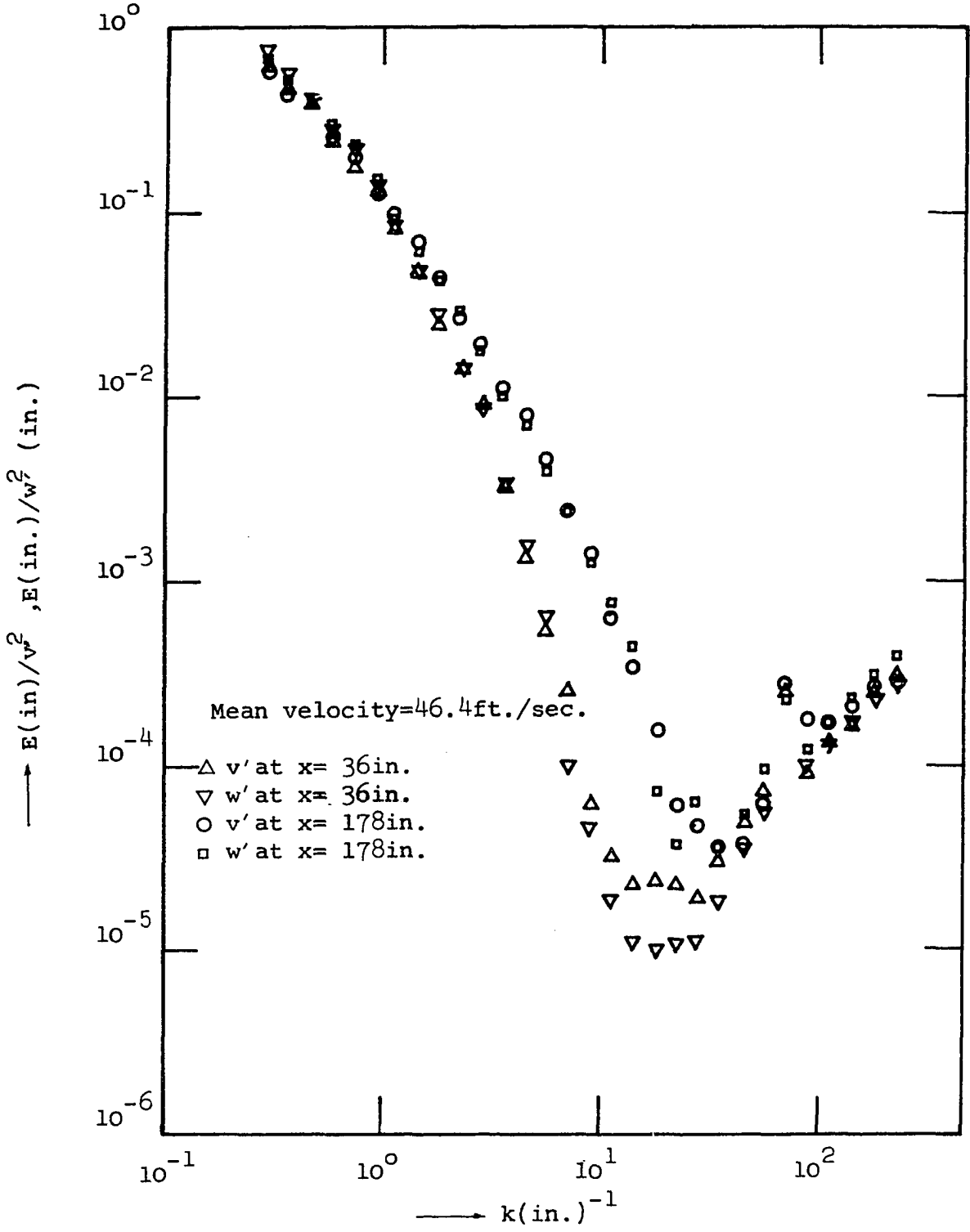


Fig.33 Energy spectra of  $v'$  and  $w'$  in free stream turbulence in the wind tunnel.

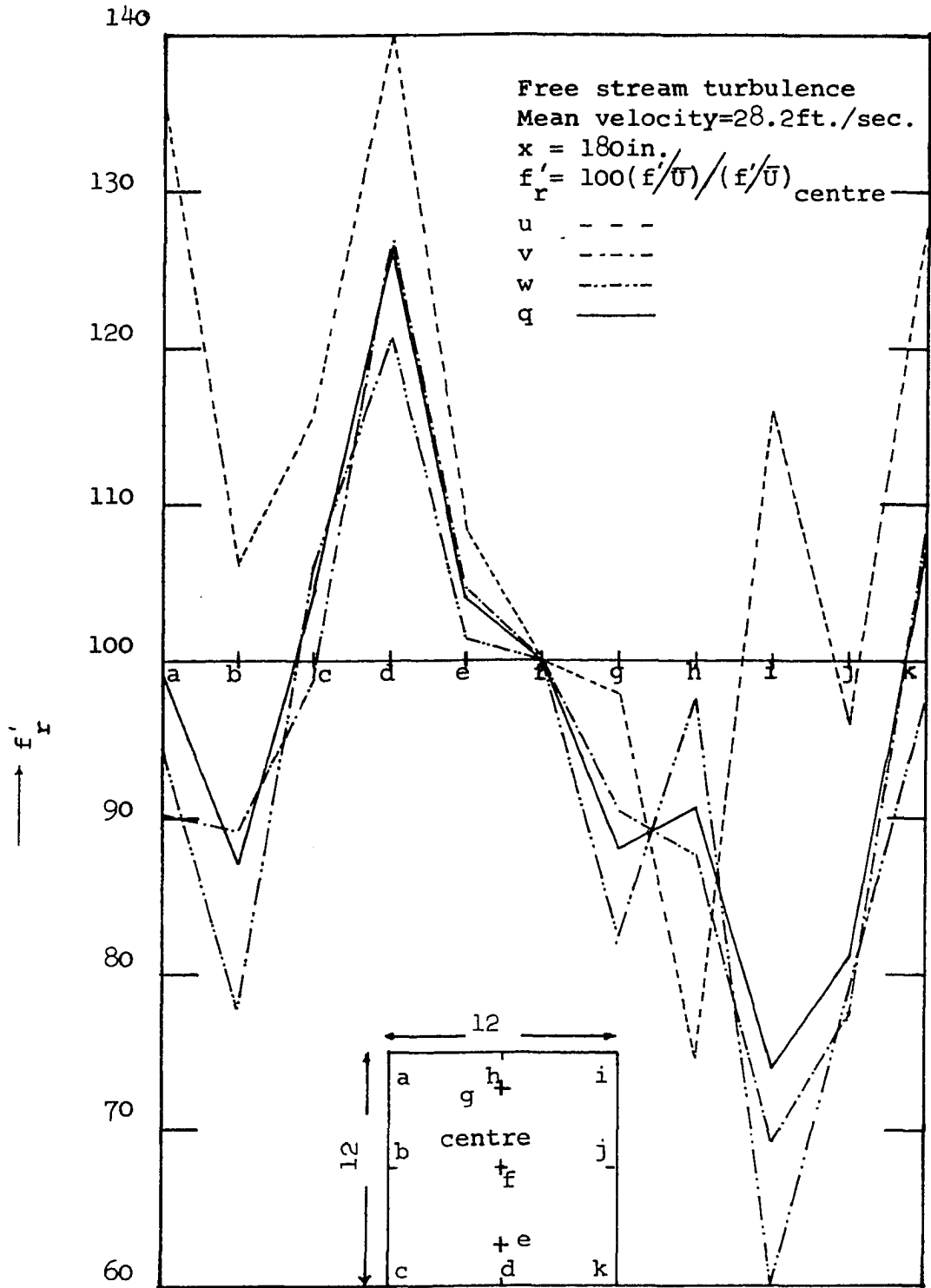
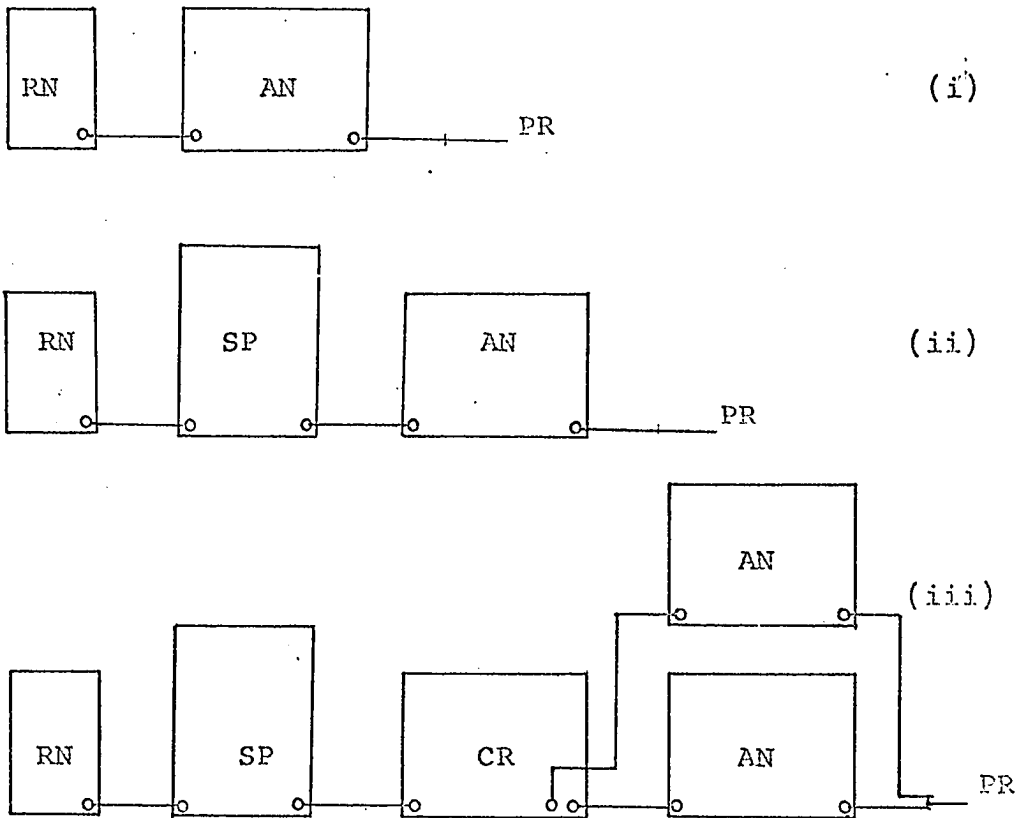


Fig. 34 Homogeneity of turbulence in a plane normal to the direction of flow.

PR Hot wire probe  
 AN Hot wire anemometer  
 RN Random noise voltmeter  
 SP Spectrometer  
 CR Random signal indicator and correlator.



- (i) Measurement of  $u, v,$  and  $w$   
 (ii) Measurement of energy spectra for  $u$   
 (iii) Measurement of energy spectra for  $v$  and  $w$

Fig.35 Arrangement of measuring instruments for different turbulence quantities.

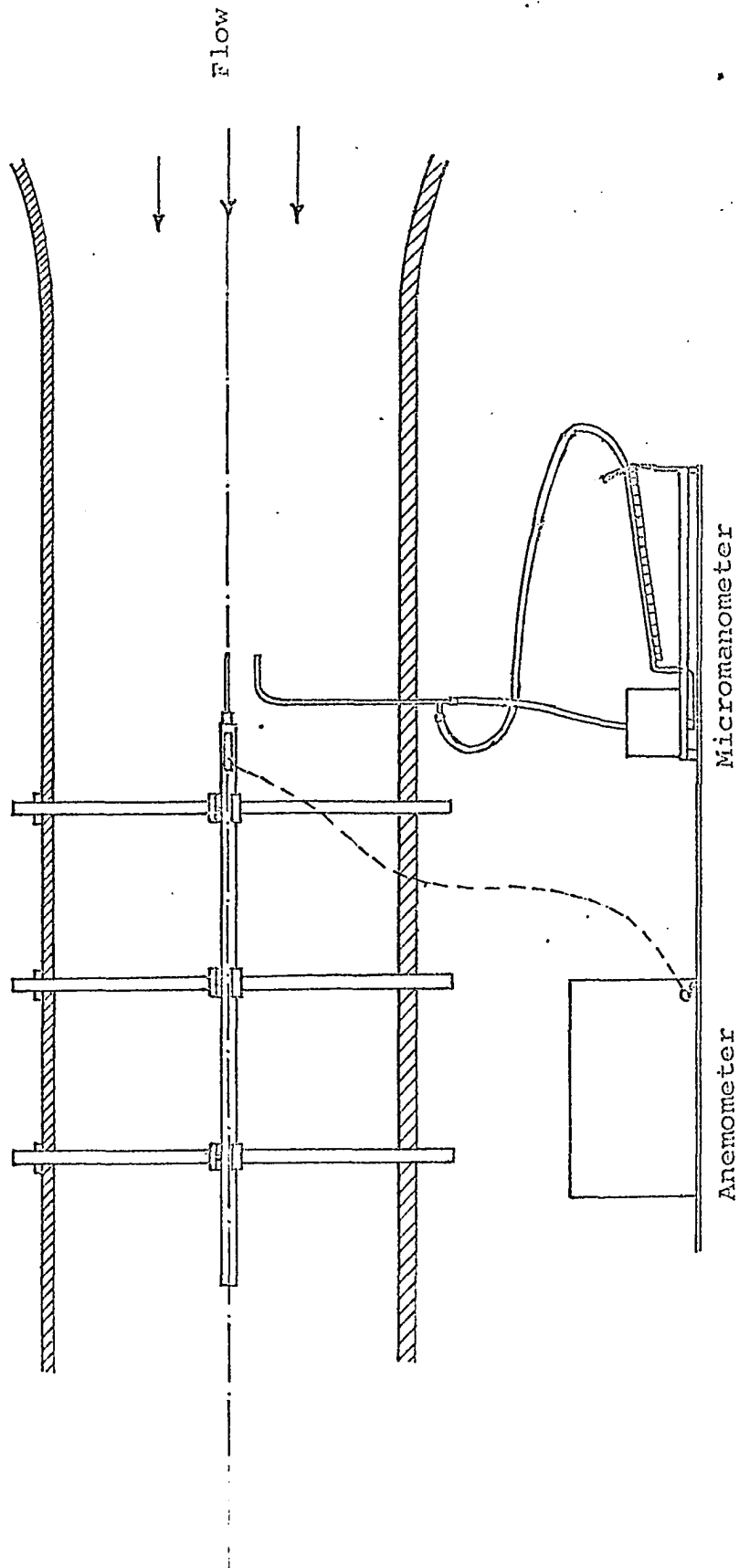
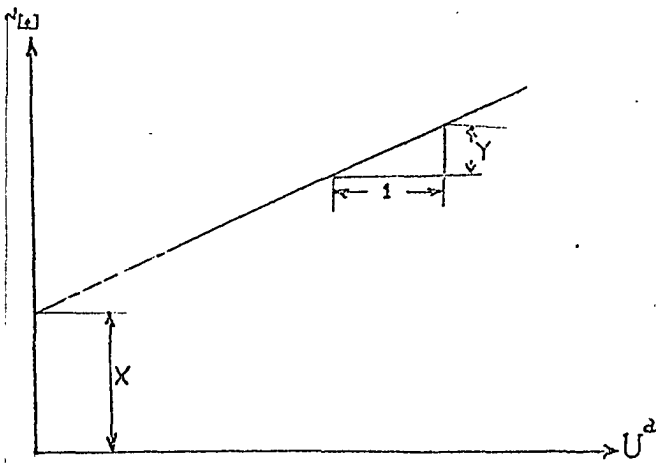
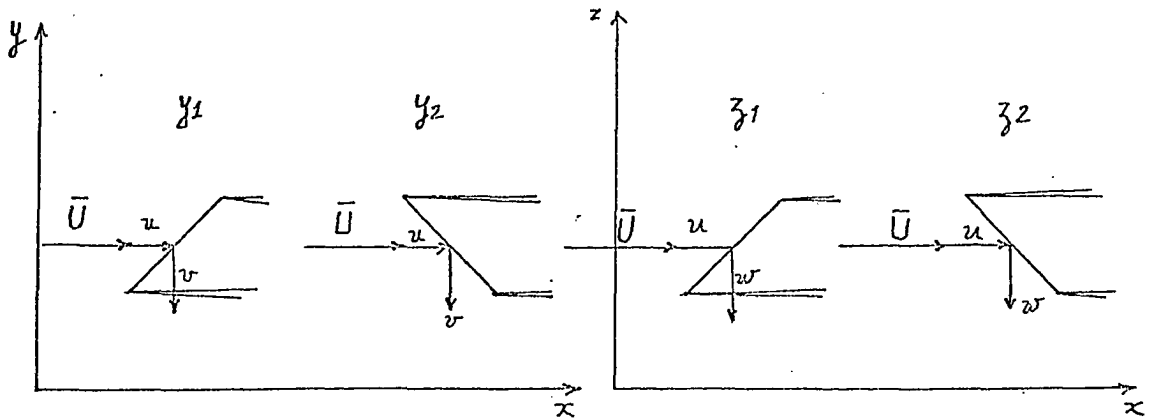
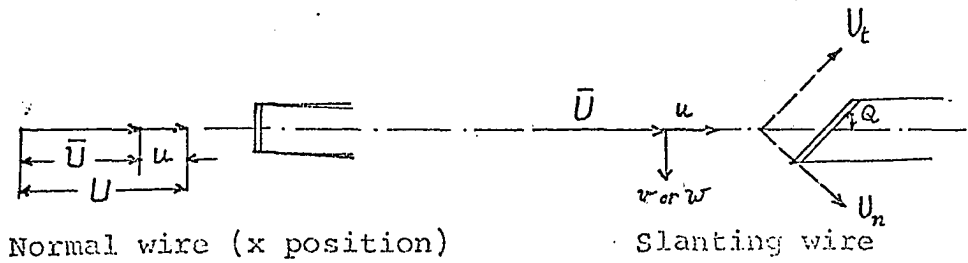


Fig. 36 Schematic view of the probing arrangement in the test section (pitot static probe is inserted only for calibration of hot wire.)



(i) Linear relationship between  $E^2$  and  $U^a$  for a hot wire.



(ii) Positions of normal and slanting wires w.r.t. the flow direction for measuring the three turbulence intensities.

fig.37a





(a) Magnified view of normal hot wire probe.



(b) Magnified view of slanting hot wire probe.

Fig.37 b



(c) Magnified view of X hot wire probe.

Fig. 37 b

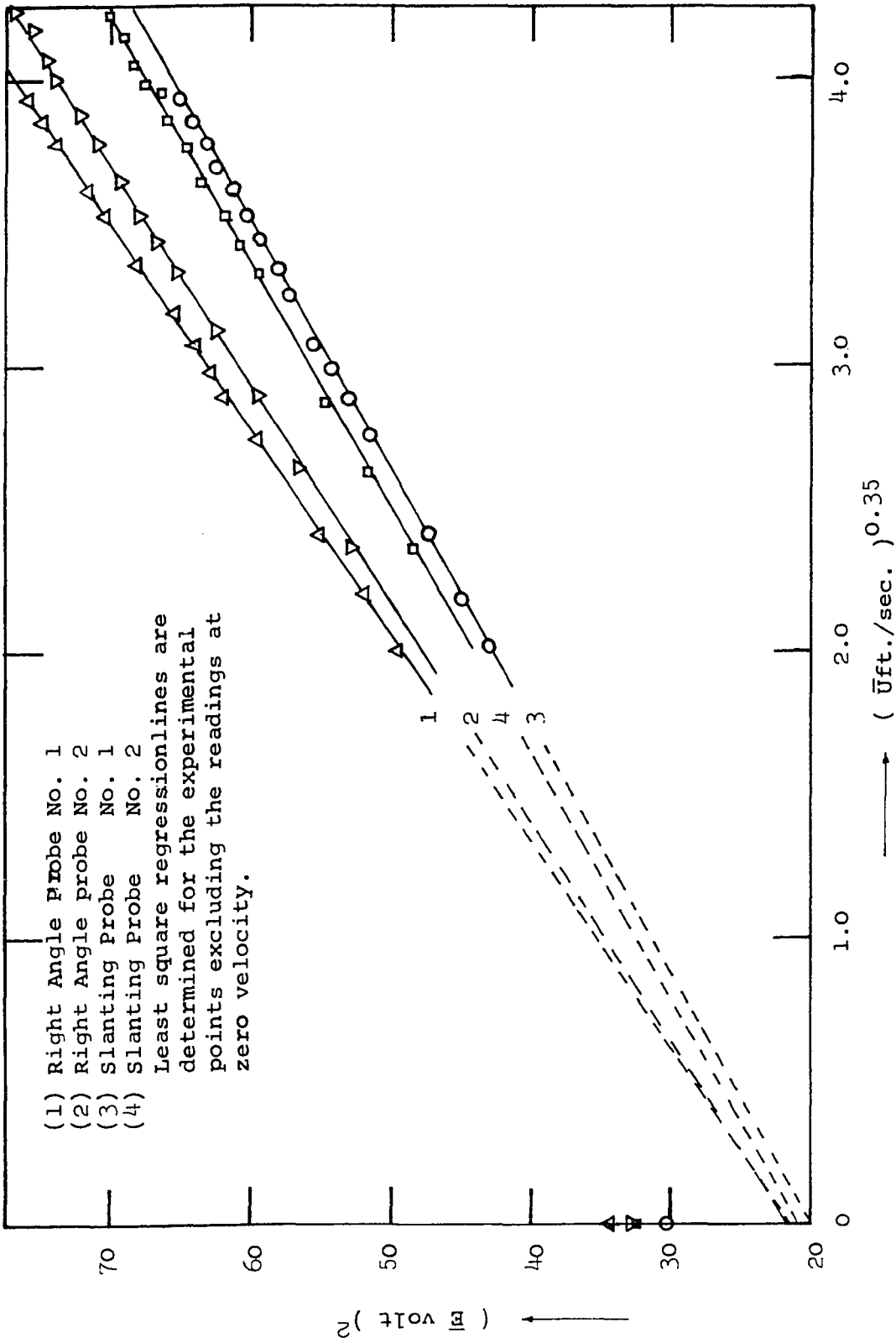


Fig.38 Calibration of the right angle and slanting hot wire probes used for experimentation.

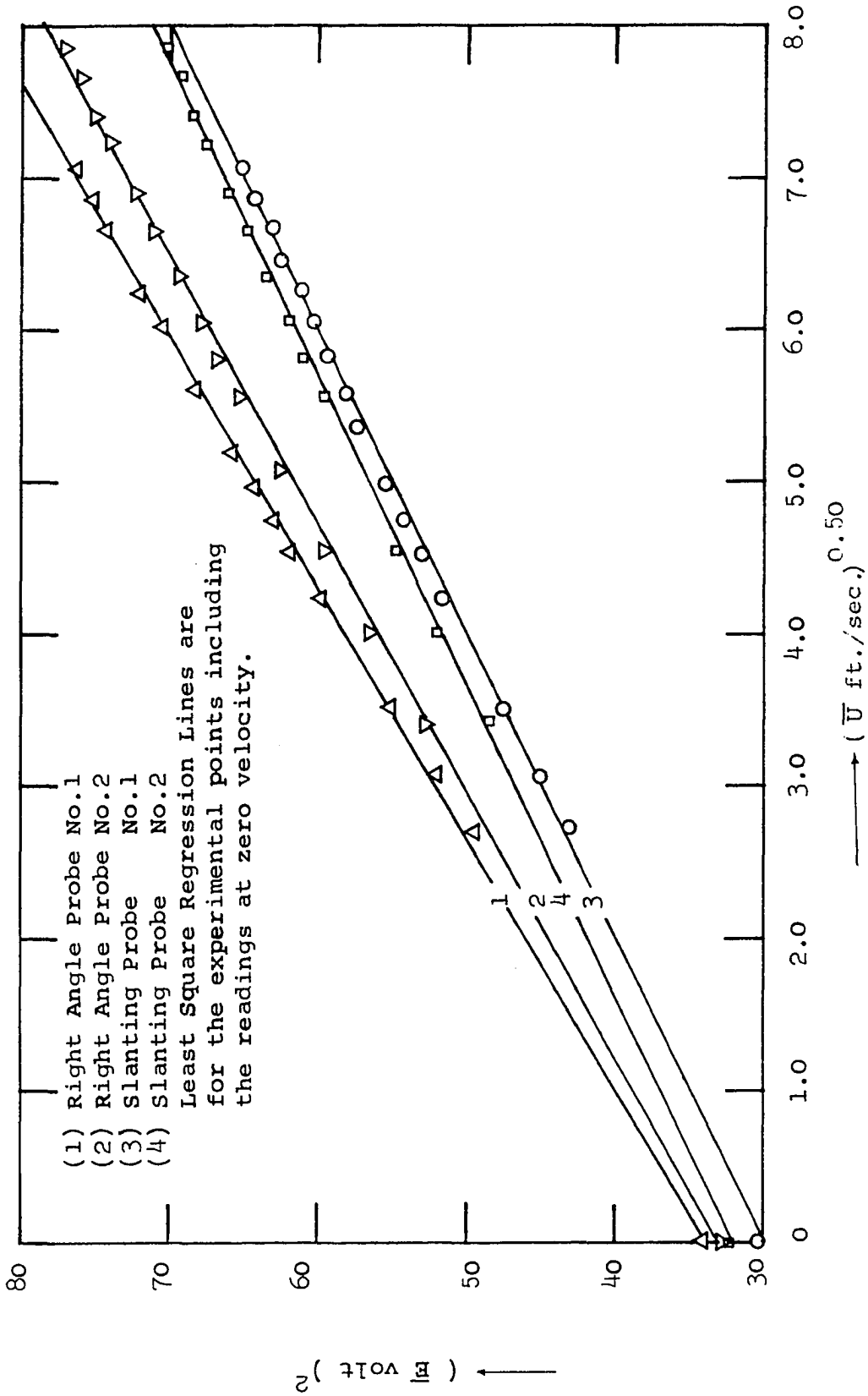


Fig.39 Calibration of the right angle and slanting hot wire probes used for experimentation.

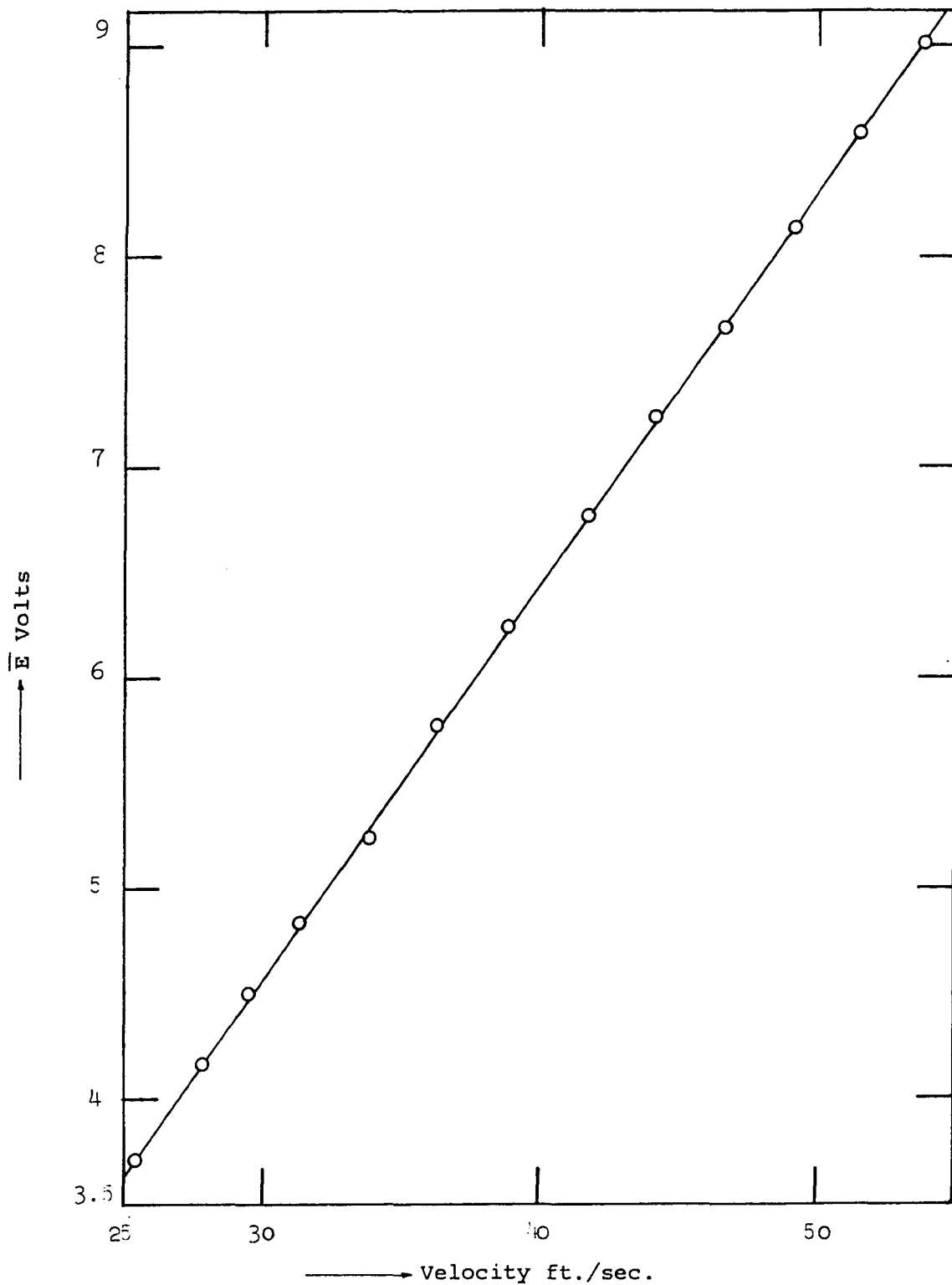
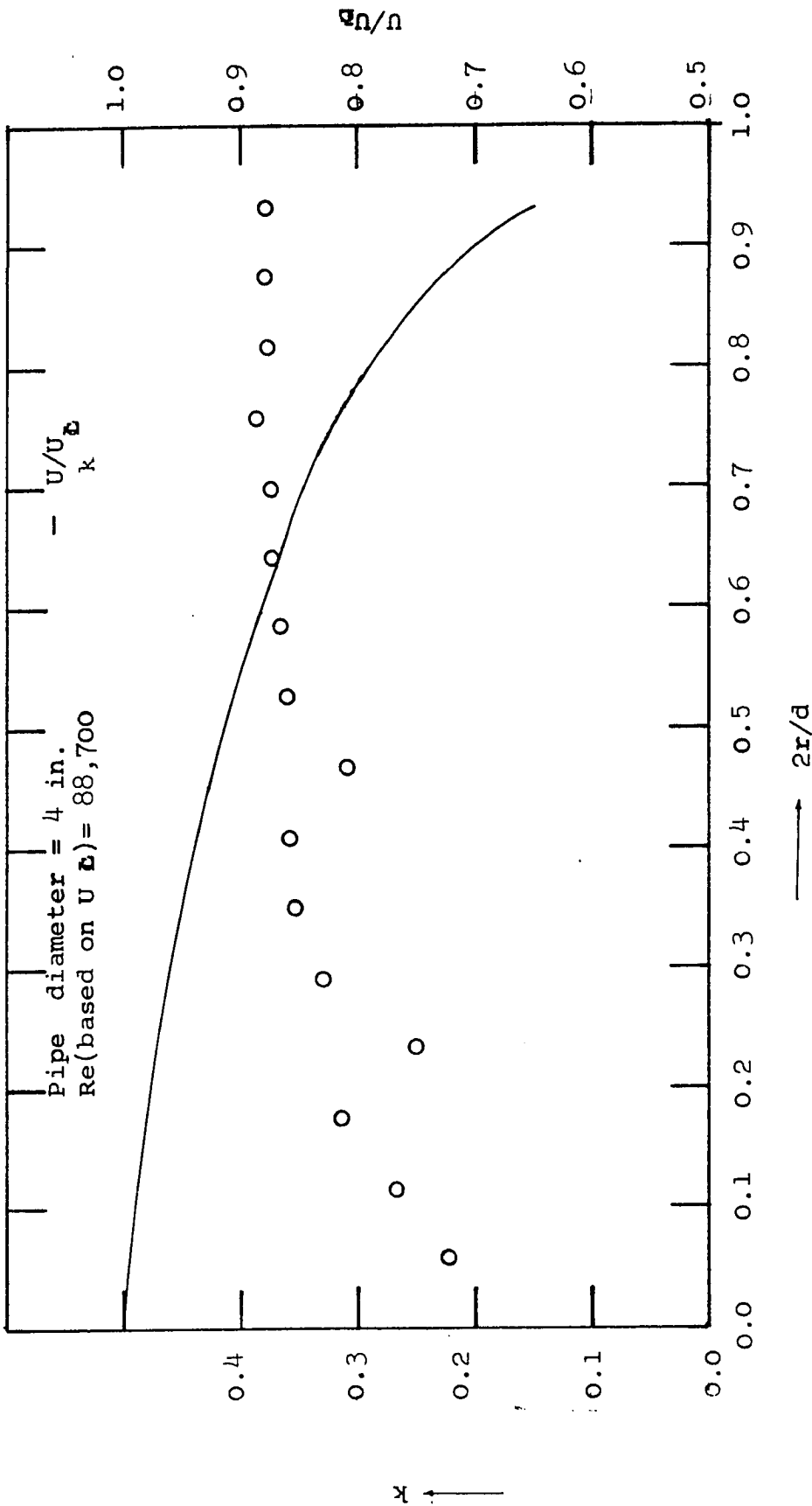


Fig. 40 Calibration of a slanting hot wire probe using linearizer in the circuit, assuming velocity exponent = 1/2.22



Mean velocity profile in turbulent flow in a pipe and values of  $k$  of slanting hot wire determined from the known Reynolds shear stress distribution.

Fig. 41

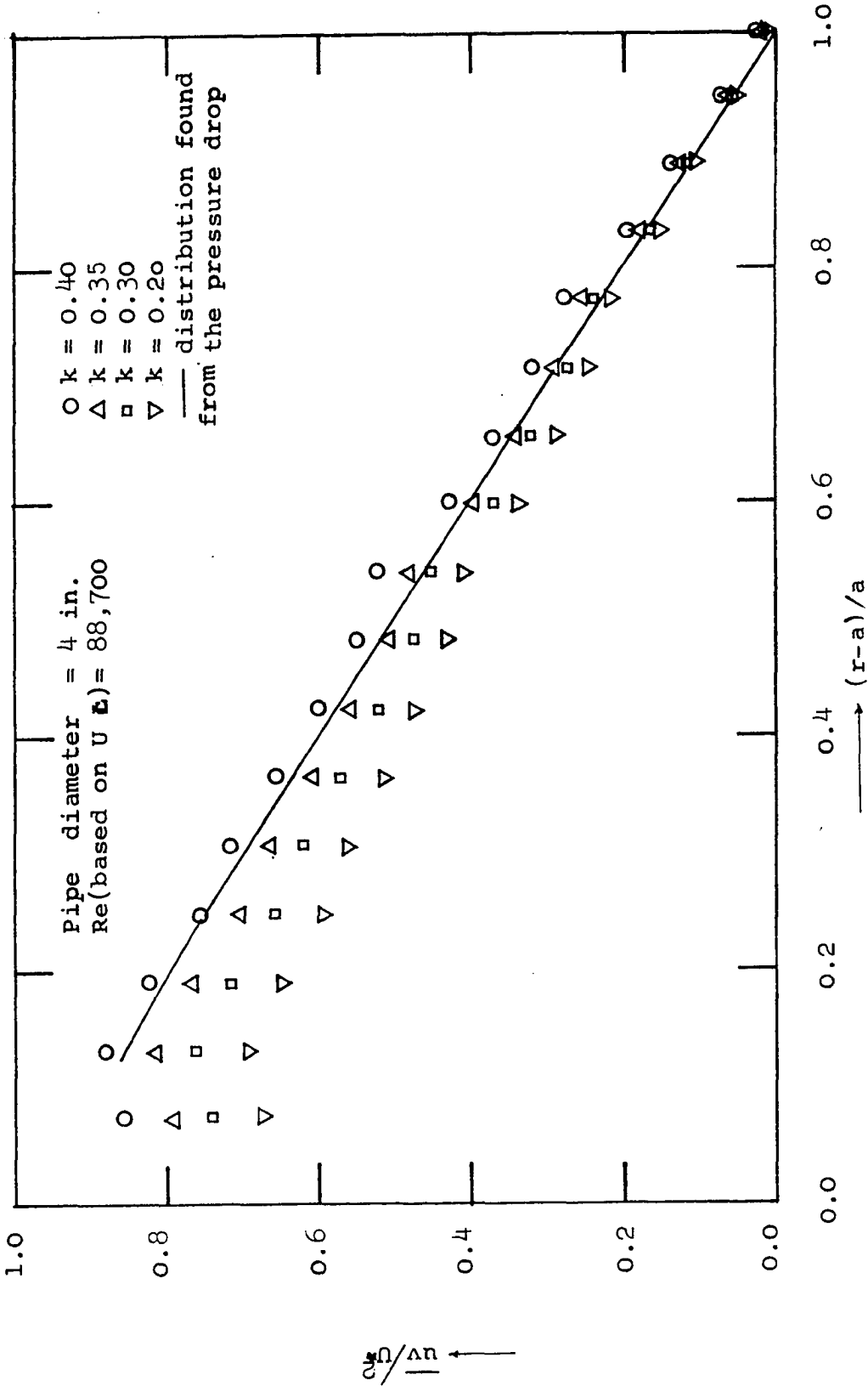


Fig. 42 Comparison of radial Reynolds shear stress distribution by hot wire anemometer assuming different values of  $k$ , with that obtained from pressure drop along the pipe.

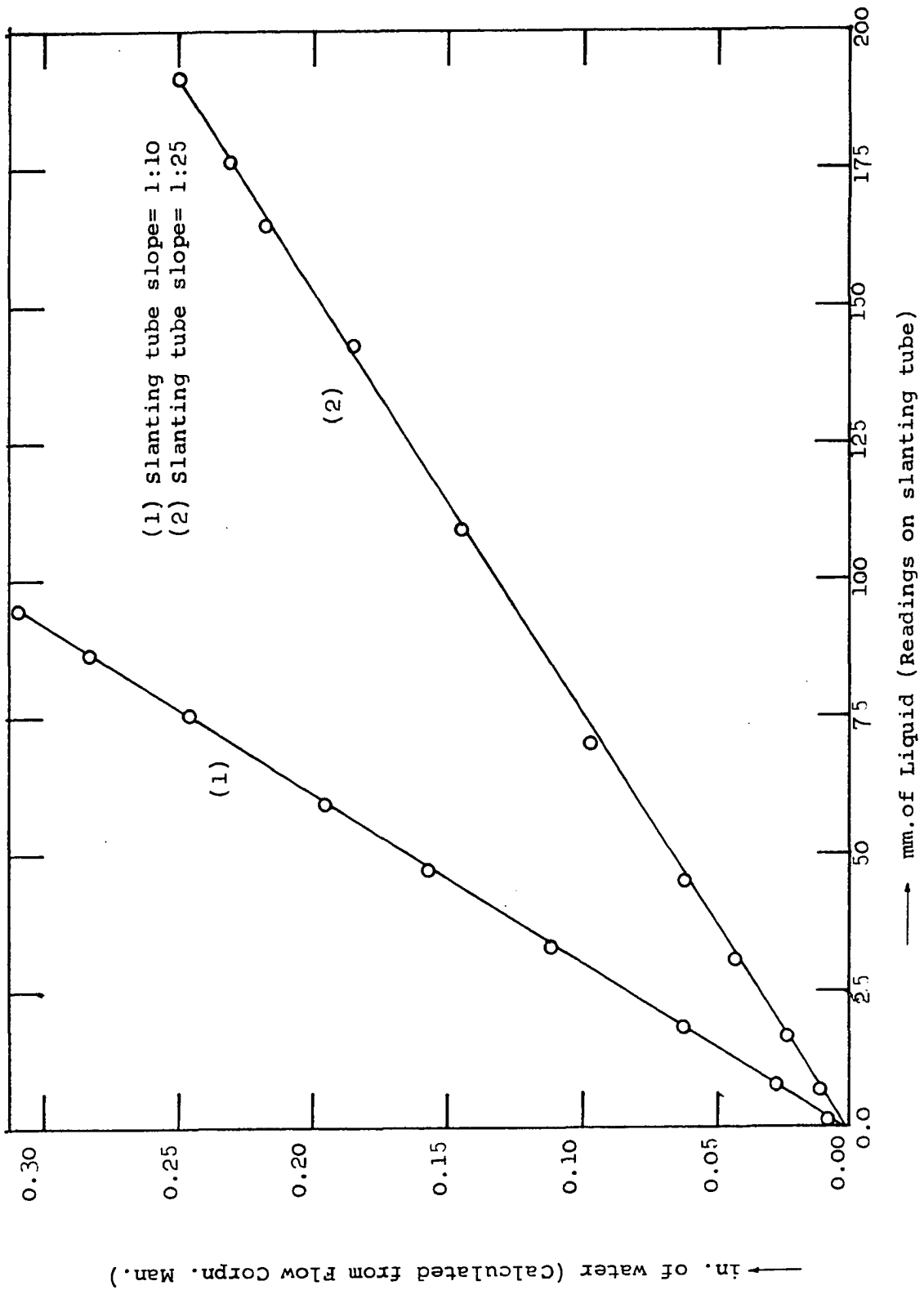


Fig. 43 Calibration of WL slanting tube micromanometer against Flow Corporation Micromanometer.



## VITA AUCTORIS

- 1943 Born in Gawalior, India, on November 11.
- 1959 Completed Secondary School from Government Boys' Secondary School, Behar Colony, Karachi, Pakistan.
- 1961 Passed Intermediate Science Examination from S.R.A. College, Karachi.
- 1965 Received Bachelor of Engineering (Mechanical) Degree from the University of Karachi, Karachi, Pakistan.
- 1966 Joined N.E.D. Government Engineering College, Karachi, as Lecturer in Mechanical Engineering.
- 1969 Candidate for the Degree of Master of Applied Science in Mechanical Engineering at the University of Windsor, Windsor, Ontario.